Vibration Control of Building Structures by Active Tuned Mass Damper

アクティブ動吸振器による建築構造物の振動制御

Isao Nishimura
西村　功

June 1994
平成六年六月

①

Vibration Control of Building Structures

by

Active Tuned Mass Damper

This is the thesis submitted to
the Graduate School of the University of Tokyo
as the requirement for the doctoral degree
from the School of Engineering.

By

Isao Nishimura

1994

CONTENTS

Introduction

The theme of this paper is the optimization of the active tuned mass damper (TMD), otherwise known as the dynamic absorber which has been a well known vibration control tool among mechanical engineers for many years. The history of the dynamic absorber can be traced back to the invention by Frahm [1] in 1909. It is a tiny little oscillator, which is composed of a mass and a spring, for the purpose of reducing the response vibration of a relatively large mass system subjected to a sinusoidal excitation. Later, this intriguing device came to be known as Frahm's dynamic absorber.

In 1928, there was a paper written by Ormondroyd and Den Hartog [2] who first studied this device theoretically. They discovered the fact that the addition of a damping material to the dynamic absorber significantly enhances the vibration control performance under a harmonic excitation. Their contribution to the refinement of the device was significant, and it came to be known to engineers and scientists after the first edition of *Mechanical Vibration* was published in 1934. The importance of their work does not only consist in the refinement of the dynamic absorber but in the development of a general optimization method in the frequency domain. This optimization procedure, however, had a rather unexpected depreciation in spite of its remarkable debut. It was never regarded as a general methodology applicable to other types of optimization, much less to active control.

As far as the active vibration control of building structures is concerned, the concept of the method was first pointed out by Yao in 1972 [3]. The importance of his paper lies in the positive suggestion of the active control as one of the seismic design methods at the time when nobody had the slightest idea of replacing the matured structural design methods by an active control approach. Little attention was paid to his work until 1977, when MTS System Corporation (a hydraulic power system engineering company) installed a passive TMD into a high rise building (John Hancock Tower 60-story or 240 meters high) in Boston. Their system used a hydraulic actuator as a damping material. Two identical machines were set on the 58th floor to attenuate the response vibration induced by strong wind blows. The auxiliary mass weight of each machine is approximately 300 ton, which is just a huge lump mass of

lead. The details of their work were reported by McNamara [4]. The second project conducted by MTS is another passive TMD installed into New York Citicorp Center building [5],[6],[7]. The system constitution is almost identical to the previous one except that the weight is approximately 400 ton made of a concrete block and the lateral stiffness is provided by pneumatic springs. But this project might have had a different progress. Lund, who was one of the MTS engineers and studied the feasibility of active control, wrote a paper associated with this project [8]. According to his paper, it is clear that he tried to increase the amplitude of the TMD by means of a hydraulic actuator so that the control performance would be augmented. This might have been the first active control attempt in civil engineering with an actual target project. However, he could not explicitly describe a control algorithm suitable for this purpose. Instead of working independently, he seemed to have collaborated with a research team of State University of New York at Buffalo. Indeed, Lund's work was further studied by Chang and Soong [9]. They regarded the active TMD as a typical example problem of the modern control technique or the state space method with a linear quadratic regulator. Unfortunately, the simple application of the modern control method did not yield a noticeable result that could have changed the design of the Citicorp TMD.

Just a few years prior to this movement in civil engineering field, there was a work done by Morison and Karnopp [10]. They were mechanical engineers who were interested in the active TMD. Their work was the first theoretical attempt to improve the control performance of the passive TMD by means of an active device supplemented to it. They employed the modern control technique to raise the TMD performance and obtained several interesting solutions by crunching out the Algebraic Riccati Equation. One ironical weakness of this sophisticated method is that we could not understand what we are doing. Even after we obtain a solution, the physical meaning of the feedback gain is far from comprehension. As Morison stated in his paper [10], the active feedback gain could not be determined by intuition. And the physical meaning of the feedback gain was not even discussed. Indeed, what can be obtained by the linear quadratic optimization is a numerical solution for a particular problem. As a result, they came to believe that the active TMD operation was completely different from the passive TMD. In fact, they did

not notice the fact that the tuning adjustment was indispensable for the optimization of the active TMD.

This is the background of the active TMD research before 1988. In civil engineering, methods for the attenuation of structural response under seismic excitation did not receive much attention until the importance was recognized at the time of the 9WCEE (9th World Conference of Earthquake Engineering) held at Tokyo and Kyoto in 1988. The Steering Committee of the conference organized a special theme session titled "Seismic Response Control of Structural Systems". The session highlighted recent developments in seismic response reduction and control methodologies, with emphasis on seismic load reduction, seismic load isolation and response control [11],[12]. This event accelerated application projects of active control in civil engineering of Japan, though the emphasis was more focused on wind blow disturbances rather than ground motion. The first application reported was the work by Kobori [13], followed by others [14], [15], [16], [17]. Since then, there have been numerous works reported with actual application projects. But most of them were related with specific devices of their own and the reported results were only numerical studies obtained by way of solving Riccati equations. Hence, the analytical solution for the active TMD was not still obtained in general. And the importance of tuning adjustment was not precisely understood.

In 1992, it was discovered that the analytical solution is obtainable if the acceleration of the primal structure is used as the basic feedback gain to control the active TMD [18]. According to the modern control method, it is impossible to use the acceleration signal as a feedback gain for a second order dynamic system. Therefore the modern control technique, especially the optimization procedure, could not be used to derive the solution for the acceleration feedback method. The basic concept of this new control strategy was proposed on the occasion of the Japan National Symposium on Active Structural Response Control held at Tokyo March, in 1992 [18]. The concise version of the paper was presented at the First European Conference on Smart Structures and Materials held at Glasgow [19]. The experimental results were also reported at the First International Conference on Motion and Vibration Control held at Yokohama in 1992 [21].

The acceleration feedback method clarified the physical meaning of the active TMD operation, and revitalized Den Hartog's method. Several enigmatic problems that had never been explained properly were analytically solved and expressed in a closed form solution. The formulation of the solutions and the configuration of the response functions are simple, precise and beautiful. The optimum tuning adjustment for the active TMD is made clear in comparison with the passive TMD. The minimization of control force, power, and energy is also achieved by the acceleration feedback method. This paper devoted 90% of its contents to the explanation of the acceleration feedback method, and 10% to the introduction of a remarkable invention, the composite TMD, which is related to this algorithm.

Independently from these movements taking place in the mechanical and civil engineering fields, the composite TMD was invented by Yamada [21] in 1986. The remarkable idea which makes this invention unique is the replacement of the reaction control force by the inertia force created by the motion of additional secondary mass actively mounted on the passive primal TMD. From the very beginning, Yamada apparently recognized the intrinsic essence that is indispensable for controlling the active TMD in general. The possibility of considerable reduction of the active control force and power was suggested by the application paper of the invention submitted to the Japan Patent Bureau. However, the suitable control algorithm for the device was unknown at that time, mainly because the displacement required for the active secondary mass would be very large if the modern control method was simply applied. This invention motivated a research to find the general analytical solution for this problem. The acceleration feedback algorithm was later recognized to be an appropriate control law for the composite TMD. The replacement of the reaction force by the inertia force was clarified in the paper [23], followed by other papers [24],[25]. Then the appropriate control algorithm for the active-passive composite TMD was procured, though further study will be necessary for identifying the closed form solution.

This is the brief history of the tuned mass damper and the background of the research of this paper. In recognition of the weak points of both the classical passive TMD and the modern control method, the author attempts to improve the control algorithm of the active TMD so as to make it one of the

feasible choices for vibration control of large civil engineering structures. It is true that the tuned mass damper can reduce only one modal vibration of a multi-degree-of-freedom system. But the first modal vibration has a predominant importance for many cases. Therefore, in this paper a single-degree-of-freedom model is thought to be a target system for the active TMD. The followings are the issues of this research.

1. It is natural that the response motion of the auxiliary system is enlarged as a result of active control, whatever the control algorithm may be. Hence it is important to reduce the auxiliary system response as much as possible without degrading the control effect.

2. Only numerical solutions are available, if we faithfully follow the modern control method which does not explain the physical meaning of the active TMD operation. Hence it is aimed that the optimal control algorithm is established to obtain a closed form solution that can physically explain the operation of the active TMD.

3. When the active control method is applied to a large civil engineering structure, it is indispensable to reduce the control force, power, and energy as much as possible without degrading the control effect of the active TMD. The stiffness and damping parameters of the device will be optimized so as to reduce the control requirement. The derivation of the formulae will be carried out in the frequency domain under a white noise excitation as well as a harmonic excitation.

4. The effect of disturbance excitation acting on the building structure is considered for the above optimization process. First, the physical meaning of the acceleration feedback method is clarified under a harmonic excitation. Then, the optimum tuning frequency and damping factor are obtained both under a harmonic and a white noise excitation. Finally, the difference between the

wind blow disturbances and the earthquake ground motions is also considered for the parameter optimization.

5. There will be carried out numerical calculations to verify the statistically expected control performance of the acceleration feedback algorithm. Several recorded earthquake disturbances are used to evaluate the control energy minimization in a deterministic sense instead of a stochastic sense. There will be shown plenty of examples that can strongly support the validity of the optimal parameter formulae under earthquake excitations.

6. The feasibility and practicability of the active control method is the final goal of this research. The theoretically expected control performance is experimentally verified by a shaking table test. Attention is paid to the preliminary system identification part of the test, because the consistency with the theory is of the first importance for this part of the research.

In chapter 1 there are introduced and reviewed the classical passive TMD parameter optimization and the active TMD optimum control algorithm. The analytical optimum solutions are obtained in chapter 2 according to the acceleration feedback method. The optimum solutions of the active TMD will be shown to have a physical consistency with the passive TMD, which is also described in chapter 2. The solutions are achieved under several different types of disturbances such as harmonic, white noise, and non-stationary random excitations. The numerical solutions under several earthquake disturbances are discussed in chapter 3 for the purpose of verifying the energy equilibrium that is predicted in a probabilistic sense in chapter 2. Finally, the theoretically estimated vibration control performance is experimentally studied in chapter 4. The experimental results are assertive and encouraging so that the acceleration feedback method is seen to be the most effective and feasible control algorithm for the active TMD.

Isao Nishimura

Chapter 1

Review of the Past Methods

The principle of a vibration absorber or a tuned mass damper (TMD) has been widely known as one of the passive vibration control methods for many years [1], [2] (Figure 1.1). It is said that the original TMD (without damping instrument) was invented by Frahm in 1909 [1]. Then, it was intensively studied by Ormondroyd and Den Hartog, who suggested the optimum tuning adjustment and damping selection in the frequency domain. In this chapter, the method initiated by them is reviewed to examine the feasibility of the passive TMD applied into large building structures. Then, the weak points of the device are stated for the purpose of improving the TMD control performance.

The actively controlled TMD was proposed by Morison and Karnopp in 1973 [10] (Figure 1.2). They studied the dynamic behavior of a primal system, a single-degree-of-freedom system, with an actively controlled tuned mass damper mounted on it. The controller was supposed to generate an adequate force to activate the auxiliary mass so that the vibration control performance of the TMD could be augmented. The theoretical tool adopted in their research was the modern control technique described in the state space or in the time domain. They employed the linear quadratic optimum regulator to specify the feedback gains for controlling the TMD. Although the system constitution of their active TMD stemmed from the classical passive TMD, there was no continuity between the two methods. As a matter of fact, the tuning adjustment was not even thought to be indispensable for their active TMD algorithm.

In the civil engineering field, Lund was one of those who first studied the feasibility of the active TMD by using an actuator and a pneumatic spring [8]. His idea was further investigated by Chang and Soong who, however, only applied the linear quadratic optimum control law to determine an appropriate feedback gain for the active TMD [9]. So, they did not optimize the TMD parameters, just like Morison and Karnopp. In this chapter, the modern control method is reviewed and its weak points are clarified in order to develop an alternative active control algorithm.

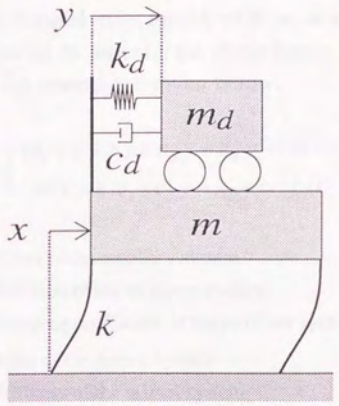

Figure 1.1 Passive Tuned Mass Damper

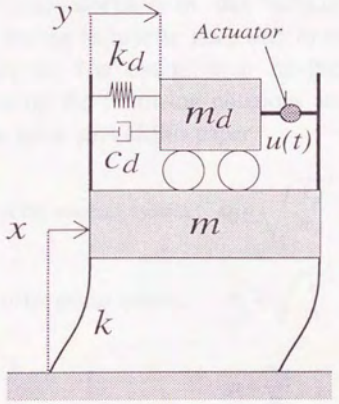

Figure 1.2 Active Tuned Mass Damper

1.1 The Principle of Passive Tuned Mass Damper

We suppose that a large lumped mass model with an auxiliary system, which is a passive TMD, is subjected to an external disturbance. (See Figure 1.1.) The equations of motion of the system are given below.

$$\begin{cases} m_d(\ddot{y}+\ddot{x}) + c_d\dot{y} + k_d y = 0 & (1.1) \\ m\ddot{x} + kx - c_d\dot{y} - k_d y = f_w(t) & (1.2) \end{cases}$$

where m_d : Mass of the auxiliary system
k_d : Stiffness of the auxiliary system
c_d : Damping coefficient of the auxiliary system
m : Mass of the primal system
k : Stiffness of the primal system
$f_w(t)$: External disturbances applied to the mass of the primal system

If the natural frequency of the auxiliary system is close to that of the primal system, the motion of the TMD mass has approximately 90° phase lag behind the primal system vibration. Therefore, the inertia force created by the TMD mass motion works as a damping force on the primal system. This is the basic principle of the passive TMD. However, its control performance is not so easily attained in the real world. In this section, the work done by Ormondroyd and Den Hartog is briefly reviewed to clarify the weak points associated with the device. The optimization of the TMD parameters is conducted after introducing the following notations and substitutions for the sake of continuity of the latter part of this paper.

Natural frequency of the auxiliary system : $\omega_d = \sqrt{\frac{k_d}{m_d}}$ (1.3)

Natural frequency of the primal system : $\omega_o = \sqrt{\frac{k}{m}}$ (1.4)

Mass ratio : $\mu = \frac{m_d}{m}$ (1.5)

Frequency ratio : $$\xi = \frac{\omega_d}{\omega_o} \tag{1.6}$$

Damping factor : $$\eta = \frac{c_d}{2\, m_d\, \omega_d} \tag{1.7}$$

We supposed that $f_w(t)$ is a harmonic excitation given by

$$f_w(t) = m\,(\omega_o)^2 F\, e^{i\omega t} \tag{1.8}$$

In this case, the solution can be shown to have the form

Primal system response : $$\begin{cases} x(t) = & X\, e^{i\omega t} \\ \dot{x}(t) = & i\omega X\, e^{i\omega t} \\ \ddot{x}(t) = & -\omega^2 X\, e^{i\omega t} \end{cases} \tag{1.9}$$

Auxiliary system response : $$\begin{cases} y(t) = & Y\, e^{i\omega t} \\ \dot{y}(t) = & i\omega Y\, e^{i\omega t} \\ \ddot{y}(t) = & -\omega^2 Y\, e^{i\omega t} \end{cases} \tag{1.10}$$

where ω : Excitation frequency
F : Complex amplitude of the excitation
X : Complex amplitude of the primal system response
Y : Complex amplitude of the auxiliary system response

After some manipulation of the previous equations, we obtained

$$\begin{bmatrix} -f^2 + \xi^2 + 2f\xi\eta i & -f^2 \\ -\mu f^2 & 1-(1+\mu)f^2 \end{bmatrix} \begin{bmatrix} Y \\ X \end{bmatrix} = \begin{bmatrix} 0 \\ F \end{bmatrix} \tag{1.11}$$

where $f = \frac{\omega}{\omega_o}$: Normalized excitation frequency

which can be solved and we obtain

The frequency response of the primal system:

$$\left|\frac{X}{F}\right|(f)=\sqrt{\frac{(\xi^2-f^2)^2+(2\eta\xi f)^2}{\left[f^4-(1+\xi^2+\mu\xi^2)f^2+\xi^2\right]^2+\left[2\eta\xi f(1-f^2-\mu f^2)\right]^2}} \tag{1.12}$$

The frequency response of the auxiliary system:

$$\left|\frac{Y}{F}\right|(f)=\sqrt{\frac{f^4}{\left[f^4-(1+\xi^2+\mu\xi^2)f^2+\xi^2\right]^2+\left[2\eta\xi f(1-f^2-\mu f^2)\right]^2}} \tag{1.13}$$

Then, the optimum parameters are defined in such a manner that the peaks of the primal system response curve are reduced as much as possible. (There are two peaks in the response curve. See Figure 1.3.) This optimization methodology is to be referred to [1], or other text books [26],[27]. The classical optimum parameter formulae are cited and given by

$$\xi_{opt}=\frac{1}{1+\mu} \tag{1.14}$$

$$\eta_{opt}=\sqrt{\frac{3\mu}{8(1+\mu)}}=\sqrt{\frac{3}{4(\alpha_{max}{}^2+1)}} \tag{1.15}$$

$$\alpha_{max}=\sqrt{\frac{\mu+2}{\mu}} \tag{1.16}$$

where ξ_{opt} : Optimum tuning frequency ratio

η_{opt} : Optimum damping factor

α_{max} : Optimized maximum response of the primal system

1.2 Response Peak of the Auxiliary System

In this section, the auxiliary system response is considered as an optimization index. It is understood from (1.13) that the auxiliary system has a locked point at the frequency

$$f_3 = \sqrt{\frac{1}{1+\mu}} \tag{1.17}$$

Then, the locked response is given by

$$\beta_{max} = \frac{1+\mu}{\mu} \tag{1.18}$$

No matter how large the damping factor η_{opt} may be, the peak of the auxiliary system response is not smaller than the value specified by (1.18). Therefore, there exists the minimum damping factor that places the maximum response of the auxiliary system equal to β_{max} at f_3. After some manipulation of (1.13), the minimum damping factor according to the definition above is obtained and given by

$$\eta_{opt} = \sqrt{\frac{\mu}{2(1+\mu)}} = \sqrt{\frac{1}{\alpha_{max}^2 + 1}} \tag{1.19}$$

The damping factor according to (1.19) is larger than the value specified by (1.15). However, this small discrepancy between (1.15) and (1.19) does not significantly influence the primal system response. It is true that the peak of the primal system is just a little more reduced according to (1.15) rather than (1.19), but the damping augmentation makes the TMD performance more robust in case of a possible miss-tuning adjustment, which makes (1.19) more favorable from an engineering point of view. An example numerical study is conducted to show the difference between the two equations. The optimum parameters according to (1.14)~(1.16) under the mass ratio $\mu = 0.02$ is given in Table 1.1, where the alternative optimum value due to (1.19) is also indicated. The response curves of the primal system due to (1.15) and (1.19) are shown in Figure 1.3, while the corresponding auxiliary system responses are shown in Figure 1.4.

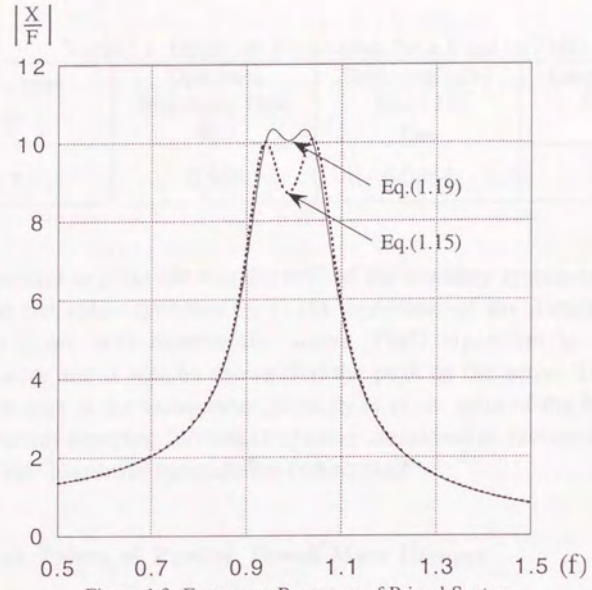

Figure 1.3 Frequency Response of Primal System

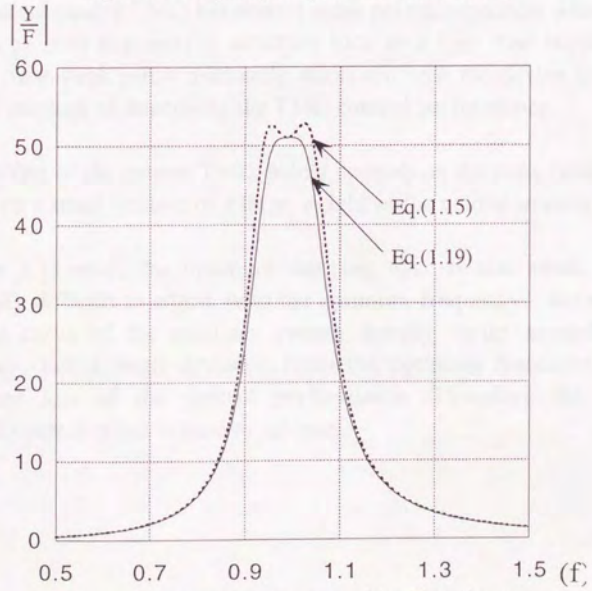

Figure 1.4 Frequency Response of Auxiliary System

Table 1.1 Optimum Parameters for a Passive TMD

Mass ratio μ	Optimum frequency ratio ξ_{opt}	Damping ratio Eq.(1.15) η_{opt}	Damping ratio Eq.(1.19) η_{opt}
0.02	0.980	0.0857	0.099

It is important to point out that the peak of the auxiliary system response is not less than the value specified by (1.18) regardless of the damping factor. In chapter 2, we will discuss the active TMD algorithm to improve the performance and it will be shown that the peak of the active TMD auxiliary system is kept at the same value given by (1.18) in spite of the feedback gain. The optimum damping formula (1.19) is reconsidered in section 2.3, where the active TMD parameter optimization is discussed.

1.3 Weak Points of Passive Tuned Mass Damper

The classical passive TMD has several weak points, especially when it is applied to a large civil engineering structure such as a high rise building. In this section, these weak points inherently associated with the device are pointed out with the purpose of improving the TMD control performance.

1. The effect of the passive TMD solely depends on the mass ratio μ, which is usually very small because of a large weight of the primal structure.

2. When μ is small, the optimum damping η_{opt} is also small. Hence it is practically difficult to adjust ω_d to the optimum frequency. Because the phase response curve of the auxiliary system sharply varies around the natural frequency. Just a small deviation from the optimum frequency results in a significant loss of the control performance. Therefore the theoretically expected control effect is hard to achieve.

3. The smaller the damping factor η_{opt} is, the longer time the auxiliary system takes until it reaches the steady state response condition. Hence, at the beginning of the disturbance excitation, it does not work effectively to suppress the response motion of the primal system.

4. When μ and η_{opt} are small, the auxiliary system response becomes very large. Because the auxiliary mass won't stop quickly on account of the small damping. The free vibration continues for a long time even after the disturbance input recedes from the primal structure. So the unnecessary response motion of the TMD is inevitable under random excitations.

All the above weak points are removed, if the mass ratio of the passive TMD is quite large. If the mass ratio μ exceeds a critical level, the tuning adjustment is less important. In fact, there is a paper by Akiyama who studied the elasto-plastic damping given to the passive TMD which is roughly tuned or even not-tuned intentionally [39]. His attempt is based on the empirical recognition that the energy input into a structure under earthquake disturbances is quite invariant or not much influenced by the material non-linearity of the target system [38]. Hence, if the total input energy is mostly dissipated at the top story of a building structure, the rest of the frame work is expected to remain intact after the event of a major earthquake. According to his study, the minimum required mass ratio for such a large TMD is roughly more than 0.1, which might be one whole story or two, which will be additionally constructed to the top of a building structure.

On the contrary, the active control aims to compensate for the weak points of the passive TMD without increasing its actual weight. In the coming section, the active control approach is reviewed to make clear the difference from the passive TMD optimization.

1.4 Active Control by the Modern Control Method

An actuator as a control device was installed between the primal and auxiliary systems and was first investigated by Morison and Karnopp. This is the actively controlled TMD configuration long investigated by many researchers ever since then (Figure 1.2). The theoretical methodology adopted by them

was the orthodox modern control approach, which is briefly reviewed in this section.

In general, it is possible to place the closed-loop poles of the characteristic polynomial of the system anywhere we wish them in the complex s plane, provided that all the necessary state variables are accessible for measurement and the controller is placed at a position where the system is controllable. The location of the closed-loop poles is a matter of significance, because it can completely specify the characteristic polynomial of the system dynamics. Therefore the purpose of the modern control technique is nothing more than a relocation of root locus by feedback method.

Although the zeros of the closed-loop transfer function (root locations of the numerator of the Laplace transform of the system function) also play an important role to specify the dynamic behavior of the system, they have received little attention until recently. In fact, the optimization of controller's location, the optimization of the controllers' power and energy, the effect of disturbances on the system response are the typical problems that should have been more seriously.

To illustrate those left over problems associated with the conventional linear quadratic optimization approach, the state space method is simply applied to the active TMD and the optimum solution is reviewed. This section's formulations and derivations are mostly referred to [31], [32]. The equations of motion of the active TMD are given by

$$\begin{cases} m_d(\ddot{y}+\ddot{x}) + c_d\dot{y} + k_d y + u(t) = 0 & (1.20) \\ m\ddot{x} + kx - c_d\dot{y} - k_d y - u(t) = f_w(t) & (1.21) \end{cases}$$

where $u(t)$: the control force applied by an actuator

According to the modern control linear quadratic optimum formation, the disturbance excitation $f_w(t)$ is supposed to be zero. Then, the above equation is converted into

$$\{\dot{x}(t)\} = A\{x(t)\} + B\,u(t) \qquad (1.22)$$

where

$$A = \begin{bmatrix} \begin{bmatrix} 0 & 0 \\ 0 & 0 \end{bmatrix} & I \\ -M^{-1}K & -M^{-1}C \end{bmatrix}, \quad B = \begin{bmatrix} \begin{bmatrix} 0 \\ 0 \end{bmatrix} \\ -M^{-1}\begin{bmatrix} 1 \\ 0 \end{bmatrix} \end{bmatrix} \tag{1.23}$$

$$\{x(t)\} = \begin{bmatrix} y \\ x \\ \dot{y} \\ \dot{x} \end{bmatrix}, \quad \{\dot{x}(t)\} = \begin{bmatrix} \dot{y} \\ \dot{x} \\ \ddot{y} \\ \ddot{x} \end{bmatrix} \tag{1.24}$$

$$M = \begin{bmatrix} m_d & m_d \\ m_d & m + m_d \end{bmatrix}, \; C = \begin{bmatrix} c_d & 0 \\ 0 & 0 \end{bmatrix}, \; K = \begin{bmatrix} k_d & 0 \\ 0 & k \end{bmatrix}, \; I = \begin{bmatrix} 1 & 0 \\ 0 & 1 \end{bmatrix} \tag{1.25}$$

It is noted that the control algorithm according to the modern control technique, in general, is given by

$$u(t) = -G\,\{x(t)\} \tag{1.26}$$

The gain matrix for this particular problem is

$$G = \begin{bmatrix} g_1, g_2, g_3, g_4 \end{bmatrix} \tag{1.27}$$

With the control law of (1.26), (1.22) becomes

$$\{\dot{x}(t)\} = A_c\,\{x(t)\} \tag{1.28}$$

where

$$A_c = A - B\,G \tag{1.29}$$

so that the characteristic polynomial for A_c is given by

$$\left| s\,I - A_c \right| = \left| s\,I - A + B\,G \right| = 0$$

or equivalently

$$s^4 + a_1 s^3 + a_2 s^2 + a_3 s + a_4 = 0 \tag{1.30}$$

These coefficients of a_1~a_4 are the function of feedback gains. If we select the four gains properly, it is possible to locate all the coefficients anywhere we wish them to be. This system has the 4-th order dynamic matrix A given by (1.23) and the characteristic polynomial by (1.30), which means the characteristic equation has 4 poles in the complex s plane. And there are also 4 state variables available for feedback control as indicated by (1.27). Therefore they can completely specify the location of the poles of the system transfer function. The only question raised here is where they should be placed. A customary answer to this question is given simply by solving the well known Riccati equation. To simplify this problem, the steady state solution or the Algebraic Riccati Equation is reviewed and an example solution for this particular active TMD is demonstrated in the following section.

1.5 Linear Quadratic Optimization and Pole Placement

In a general sense, there are several reasons for seeking an optimum controller. According to the modern control theory, it is possible to place the closed-loop poles anywhere we want them to be in a single-input and single-output system, provided that the system is controllable and observable [32]. However, as was pointed out in Morison's paper, it is hardly possible to use one's insight to find the desirable closed-loop pole locations for the active TMD.

Another reason for seeking the optimum control is that in a multiple-input or multiple-output system, it is not generally possible to completely specify the pole locations of the closed-loop. Because in a case of k-th order system with m-inputs there are km parameters to be determined, but there are only k possible closed-loop pole locations. There are too many ways to realize the controller with the same closed-loop pole locations. Obviously, in this particular active TMD case, the target system is 4-th order with only one controller. And all the accessible state variables are the displacement and velocity of the primal and auxiliary systems, in other words there are 4 variables available for feedback quantities. Therefore, in this particular problem there is no such problem of too much freedom as in a general case which necessitates a procedure to diminish this cumbersome situation. Seemingly this is a lucky situation for the active TMD optimization. But careful

consideration is necessary. The above condition does not mean that 4 variables are necessary to specify the characteristic polynomial of the optimum dynamics. There is a possibility that only one variable is enough to obtain the optimum feedback algorithm. The linear quadratic regulator method, however, does not answer this problem which is discussed in the next section.

In this section we treat the first order differential equation in a general manner to trace the optimization procedure according to the modern control theory so that Morison's active TMD optimization process is reviewed. The dynamic process considered here is

$$\{\dot{x}(t)\} = A\{x(t)\} + B\,u(t) \tag{1.31}$$

The gain matrix we wish to determine is

$$u(t) = -G\{x(t)\} \tag{1.32}$$

Substitution of (1.32) into (1.31) yields

$$\{\dot{x}(t)\} = A_c\{x(t)\} \tag{1.33}$$

where

$$A_c = A - B\,G \tag{1.34}$$

In this particular case, A_c is a constant matrix so that the state transition matrix is given by

$$\{x(\tau)\} = e^{A_c(\tau - t)}\{x(t)\} \tag{1.35}$$

The target performance index is expressed in a quadratic form as

$$J = \int_t^T \left[\{x(\tau)\}^t\, Q\,\{x(\tau)\} + u(\tau)\, R\, u(\tau) \right] d\tau$$

$$= \int_t^T \left[\{x(\tau)\}^t\, (Q + G^t R\, G)\,\{x(\tau)\} \right] d\tau \tag{1.36}$$

where t : the initial time when the disturbance begins.
$T - t$: the duration while the system is interesting.

The optimum feedback gain G is so determined as to minimize the above performance index where Q and R are the weighting matrices according to the desired control performance. Using the state transition matrix, (1.36) is converted into

$$J = \int_t^T \left[\{x(t)\}^t \left[e^{A_c(\tau - t)} \right]^t (Q + G^t R G) \left[e^{A_c(\tau - t)} \right] \{x(t)\} \right] d\tau$$

$$= \{x(t)\}^t \int_t^T \left[e^{A_c^t(\tau - t)} (Q + G^t R G) e^{A_c(\tau - t)} \right] d\tau \{x(t)\}$$

$$= \{x(t)\}^t M(t, T) \{x(t)\} \tag{1.37}$$

where

$$M(t, T) = \int_t^T e^{A_c^t(\tau - t)} (Q + G^t R G) e^{A_c(\tau - t)} d\tau \tag{1.38}$$

$\{x(t)\}^t$: transpose vector of $\{x(t)\}$

G^t : transpose matrix of G

For the purpose of finding the optimum feedback gain G, we must minimize M by selecting A_c, or the resulting closed loop dynamic matrix. Differentiating (1.36), we obtain

$$\frac{dJ}{dt} = -\{x(t)\}^t (Q + G^t R G) \{x(t)\} \tag{1.39}$$

but, from (1.37)

$$\frac{dJ}{dt} = \{\dot{x}(t)\}^t M \{x(t)\} + \{x(t)\}^t \frac{dM}{dt} \{x(t)\} + \{x(t)\}^t M \{\dot{x}(t)\}$$

$$= \{x(t)\}^t \left(A_c^t M + \frac{dM}{dt} + M A_c \right) \{x(t)\} \tag{1.40}$$

therefore

$$-Q - G^t R G = A_c^t M + \frac{dM}{dt} + M A_c \tag{1.41}$$

or

$$-\frac{dM}{dt} = MA_c + A_c^t M + Q + G^t R G \tag{1.42}$$

This equation is to be satisfied by M under the condition of

$$M(T, T) = 0 \tag{1.43}$$

If we wish to minimize the index in case of steady state condition or

$$J = \int_t^\infty \left[\{x(\tau)\}^t Q \{x(\tau)\} + u(\tau) R u(\tau) \right] d\tau \tag{1.44}$$

then , M should be constant or

$$\frac{dM}{dt} = 0 \tag{1.45}$$

or (1.42) is converted into

$$MA_c + A_c^t M + Q + G^t R G = 0 \tag{1.46}$$

Suppose that we have the optimum G_{opt} and the minimized M_{min}, then the other cases are

$$\begin{cases} M = M_{min} + \delta M & (1.47) \\ G = G_{opt} + \delta G & (1.48) \end{cases}$$

Substitution of (1.47) and (1.48) into (1.46) yields

$$\begin{aligned} &(M_{min} + \delta M)(A - B G_{opt} - B \delta G) + (A^t - G_{opt}^t B^t - \delta G^t B^t)(M_{min} + \delta M) \\ &\quad + Q + (G_{opt} + \delta G)^t R (G_{opt} + \delta G) = 0 \end{aligned} \tag{1.49}$$

On the other hand G_{opt} and M_{min} should satisfy

$$M_{min}(A - B G_{opt}) + (A^t - B^t G_{opt}^t) M_{min} + Q + G_{opt}^t R G_{opt} = 0 \tag{1.50}$$

Subtracting (1.50) from (1.49), we obtain

$$\delta M (A - B G_{opt} - B \delta G) + (A^t - G_{opt}^t B^t - \delta G^t B^t) \delta M =$$
$$\delta G^t (B^t M_{min} - R G_{opt}) + (M_{min} B - G_{opt}^t R) \delta G - \delta G^t R \delta G \quad (1.51)$$

which is rewritten as

$$\delta M A_c + A_c^t \delta M =$$
$$\delta G^t (B^t M_{min} - R G_{opt}) + (M_{min} B - G_{opt}^t R) \delta G - \delta G^t R \delta G \quad (1.52)$$

If M_{min} is the minimum solution, then the following equation should be satisfied from the definition.

$$\{x(t)\}^t M_{min} \{x(t)\} \leq \{x(t)\}^t (M_{min} + \delta M) \{x(t)\}$$
$$= \{x(t)\}^t M_{min} \{x(t)\} + \{x(t)\}^t \delta M \{x(t)\} \quad (1.53)$$

This equation implies that δM matrix should be positive definite for any initial condition $\{x(t)\}$. Recalling Lyapunov equation given by (1.54), the theorem asserts that if matrix A has its eigen values in the negative plane, or the system is stable, for any positive semi-definite matrix Q, the solution matrix P is positive-definite [31].

$$P A^t + A P = -Q \quad (1.54)$$

From (1.53), δM should be positive, at least, semi-definite matrix. The third term of the right hand side of (1.52) is to be converging to zero, if G is close to G_{opt}. Hence, the rest of the two linear terms should be positive and semi-definite for any given δG in order that the solution matrix δM should be positive and definite. In other words, the following equation should be satisfied.

$$B^t M_{min} - R G_{opt} = 0 \quad (1.55)$$

Finally it is summarized as follows. The optimum feedback gains G_{opt} in the steady state is given by

$$G_{opt} = R^{-1} B^t M_{min} \tag{1.56}$$

where M_{min} satisfies

$$M_{min} A + A^t M_{min} - M_{min} B R^{-1} B^t M_{min} + Q = 0 \tag{1.57}$$

where Q and R are given in advance, depending on the expected control performance. The equation (1.57) is the well known Algebraic Riccati Equation, which can be solved numerically by several methods.

1.6 Numerical Example

An example calculation is conducted to clarify the methodology for the control of the active TMD. First of all, we should select the parameters for a primal system. The weight and stiffness of a single-degree-of-freedom model shown in Figure 1.2 are given in Table 1.2. It is also necessary to specify the damping coefficient and stiffness of the TMD. The tuning adjustment is not required for this method. Because the feedback gain is expected to adjust the pole location, if necessary. What can be obtained by passive restoring devices and viscous damping materials can also be achieved by actuator's control force. But we must be careful to select k_d and c_d , because the selection of the passive members might effect the control force requirement. Unfortunately, we have no leading principle for this purpose. There have been numerous researches carried out recently in Japan, mainly from this point of view [14],[15],[16],[17]. But the selection of these passive parameters was intuitively conducted in most of the researches. Indeed, the optimum parameters of the passive TMD with the same mass ratio have been the most eligible and favorable candidates without any reason. Another cumbersome task to be finished is the selection of the weighting matrix and factor which are to be given in advance. The linear quadratic optimization is only possible after the weighting matrix and factor are determined. As is seen in the previous section, the feedback gains are implicitly related to the root location of the characteristic polynomial of the system. But the feedback gains and weighting factors do not have a discernible

relation. Hence we need to carry out several numerical studies before we come to be satisfied with the final result. There have been carried out several calculations until the final satisfactory weighting matrix and factor are found, they are determined as

$$Q = \begin{bmatrix} 0\,0\,0\,0 \\ 0\,1\,0\,0 \\ 0\,0\,0\,0 \\ 0\,0\,0\,0 \end{bmatrix} \quad , \quad R = 10.0 \tag{1.58}$$

According to the weighting matrix, it is aimed that the response of the primal system is only in consideration, because the factor appears only with respect to the response displacement of the primal system. The optimum feedback gain associated with the weighting factors given by (1.58) is

$$u(t) = g_1 y + g_2 x + g_3 \dot{y} + g_4 \dot{x} \tag{1.59}$$

The system parameters are given in Table 1.2 from which the system matrices A, B can be shown to have the values as

$$A = \begin{bmatrix} 0 & 0 & 1 & 0 \\ 0 & 0 & 0 & 1 \\ -1.01 & 1.0 & -0.101 & 0 \\ 0.01 & -1.0 & 0.001 & 0 \end{bmatrix}, B = \begin{bmatrix} 0 \\ 0 \\ -101.0 \\ 1.0 \end{bmatrix} \tag{1.60}$$

Table 1.2 Parameters of an example numerical study of an active TMD

	Auxiliary system	Primal system
Parameters	$m_d = 0.01$ $\omega_d = 1.00$ $k_d = 0.01$ $c_d = 0.001$	$m = 1.00$ $\omega_o = 1.00$ $k_o = 1.00$

After substituting (1.60) into (1.57), we solve it in terms of M_{min} which is given by

$$M_{\min} = \begin{bmatrix} 0.000 & 0.000 & 0.000 & 0.031 \\ 0.000 & 2.484 & -0.030 & 0.002 \\ 0.000 & -0.030 & 0.000 & 0.026 \\ 0.031 & 0.002 & 0.026 & 2.534 \end{bmatrix} \tag{1.61}$$

Numerical calculation is necessary for solving the Algebraic Riccati Equation. The recursive method of Lyapunov equation was used for this purpose [31]. The final solution M_{min} is a symmetric matrix as shown in (1.61). Substitution of (1.61) into (1.56) yields

$$G_{opt} = \begin{bmatrix} 0.00 & 0.306 & -0.00688 & -0.00756 \end{bmatrix} \tag{1.62}$$

We came to understand that the tuning adjustment is not requested for this example problem because the initial stiffness is not changed by g_1 that is zero. It is also understood that the active damping factor is approximately 35%, because g_3 is -0.00688. The physical meaning of g_2 is not certain. Obviously more studies, for example dynamic response analyses under several disturbances, are necessary to be content with the result given by (1.62) . The rest of the task is quite subjective and time consuming before reaching to an adequate solution.

1.7 Weak Points of Linear Quadratic Optimization

There are several weak points associated with the conventional linear, quadratic optimization method by solving Algebraic Riccati Equation to specify the feedback gains for the active TMD. First of all, it is impossible to find out the optimum passive tuning frequency, which was already pointed out by Morison [10]. As a matter of fact, it is not necessary to adjust the natural frequency of the auxiliary system to that of the primal system. It is true that this is one of the beneficial aspects of the active approach which is free from tuning adjustment, but it is important to find out the appropriate tuning frequency for

reducing the control force and power necessary for the actuator. This issue is discussed in the following chapter.

Another significant problem associated with the conventional linear quadratic optimum law is that the displacement of the primal system is a necessary state variable for the feedback quantity. But it is not always easy to employ an adequate sensor for this purpose, above all, the displacement signal contains quite a large amount of low frequency component which is not a useful source for the dynamic vibration control purpose. For example, the lateral story drift of a building is caused by a steady constant wind blow acting on one side of the structure, which means that the structure's main frame should be responsible for resisting such a static load.

A third problem is that the final result of the feedback gain does not explicitly show the physical meaning of the algorithm. As a result, we are totally at a loss when to judge the result is acceptable or not. Hence other additional numerical studies are necessary to ascertain the optimum solution is really satisfactory. Indeed, the control performance, including energy dissipation efficiency, is not optimized by the modern control method.

Moreover, the disturbance influences on the control performance and the response of the primal system are totally neglected during the whole optimization process, while the passive TMD optimization procedure explicitly deals with the effect of the disturbances. According to the modern control law, the disturbance is assumed to be zero to obtain the optimum feedback gains. This means that the free vibration from a given initial condition is only considered for the optimization index. Hence there is no guarantee that the solution by the linear quadratic optimization is always appropriate for the system subjected to random disturbances such as earthquakes.

As is reviewed in this chapter, there are many problems that have not yet been considered deeply. In the following chapter, we will discuss an alternative control algorithm suitable for the active TMD, whose physical function is carefully observed to propose a new control algorithm.

Chapter 2

Formulation of the Optimum Control Algorithm

As we reviewed in the previous chapter, the active TMD has been investigated by several people, however, it has been viewed as a simple application problem of the state space method with linear quadratic optimization. But there are several problems left over and they have not received much attention until quite recently. One of these problems is how to operate the machine most efficiently in order to subdue the response motion of the primal system. It is expected that the response motion of the auxiliary system is ordinarily increased as a result of active control, whatever the control law may be. Hence it is desired not only to increase the control effect but also to restrict the auxiliary mass motion as much as possible. In conjunction with the modern control theory, the linear quadratic optimization was favorably used to answer this problem. But the adequate selection of the weighting matrix and factor is another trade off problem to consider, which is a highly subjective matter and has no general methods to follow. Another serious problem is that the TMD passive parameters such as stiffness and damping can not be generally optimized according to this method. These passive parameters play a very important role to economize the required control force and power. This problem was recently pointed out by several papers [15], [16], [17]. However, the optimization of these passive parameters have not yet achieved by the modern control method.

In this chapter, a unique control algorithm suitable for the active TMD is proposed and its physical meaning is explained to clarify the control strategy. The theoretically expected control performance and superiority of the proposed method are explained in comparison with both the passive and active TMDs. This algorithm, which uses the acceleration of the primal structure as the main feedback quantity, explicitly treats the disturbance effect to improve its control performance. Therefore, it is necessary to consider the influence of disturbance excitations on the control performance. As the first step, a set of optimum parameters of the active TMD are obtained under a harmonic wind turbulence, which is then replaced by a white noise disturbance. After the optimum parameters are selected, it is pointed out that there is a way to reduce

the control force without degrading the control effect, which is obtained under a white noise excitation as well as a harmonic excitation. As the final step, what is predicted in a stochastic sense is numerically evaluated under several earthquake disturbances.

2.1 The Principle of the Absolute Acceleration Feedback Method

The motion of the passive TMD auxiliary mass has an approximately 90° phase lag behind the vibration of the primal system. Therefore, the inertia force created by the passive TMD works as a damping effect on the primal system. If the motion of the TMD is enhanced by an active device, the control performance of the TMD is expected to increase. This is the basic idea of the active TMD control strategy. The equations of motion of the active TMD shown in Figure 2.1 are given by (2.1) and (2.2). Substitution of (2.1) into (2.2) yields (2.3). When (2.1) and (2.3) are carefully observed, it is understood that the term $-m_d \ddot{x}$ is an *input force* to the auxiliary system and $-m_d \ddot{y}$ is an *output force* to the primal system. If the auxiliary system parameters are optimized in the sense of passive TMD and the *input force* is increased by means of an active controller, the efficiency of the TMD is expected to increase. Because the *output force*, which actually is the damping effect on the primal system, will be increased in proportion to the *input force*. The block diagrams of the passive TMD and the acceleration feedback method are shown in Figure 2.2, where the relation between the two is made clear and the control strategy is illustrated. Hence the problem to be considered for this algorithm is how to optimize the active TMD in the sense of passive TMD. Based on the above discussion, a new algorithm given by (2.4) is proposed.

$$\begin{cases} m_d \ddot{y} + c_d \dot{y} + k_d y = -m_d \ddot{x} + u(t) & (2.1) \\ m \ddot{x} + k x - c_d \dot{y} - k_d y = f_w(t) - u(t) & (2.2) \end{cases}$$

$$(m + m_d)\ddot{x} + k x = f_w(t) - m_d \ddot{y} \qquad (2.3)$$

$$u(t) = -G\ddot{x} = -mg\ddot{x} \qquad (2.4)$$

where G : Feed back gain g : Normalized feed back gain

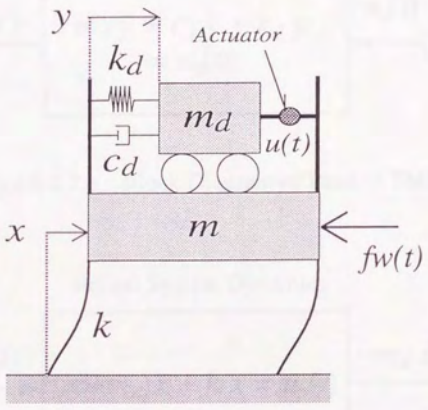

Figure 2.1 Active TMD under Wind Disturbance

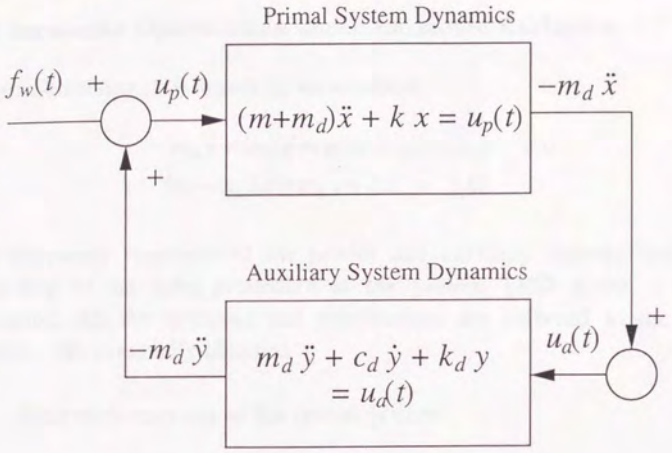

Figure 2.2.a Block Diagram of Passive TMD

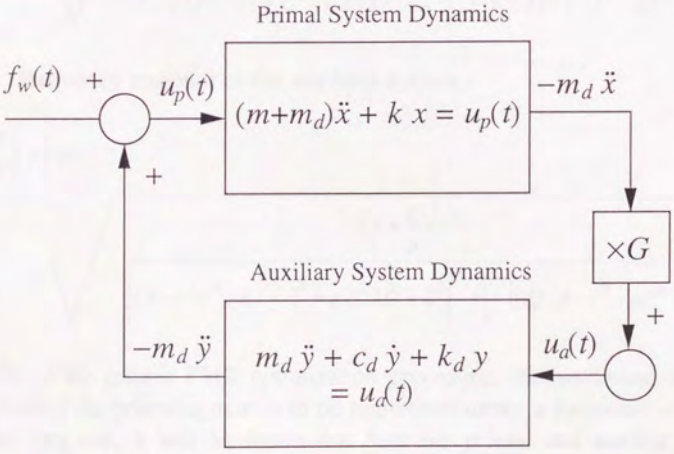

Figure 2.2.b Block Diagram of Active TMD

2.2 Parameter Optimization under Harmonic Excitation

After substituting (2.4) into (2.1), we obtained

$$\begin{cases} m_d \ddot{y} + (m_d + m\,g)\ddot{x} + c_d \dot{y} + k_d y = 0 & (2.5) \\ (m + m_d)\ddot{x} + m_d \ddot{y} + k x = f_w(t) & (2.6) \end{cases}$$

The frequency responses of the primal and auxiliary systems are obtained according to the same procedure as the passive TMD under a harmonic excitation. All the notations and substitutions are referred to the previous chapter. We eventually obtained

Frequency response of the primal system :

$$\left|\frac{X}{F}\right|(f) = \sqrt{\frac{(\xi^2 - f^2)^2 + (2\eta\xi f)^2}{\left[(1-g)f^4 - (1+\xi^2+\mu\xi^2)f^2 + \xi^2\right]^2 + \left[2\eta\xi f(1-f^2-\mu f^2)\right]^2}} \quad (2.7)$$

Frequency response of the auxiliary system :

$$\left|\frac{Y}{F}\right|(f) = \sqrt{\frac{(1+\frac{g}{\mu})^2 f^4}{\left[(1-g)f^4 - (1+\xi^2+\mu\xi^2)f^2 + \xi^2\right]^2 + \left[2\eta\xi f(1-f^2-\mu f^2)\right]^2}} \quad (2.8)$$

Similar to the passive TMD optimization procedure, the maximum frequency response of the primal system is to be minimized under a harmonic excitation. In the long run, it will be shown that both the primal and auxiliary system responses are optimized simultaneously.

It is well known that the response function of the primal system with the passive TMD has two locked frequencies, where the corresponding responses

are not influenced by the damping factor. Similarly, the response function of the primal system with the active TMD has two locked points $(f_1,\alpha),(f_2,\alpha)$,which should satisfy (2.9).

$$\lim_{\eta\to 0}\left|\frac{X}{F}\right|^2 = \lim_{\eta\to\infty}\left|\frac{X}{F}\right|^2 = \alpha^2 \tag{2.9}$$

Equation (2.9) is identical to (2.10) which yields (2.11). Hence, the two locked frequencies f_1, f_2 should satisfy (2.12) and (2.13) at the same time.

$$\left[\frac{1}{1-(1+\mu)f^2}\right]^2 = \left[\frac{(\xi^2-f^2)}{(1-g)f^4-(1+\xi^2+\mu\xi^2)f^2+\xi^2}\right]^2 = \alpha^2 \tag{2.10}$$

$$f^4-\frac{2(1+\xi^2+\mu\xi^2)}{2+\mu-g}f^2+\frac{2\xi^2}{2+\mu-g} = 0 \tag{2.11}$$

$$\begin{cases} (f_1)^2+(f_2)^2=\dfrac{2(1+\xi^2+\mu\xi^2)}{2+\mu-g} & (2.12) \\ (f_1)^2(f_2)^2=\dfrac{2\xi^2}{2+\mu-g} & (2.13) \end{cases}$$

In addition to this, the two locked points should have the same response peak α, which means (2.14) or (2.15).

$$\frac{-1}{1-(1+\mu)(f_1)^2} = \frac{1}{1-(1+\mu)(f_2)^2} = \alpha \tag{2.14}$$

$$(f_1)^2+(f_2)^2=\frac{2}{\mu+1} \tag{2.15}$$

Substitution of (2.15) into (2.12) yields

$$\xi^2=\frac{1-g}{(\mu+1)^2} \tag{2.16}$$

Equations (2.17) and (2.18) are the solutions of (2.11) under the condition of (2.16).

$$(f_1)^2 = \frac{1}{1+\mu}\left[1+\sqrt{\frac{\mu+g}{2+\mu-g}}\right] \tag{2.17}$$

$$(f_2)^2 = \frac{1}{1+\mu}\left[1-\sqrt{\frac{\mu+g}{2+\mu-g}}\right] \tag{2.18}$$

Finally, the locked response value α, which is optimized, is obtained and given by

$$\alpha_{max} = \frac{-1}{1-(1+\mu)(f_1)^2} = \sqrt{\frac{2+\mu-g}{\mu+g}} \tag{2.19}$$

Thus, the feed back gain is expressed in terms of α_{max}

$$\text{Feedback gain :} \qquad g = \frac{2+\mu-\mu\,\alpha_{max}^{\,2}}{\alpha_{max}^{\,2}+1} \tag{2.20}$$

Substitution of (2.20) into (2.16) yields

$$\text{Optimum Frequency Ratio :} \quad \xi_{opt} = \sqrt{\frac{\alpha_{max}^{\,2}-1}{(\mu+1)(\alpha_{max}^{\,2}+1)}} = \frac{\sqrt{1-g}}{1+\mu} \tag{2.21}$$

The optimum damping factor is to be determined in such a manner that the peak of the response function should coincide with the two locked points under the same damping factor. However, the one which gives the peak at f_1 is different from the other one that gives the maximum at f_2. So, we must be content with an approximated value given by (2.22), which has the consistency with (1.15) of the passive TMD formula. The author numerically checked the validity of (2.22) under various combinations of the parameters and found it gives a plausible approximation.

$$\text{Optimum Damping factor :} \quad \eta_{opt} = \sqrt{\frac{3}{4(\alpha_{max}^{\,2}+1)}} = \sqrt{\frac{3(\mu+g)}{8(1+\mu)}} \tag{2.22}$$

2.3 Numerical Analysis under Harmonic Excitation

In this section, an example numerical calculation is conducted to exhibit the performance of the proposed methodology, which reveals the hidden relationship between the active and passive TMDs that have been regarded as independent subjects until recently. According to the given formulae by (2.20)~(2.22), an example calculation is demonstrated for quantitative evaluation of the proposed algorithm. Suppose that we want α_{max} to be 3.0 (e.g., the peak of the primal system frequency response is 3.0), we get the corresponding feed back gain and the optimum TMD parameters which are given in Table 2.1 where the mass ratio is fixed to 0.01. The passive TMD with the same mass ratio is also calculated and given in Table 2.1 for comparison. The optimum damping factor for the active TMD is about 4.5 times as large as that of the passive TMD, which means that the free vibration of the active TMD is heavily reduced. And the tuning adjustment of the device is significantly facilitated, because the phase response curve of the auxiliary system does not sharply change around the tuning frequency on account of the increased damping factor. The optimum tuning frequency of the active TMD is slightly lower than that of the passive TMD, which looks similar to the situation under a passive TMD with a large mass ratio. Hence all of the weak points of the passive TMD are removed by the acceleration feedback algorithm.

Equations (2.7) and (2.8) give us the frequency responses of the primal and auxiliary systems, which are shown in Figure 2.3.a and 2.3.b where the passive TMD is also indicated for comparison. It is understood from Figure 2.3.b that the peak of the active auxiliary system response is almost equal to that of the passive TMD. On the other hand, the peak response of the primal system with the active TMD is around 3.0, as is expected from the formula, while the passive TMD is about 14. This result indicates that not only the primal system response is optimized but also the auxiliary system response is optimized as well. Because the peak of the active TMD is not higher than that of the passive TMD. The reason for this incidental optimization is that the feedback force basically accelerates the auxiliary mass while the increased damping force restricts the mass motion so that they are canceling each other at the tuning frequency. Apart from the discussion above, there is another important feature with respect to the auxiliary system response. It is understood from (2.8) that there is a locked point (f_3, β_{max}), which is not

influenced by the damping factor, in the response curve of the auxiliary system. In fact, no matter what the damping factor may be, (2.8) is satisfied at the point (f_3, β_{max}) specified by (2.23) and (2.24) .

$$\beta_{max} = \frac{\mu + 1}{\mu} \tag{2.23}$$

$$f_3 = \sqrt{\frac{1}{\mu + 1}} \tag{2.24}$$

$$\eta_{opt} = \sqrt{\frac{1}{(\alpha_{max}{}^2 + 1)}} = \sqrt{\frac{(\mu + g)}{2(1 + \mu)}} \tag{2.25}$$

where β_{max} : Maximum Response (Auxiliary System)
f_3 : Locked Frequency (Auxiliary System)
η_{opt} : Optimum damping factor

This result is important, because the peak response β_{max} does not contain any parameters but mass ratio μ . Hence this equation is not only valid for an active TMD but also for a passive TMD. It should be also noted that the peak response is not less than β_{max} that is given by (2.23). Hence there is the minimum damping factor that makes the peak response equal to β_{max} , which is exactly the same as the passive TMD response peak. (See section 1.2.) After a long and careful manipulation of (2.8), we obtained the optimum damping η_{opt} given by (2.25), which is incidentally consistent with (1.19). Equation (2.25) slightly differs from (2.22), however both of them make no significant difference as far as the final frequency responses are concerned, which is similar to the passive TMD optimum damping modification. (See Figure 1.3 and Figure 1.4.)

In the first place, it was thought to be indispensable to increase the amplitude of the auxiliary system to attenuate the primal system response, but it turned out to be also important to restrict the auxiliary system response by increasing the damping factor. At the first glance this result seems inconsistent, but the cause and effect relation of this phenomenon can reasonably explain this intriguing result as follows.

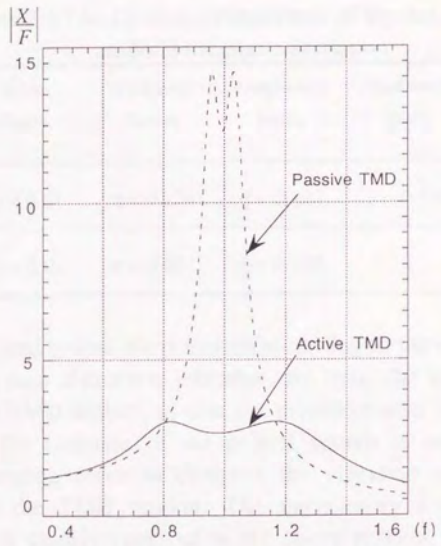

Figure 2.3.a Primal System Frequency Response

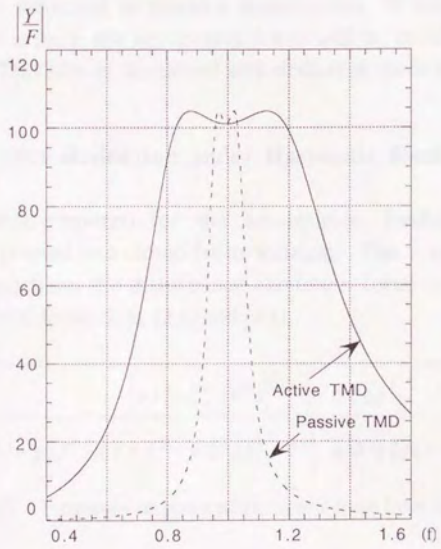

Figure 2.3.b Auxiliary System Frequency Response

Table 2.1 The Optimum Parameters of the Active TMD under a harmonic excitation

	Mass Ratio	Damping Factor	Frequency Ratio	Feed Back Gain	Maximum Response
Active TMD	$\mu = 0.01$	$\eta = 0.274$	$\xi = 0.890$	$g = 0.192$	$\alpha = 3.00$
Passive TMD	$\mu = 0.01$	$\eta = 0.061$	$\xi = 0.990$	*	$\alpha = 14.18$

As the primal system starts motion according to the external disturbance, the auxiliary system also starts vibration. At first, the acceleration feedback gain drives the TMD motion so that the primal system vibration is reduced swiftly. After the response of the primal system is subdued, the actuator generates a damping force to dissipate the vibration energy that is once accumulated in the TMD motion. The unnecessary free vibration of the auxiliary mass is quickly removed in the above process so that the efficient control performance is achieved as a result. These two control operations, the driving and damping forces, are acting on the TMD simultaneously, when the whole system is subjected to random disturbances. If one actuator generates these two forces at once, the net control force will be smaller than the original driving force. This idea is developed and studied in the following sections.

2.4 Control Force Reduction under Harmonic Excitation

The control force required for the acceleration feedback method can be obtained and expressed in a closed form solution. The transfer function of the control force $u(t)$ from the disturbance excitation force is given below, which is directly obtained from (2.5), (2.6) and (2.8).

$$U(f) = \sqrt{\frac{\left[gf^2(\xi^2 - f^2)\right]^2 + \left[2\eta\xi gf^3\right]^2}{\left[(1-g)f^4 - (1+\xi^2+\mu\xi^2)f^2 + \xi^2\right]^2 + \left[2\eta\xi f(1-f^2-\mu f^2)\right]^2}} \qquad (2.26)$$

where $U(f)$: Frequency response of the control force from disturbance force

Considering the physical principle of the control algorithm, we can naturally expect that the combination of the damping force $c_d \dot{y}$ and the driving force $g \ddot{x}$ will be smaller than the original feedback control force by (2.26). The simple explanation for this reasoning is that the driving force is supposed to accelerate the TMD mass while the damping force subdues its motion, which means that they are canceling each other in a rough sketch. Hence the control algorithm is slightly modified and given by (2.27) instead of (2.4).

$$u(t) = -m g \ddot{x} - g_v \dot{y} \tag{2.27}$$

where $$c_d + g_v = c_{opt} = 2 m_d \omega_o \xi_{opt} \eta_{opt} \tag{2.28}$$

Driving control force : $-m g \ddot{x}$

Damping control force : $-g_v \dot{y}$

It is noted that even though the algorithm is modified from (2.4) to (2.27), the optimization procedure and its results are not influenced at all by this alteration. Because the total damping factor, which is already optimized, is not changed, but is partly contributed by the active damping force and partly by the passive damper. In fact, there is an optimum combination of the passive and active damping factors so that the total control force generated by the actuator is minimized. The minimum control force transfer function from the external force is given by (2.29). And the optimum selection of the passive damping factor and the active damping force are given by (2.30).

$$U(f) = \sqrt{\frac{\left[g f^2 (\xi^2 - f^2)\right]^2}{\left[(1-g) f^4 - (1 + \xi^2 + \mu \xi^2) f^2 + \xi^2\right]^2 + \left[2 \eta \xi f (1 - f^2 - \mu f^2)\right]^2}} \tag{2.29}$$

$$\begin{cases} g_v = \dfrac{g}{\mu + g} c_{opt} \\ c_d = \dfrac{\mu}{\mu + g} c_{opt} \end{cases} \tag{2.30}$$

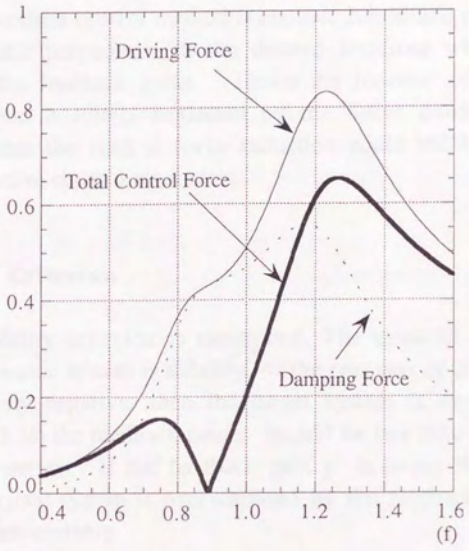

Figure 2.4 Control Force Frequency Response

For example, the parameters given in Table 2.1 are substituted into (2.26) and (2.29), then they are compared and shown in Figure 2.4 where a noticeable reduction of the control force is seen to be achieved.

What makes difference between (2.26) and (2.29) is the elimination of the second term of the numerator, which means that the zeros of the transfer function are shifted to the desired locations. As is reviewed in chapter 1, when the orthodox modern control method is applied, it is aimed to place the poles of the characteristic polynomial to the desired locations which are implicitly connected to the feedback gains. Hence the location of the zeros of the transfer function is totally neglected by the linear quadratic optimization, which means that the control force reduction could not be obtained by the conventional active control algorithm.

2.5 Stability Criterion

Finally the stability criterion is mentioned. The essential requirement for a closed-loop dynamic system is stability. If the real part of all the characteristic roots are strictly negative, then the target system is asymptotically stable. According to (2.16) the feedback gain g should be less than 1.0, which is (2.31) for stability criterion. If the feedback gain g is larger than 1.0, the inertia force of the primal system is overwhelmed by the feedback force that makes the whole system unstable.

$$g < 1.0 \tag{2.31}$$

It is to be noted that (2.31) does not contain any parameters, which simplifies the stability inspection significantly. It is also noted that the stability is not influenced by the parameter optimization at all. Even if the tuning adjustment is not precisely conducted, the stability is not at all affected by the possible miss-tuning.

2.6 Parameter Optimization under White Noise Excitation

The optimum parameters of the passive TMD under stationary random excitations were discussed in a stochastic sense by several people [28], [29],[30], who studied the effect of disturbances on the optimum damping factor and tuning frequency. In the previous sections, we treated the active TMD as an extension of the passive TMD. It is naturally expected that what can be applied to the passive TMD is also applicable to the active TMD. It is noted that the actual disturbance acting on the primal system looks more like a random process than a harmonic or sinusoidal excitation. Hence the expected optimum parameters under a stationary random process should be examined in comparison with the optimum formulae under a harmonic excitation.

First, the equations of motion of the active TMD with the acceleration feedback term, which have been obtained and expressed in (2.5) and (2.6), are converted into a transfer function expressed in Laplace transform.

$$\begin{bmatrix} m_d s^2 + c_d s + k_d & (m_d + mg)s^2 \\ m_d s^2 & (m_d + m)s^2 + k \end{bmatrix} \begin{bmatrix} Y(s) \\ X(s) \end{bmatrix} = \begin{bmatrix} 0 \\ m \end{bmatrix} F(s) \tag{2.32}$$

Hence the transfer functions of $X(s)$ and $Y(s)$ from $F(s)$ are

$$H_X(s) = \frac{s^2 + 2\omega_d \eta s + \omega_d^2}{(1-g)s^4 + 2(1+\mu)\omega_d \eta s^3 + (\omega_o^2 + (1+\mu)\omega_d^2)s^2 + 2\omega_d \omega_o^2 \eta s + \omega_d^2 \omega_o^2} \tag{2.33}$$

$$H_Y(s) = \frac{-(1+\frac{g}{\mu})s^2}{(1-g)s^4 + 2(1+\mu)\omega_d \eta s^3 + (\omega_o^2 + (1+\mu)\omega_d^2)s^2 + 2\omega_d \omega_o^2 \eta s + \omega_d^2 \omega_o^2} \tag{2.34}$$

where $X(s) = H_X(s) F(s)$, $Y(s) = H_Y(s) F(s)$

The excitation is supposed to be a stationary random process. Then the mean square response of x under a stationary random excitation is

$$E[X^2] = \int_{-\infty}^{\infty} S_X(\omega)\, d\omega = \int_{-\infty}^{\infty} H_X(i\omega)\, H_X(-i\omega)\, S_F(\omega)\, d\omega \qquad (2.35)$$

where $E[*]$ is the operator which takes the expected value of a random function. If the excitation is a stationary white noise whose power spectral density is S_o, then (2.35) is

$$E[X^2] = S_o \int_{-\infty}^{\infty} H_X(i\omega)\, H_X(-i\omega) d\omega \qquad (2.36)$$

The evaluation of this integral can be carried out in the complex s plane by means of residue theorem [37]. The closed form solutions of typical polynomial functions are referred to the Appendix [33]. As a result, we obtain

$$E[X^2] = \frac{\pi S_o}{2\,(g+\mu)\,\omega_o^3 \eta}\left[4\xi(1+\mu)\eta^2 + (1+\mu)^2\xi^3 - (2+\mu-g)\xi + \frac{1}{\xi}\right] \qquad (2.37)$$

The optimum tuning frequency ratio ξ and damping factor η are the solutions of the next condition.

$$\frac{\partial E[X^2]}{\partial \xi} = 0 \qquad (2.38)$$

$$\frac{\partial E[X^2]}{\partial \eta} = 0 \qquad (2.39)$$

They yield the following relations, respectively.

$$4\eta^2 = -3(1+\mu)\xi^2 + \frac{1}{(1+\mu)\xi^2} + \frac{2+\mu-g}{1+\mu} \qquad (2.40)$$

$$4\eta^2 = (1+\mu)\xi^2 + \frac{1}{(1+\mu)\xi^2} - \frac{2+\mu-g}{1+\mu} \qquad (2.41)$$

Hence we obtain the optimum tuning ratio and damping factor as

$$\xi_{opt} = \frac{1}{1+\mu}\sqrt{\frac{2+\mu-g}{2}} \tag{2.42}$$

$$\eta_{opt} = \sqrt{\frac{(4+3\mu-g)(\mu+g)}{8(1+\mu)(2+\mu-g)}} \tag{2.43}$$

It is noted that the optimization has been carried out with respect to the displacement response x. If the optimization is conducted to reduce the velocity response $\dot{x}$ instead of x, the solutions will be different from (2.42) and (2.43). In fact, Warburton showed the optimum parameters of the passive TMD with respect to $\dot{x}$ as well as x under white noise disturbance [28].

The index which should be reduced is given by

$$E\left[\dot{X}^2\right] = \frac{\pi S_o}{2(g+\mu)\omega_o\eta}\left[(1+\mu)\xi^3 + 2(2\eta^2 - 1)\xi + \frac{1}{\xi(1-g)}\right] \tag{2.44}$$

The derivatives of (2.44) with respect to ξ and η should be zero, which are given by (2.45) and (2.46), respectively.

$$4\eta^2 = -3(1+\mu)\xi^2 + \frac{1}{(1-g)\xi^2} + 2 \tag{2.45}$$

$$4\eta^2 = (1+\mu)\xi^2 + \frac{1}{(1-g)\xi^2} - 2 \tag{2.46}$$

Hence the optimum parameters are obtained as

$$\xi_{opt} = \sqrt{\frac{1}{1+\mu}} \tag{2.47}$$

$$\eta_{opt} = \frac{1}{2}\sqrt{\frac{\mu+g}{1-g}} \tag{2.48}$$

Interestingly, the optimum tuning frequency is not influenced by the feedback gain g so that the discrepancy between (2.47) and (2.42) becomes larger as the feedback gain increases. And this trend becomes more conspicuous when the disturbance is a harmonic excitation (See equations (2.21), (2.22).) .

2.7 Control Power Reduction under White Noise Excitation

In section 2.4, we studied the optimum passive damping factor that minimizes the required active control force under a harmonic excitation. In this section, the optimum passive damping factor under a white noise excitation is obtained. Suppose that we have one disturbance excitation acting on the primal structure, then it starts motion accordingly. But in the very beginning, the auxiliary mass does not move enough to produce control effect, because it takes time until the mass reaches the desired level of motion. When the TMD does not move enough to attenuate the primal system vibration, the actuator generates a driving force to increase the mass motion to improve control effect. After the structure motion is subdued, it is no longer necessary to sustain TMD vibration. Hence the actuator generates a damping force on the TMD so that it comes to halt as soon as possible. Depending on the command signal, the actuator switches its function from an accelerator to a brake. In other words, if the system is excited by a harmonic disturbance, these two forces cancel each other and completely vanish at the tuning frequency ξ, which is the physical meaning of Figure 2.4. This reasoning is not, however, proved to be valid when the system is under a random type of excitation. But the physical function of the actuator should be the same as in the case of a harmonic excitation. Therefore it is naturally expected that the optimum active and passive damping factors or (2.30) will be also the appropriate values under random disturbances.

In this section, the average rate of energy dissipation due to the actuator under a white noise excitation is discussed to prove the above hypothesis. In the end of this section, the optimum passive damping factor is obtained from the probabilistic point of view and it is seen to be identical to (2.30). First, let us reconsider the equation of motion of the active TMD shown in Figure 2.1.

$$\begin{bmatrix} m_d & m_d \\ m_d & m_d + m \end{bmatrix} \begin{bmatrix} \ddot{y} \\ \ddot{x} \end{bmatrix} + \begin{bmatrix} c_d & 0 \\ 0 & 0 \end{bmatrix} \begin{bmatrix} \dot{y} \\ \dot{x} \end{bmatrix} + \begin{bmatrix} k_d & 0 \\ 0 & k \end{bmatrix} \begin{bmatrix} y \\ x \end{bmatrix} + \begin{bmatrix} -1 \\ 0 \end{bmatrix} u(t) = \begin{bmatrix} 0 \\ m \end{bmatrix} f_w(t) \tag{2.49}$$

Then this equation is interpreted into

$$M\{\ddot{v}\} + C\{\dot{v}\} + K\{v\} + \{b\}u(t) = \{d\}f_w(t) \tag{2.50}$$

We multiply $\{\dot{v}\}^t$ from the left hand side of the equation, and we obtain

$$\{\dot{v}\}^t M\{\ddot{v}\} + \{\dot{v}\}^t C\{\dot{v}\} + \{\dot{v}\}^t K\{v\} + \{\dot{v}\}^t \{b\}u(t) = \{\dot{v}\}^t \{d\}f_w(t) \quad (2.51)$$

which yields

$$m\dot{x}\ddot{x} + k\dot{x}x + m_d(\dot{x}+\dot{y})(\ddot{x}+\ddot{y}) + k_d\dot{y}y + c_d(\dot{y})^2 - \dot{y}\,u(t) = \dot{x}\,m\,f_w(t) \quad (2.52)$$

Taking the integral of both sides of (2.52), we obtain

$$\frac{1}{2}m(\dot{x})^2 + \frac{1}{2}kx^2 + \frac{1}{2}m_d(\dot{x}+\dot{y})^2 + \frac{1}{2}k_d y^2 + \int_0^T c_d(\dot{y})^2 dt - \int_0^T \dot{y}\,u(t)\,dt = m\int_0^T \dot{x}\,f_w(t)\,dt \quad (2.53)$$

All the responses are converging to zero as T comes to infinity, provided that the disturbance $f_w(t)$ is zero before $t = 0$ and the system dynamics is asymptotically stable. Hence the energy equilibrium is obtained as

$$\int_0^\infty c_d(\dot{y})^2 dt - \int_0^\infty \dot{y}\,u(t)\,dt = m\int_0^\infty \dot{x}\,f_w(t)\,dt \quad (2.54)$$

or

$$E_p - E_c = E_d \quad (2.55)$$

where

E_p : Passive energy dissipation
E_c : Control energy supplied
E_d : Disturbance input energy

Let us think about the next question. Is it possible to select c_d to balance the control energy E_c equal to zero without influencing the control performance of the active TMD ? The answer to this question is positive, because the damping could be partly contributed by the actuator and partly by the passive damping device. If the total damping factor is kept at η_{opt} specified by (2.22), (2.25), or (2.43), then the responses are still optimized. Hence it is possible to select the passive c_d to balance the disturbance input energy with the passively dissipated energy so that the control energy integral over the entire excitation

period could be diminished completely. Such a condition can be realized if the passive damping coefficient c_d satisfies the following condition.

$$c_d = \frac{m\int_0^\infty \dot{x} f_w(t)\,dt}{\int_0^\infty (\dot{y})^2 dt} \tag{2.56}$$

This is a remarkable result, because the control energy does not exist in an average sense over a long period of time. There, however, arises a problem: this method is a deterministic approach which means that the most appropriate damping coefficient c_d can only be determined, if and only if we know the whole disturbance excitation $f_w(t)$ in advance. This is a rather discouraging fact, because it is impossible to predict a wind gust before it happens. However, if the input disturbance can be dealt as a stochastic process, there is a way to predict the optimum damping coefficient before the event of a random excitation, which is the topic for the rest of this section.

If the disturbance excitation is supposed to be a stochastic process, then we could take the expectation of both hand sides of (2.52) and we obtain

$$\begin{aligned} &E\left[m_d(\dot{X}+\dot{Y})(\ddot{X}+\ddot{Y})\right] + E\left[m\dot{X}\ddot{X}\right] + E\left[c_d(\dot{Y})^2\right] + E\left[k_d\dot{Y}Y\right] + E\left[k\dot{X}X\right] \\ &= E\left[\dot{Y}\,U\right] + E\left[m\dot{X}\,F\right] \end{aligned} \tag{2.57}$$

where X, Y, U and F are random variables of x, y, $u(t)$ and $f_w(t)$, respectively. From (2.57), we obtain

$$c_d E\left[(\dot{Y})^2\right] = E\left[\dot{Y}\,U\right] + m\,E\left[\dot{X}\,F\right] \tag{2.58}$$

because $E\left[X\dot{X}\right] = 0$ for any random variable X. Hence the damping coefficient can be selected to diminish the control power in the ensemble sense and it is given by

$$c_d = \frac{m\,E\left[\dot{X}\,F\right]}{E\left[(\dot{Y})^2\right]} \tag{2.59}$$

From here on, we are dealing with (2.59) to evaluate it in terms of the passive parameters under a stationary white noise excitation. First, the control algorithm is modified and given by

$$u(t) = -m\,g\,\ddot{x} - g_v\dot{y} \tag{2.60}$$

which is the same control law as (2.27). After substituting (2.60) into (2.49), we obtain

$$\begin{bmatrix} m_d s^2 + (c_d + g_v)s + k_d & (m_d + mg)s^2 \\ m_d s^2 & (m_d + m)s^2 + k \end{bmatrix} \begin{bmatrix} Y(s) \\ X(s) \end{bmatrix} = \begin{bmatrix} 0 \\ m \end{bmatrix} F(s) \tag{2.61}$$

where $c_d + g_v = c_{opt} = 2m_d\omega_d\eta_{opt}$

The transfer function of $\dot{Y}(s)$ from $F(s)$ is obtained from (2.61) and given by

$$H_{\dot{Y}}(s) = \frac{-(1+\frac{g}{\mu})s^3}{(1-g)s^4 + 2(1+\mu)\omega_d\eta_{opt}s^3 + (\omega_o^2 + (1+\mu)\omega_d^2)s^2 + 2\omega_d\omega_o^2\eta_{opt}s + \omega_d^2\omega_o^2} \tag{2.62}$$

where $\dot{Y}(s) = H_{\dot{Y}}(s)\,F(s)$

Therefore, the mean square of the random variable $\dot{Y}$ is

$$\begin{aligned} E\left[(\dot{Y})^2\right] &= \int_{-\infty}^{+\infty} S_{\dot{Y}}(\omega)\,d\omega \\ &= \int_{-\infty}^{+\infty} H_{\dot{Y}}(iw)\,H_{\dot{Y}}(-iw)\,S_F(\omega)\,d\omega = S_o\int_{-\infty}^{+\infty} \left|H_{\dot{Y}}(i\omega)\right|^2 d\omega \end{aligned} \tag{2.63}$$

where the input disturbance is supposed to be a white noise whose power spectral density is S_o, and the system function $H_{\dot{Y}}(i\omega)$ is specified by (2.62). During the calculation, the power spectral density of the white noise

disturbance is supposed to be S_o, which is related to the auto correlation function defined by

$$S_F(\omega) = \frac{1}{2\pi}\int_{-\infty}^{+\infty} R_F(\tau)\, e^{-i\omega\tau} d\tau = S_o \tag{5.64}$$

$$R_F(\tau) = \int_{-\infty}^{+\infty} S_F(\omega)\, e^{i\omega\tau} d\omega = 2\pi S_o \delta(\tau) \tag{5.65}$$

$$R_F(\tau) = E\left[f_w(t-\tau) f_w(t)\right] \tag{5.66}$$

Evaluation of the integration of (2.63) is carried out in the complex plane using the residue theorem. The general form of this type of integration is to be referred to the Appendix. Eventually the result is obtained and given by

$$E\left[(\dot{Y})^2\right] = \frac{1}{1-g}\left(\frac{\mu+g}{\mu}\right)\left(\frac{\pi}{2\,\mu\,\omega_d\,\eta_{opt}}\right) S_o \tag{2.67}$$

The rest of the task to be done is to evaluate the numerator of (2.59), which is

$$E\left[\dot{X}F\right] = E\left[\int_{-\infty}^{+\infty} \dot{h}_x(\tau) f_w(t-\tau)\, d\tau\, f_w(t)\right] \tag{2.68}$$

$$= \int_{-\infty}^{+\infty} \dot{h}_x(\tau)\, E\left[f_w(t-\tau) f_w(t)\right] d\tau \tag{2.69}$$

Substitution of (2.66) into (2.69) yields

$$E\left[\dot{X}F\right] = \int_{-\infty}^{+\infty} \dot{h}_x(\tau)\, R_F(\tau)\, d\tau \tag{2.70}$$

Incorporated with (2.65), (2.70) is converted into

$$E\left[\dot{X}F\right] = 2\pi S_o \int_{-\infty}^{+\infty} \dot{h}_x(\tau)\, \delta(\tau)\, d\tau \tag{2.71}$$

Dirac delta function is used to excite the system to evaluate the impulse response function. From (2.50) we obtain

$$M\begin{bmatrix}\ddot{h}_y(t)\\ \ddot{h}_x(t)\end{bmatrix} + C\begin{bmatrix}\dot{h}_y(t)\\ \dot{h}_x(t)\end{bmatrix} + K\begin{bmatrix}h_y(t)\\ h_x(t)\end{bmatrix} = \{d\}\ \delta(t) \tag{2.72}$$

where $h_x(t)$, $h_y(t)$ are the impulse response functions of x and y, respectively. Taking the integrals of both sides of (2.72), we obtain

$$\int_{-\varepsilon}^{+\varepsilon} M\ \{\ddot{\boldsymbol{h}}\}dt + \int_{-\varepsilon}^{+\varepsilon} C\ \{\dot{\boldsymbol{h}}\}dt + \int_{-\varepsilon}^{+\varepsilon} K\ \{\boldsymbol{h}\}dt = \int_{-\varepsilon}^{+\varepsilon} \{d\}\ \delta(t)dt \tag{2.73}$$

then

$$M\ \{\dot{\boldsymbol{h}}\}\Big|_{-\varepsilon}^{+\varepsilon} + C\ \{\boldsymbol{h}\}\Big|_{-\varepsilon}^{+\varepsilon} = \{d\} \tag{2.74}$$

or

$$M\begin{bmatrix}\dot{h}_y(+\varepsilon)\\ \dot{h}_x(+\varepsilon)\end{bmatrix} + C\begin{bmatrix}h_y(+\varepsilon)\\ h_x(+\varepsilon)\end{bmatrix} = \begin{bmatrix}0\\ m\end{bmatrix} \tag{2.75}$$

The impulse response before applying the Dirac delta function is obviously zero, so $h_x(+\varepsilon)$ and $h_y(+\varepsilon)$ come to zero as ε comes to zero. Hence we obtain

$$\begin{bmatrix}\dot{h}_y(+\varepsilon)\\ \dot{h}_x(+\varepsilon)\end{bmatrix} = M^{-1}\begin{bmatrix}0\\ m\end{bmatrix} = \frac{1}{m\,m_d(1-g)}\begin{bmatrix}m+m_d & -m_d-mg\\ -m_d & m_d\end{bmatrix}\begin{bmatrix}0\\ m\end{bmatrix} \tag{2.76}$$

which becomes

$$\begin{bmatrix}\dot{h}_y(+\varepsilon)\\ \dot{h}_x(+\varepsilon)\end{bmatrix} = \frac{1}{(1-g)}\begin{bmatrix}-1-\dfrac{g}{\mu}\\ 1\end{bmatrix} \tag{2.77}$$

Substitution of (2.77) into (2.71) yields

$$E\left[\dot{X}F\right] = 2\,\pi\,S_o\int_{-\varepsilon}^{+\varepsilon} \dot{h}_x(\tau)\,\delta(\tau)\,d\,\tau = 2\pi S_o\left[\frac{1}{2}\dot{h}_x(+\varepsilon) + \frac{1}{2}\dot{h}_x(-\varepsilon)\right] \tag{2.78}$$

which means

$$E\left[\dot{X}F\right] = \frac{1}{2} 2\pi S_o \dot{h}_x(+\varepsilon) = \frac{1}{1-g}\pi S_o \tag{2.79}$$

Finally (2.59) can be evaluated and given as

$$c_d = \frac{m E\left[\dot{X} F\right]}{E\left[(\dot{Y})^2\right]} = \frac{\mu}{\mu + g}(2m_d \omega_d \eta_{opt}) = \frac{\mu}{\mu + g} c_{opt} \tag{2.80}$$

and

$$g_d = \frac{g}{\mu + g} c_{opt} \tag{2.81}$$

This equation certifies that the passive damping optimum value under a harmonic excitation is identical to the optimum damping coefficient obtained under a white noise excitation. And also this result ascertains that the required control energy is expected to be zero at least in a stochastic sense under a random type of disturbance excitation. It is noted that the optimum damping c_{opt} does not come into the whole derivation process as a specified value. Hence (2.80) is satisfied for any optimum formula (2.22),(2.43), or (2.48). The average energy input into the system brought by the disturbance excitation is predicted by

$$E\left[\dot{X}F\right] = \frac{m}{1-g}\pi S_o \tag{2.82}$$

If the feedback gain is not so large, the total energy input into the system is not significantly influenced by the control performance.

2.8 Control Force Reduction under White Noise Disturbance

In the previous section, we obtained the optimum passive damping factor and the velocity feedback gain. There arises naturally a question: what is the optimum combination of the active and passive stiffness ? It is obviously

possible to adjust the TMD stiffness to the optimum tuning frequency either by selecting passive stiffness or by adding active restoring force. Hence, there should be a rational and meaningful method that specifies the optimum stiffness value. In this section, this problem is solved in a stochastic manner and the final solution is expressed in a closed form solution. First, the control algorithm is modified from (2.60) to (2.83), then the control force should satisfy (2.84) because of the equilibrium.

$$u(t) = -m\,g\,\ddot{x} - g_v\dot{y} - g_d y \tag{2.83}$$

$$u(t) = m_d(\ddot{y}+\ddot{x}) + c_d\dot{y} + k_d y \tag{2.84}$$

Instead of reducing the control power, it is aimed to minimize the control force by selecting an appropriate passive stiffness. Equation (2.84) is always satisfied regardless of control algorithm. So, the mean square of the control force is

$$\begin{aligned}(u(t))^2 &= m_d^2(\ddot{y}+\ddot{x})^2 + c_d^2(\dot{y})^2 + k_d^2(y)^2 \\ &+ 2m_d c_d\dot{y}(\ddot{y}+\ddot{x}) + 2m_d k_d y(\ddot{y}+\ddot{x}) + 2k_d c_d\dot{y}\,y\end{aligned} \tag{2.85}$$

The expected value of both hand sides of the above equation under a stationary random excitation is

$$\begin{aligned}E\left[U^2\right] &= m_d^2\,E\left[(\ddot{Y}+\ddot{X})^2\right] + c_d^2E\left[(\dot{Y})^2\right] + k_d^2E\left[(Y)^2\right] \\ &+ 2m_d c_d E\left[\dot{Y}(\ddot{Y}+\ddot{X})\right] + 2m_d k_d E\left[Y(\ddot{Y}+\ddot{X})\right] + 2k_d c_d E\left[\dot{Y}\,Y\right]\end{aligned}$$

or

$$\begin{aligned}E\left[U^2\right] &= k_d^2E\left[(Y)^2\right] + 2k_d m_d E\left[Y(\ddot{Y}+\ddot{X})\right] \\ &+ c_d^2E\left[(\dot{Y})^2\right] + 2c_d m_d E\left[\dot{Y}\ddot{X}\right] + m_d^2\,E\left[(\ddot{Y}+\ddot{X})^2\right]\end{aligned} \tag{2.86}$$

The problem here is how to select k_d so as to minimize the mean square of the control force. Therefore, the stiffness k_d should be selected as to minimize the right hand side of (2.86). The above equation is just a basic quadratic function in terms of k_d so that the minimum value is obtained by adjusting k_d to

$$k_d = -\frac{m_d E\left[Y(\ddot{Y}+\ddot{X})\right]}{E\left[(Y)^2\right]} \tag{2.87}$$

or

$$k_d = \frac{m_d E\left[(\dot{Y})^2\right]}{E\left[(Y)^2\right]} - \frac{m_d E\left[Y\ddot{X}\right]}{E\left[(Y)^2\right]} \tag{2.88}$$

These integrals can be evaluated by the same procedure as before. The numerator of the second term of (2.88) contains the evaluation of cross power spectral density function over the entire frequency range but the integration procedure does not change. First, we substitute (2.84) into (2.49) to obtain the Laplace transform given by

$$\begin{bmatrix} m_d s^2 + c_{opt} s + (k_d + g_d) & (m_d + mg)s^2 \\ m_d s^2 & (m_d + m)s^2 + k \end{bmatrix} \begin{bmatrix} Y(s) \\ X(s) \end{bmatrix} = \begin{bmatrix} 0 \\ m \end{bmatrix} F(s) \tag{2.89}$$

where $k_d + g_d = k_{opt}$

which yield

$$H_X(s) = \frac{s^2 + 2\omega_{opt}\eta s + \omega_{opt}^2}{(1-g)s^4 + 2(1+\mu)\omega_{opt}\eta_{opt}s^3 + (\omega_o^2 + (1+\mu)\omega_{opt}^2)s^2 + 2\omega_{opt}\omega_o^2\eta_{opt}s + \omega_{opt}^2\omega_o^2} \tag{2.90}$$

$$H_Y(s) = \frac{-(1+\frac{g}{\mu})s^2}{(1-g)s^4 + 2(1+\mu)\omega_{opt}\eta_{opt}s^3 + (\omega_o^2 + (1+\mu)\omega_{opt}^2)s^2 + 2\omega_{opt}\omega_o^2\eta_{opt}s + \omega_{opt}^2\omega_o^2} \tag{2.91}$$

where $X(s) = H_X(s)F(s)$, $Y(s) = H_Y(s)F(s)$

The evaluation of these integrals are also referred to the table of the Appendix. The results are shown below.

$$E[Y^2] = \frac{\pi S_o}{\omega_o^2}\left(\frac{1}{2\mu\omega_{opt}\eta_{opt}}\right)\left(\frac{\mu+g}{\mu}\right) \tag{2.92}$$

$$E[Y\ddot{X}] = \pi S_o\left(\frac{1}{2\mu\omega_{opt}\eta_{opt}}\right)\left(\frac{1}{1-g} - \xi_{opt}^{\ 2}\right) \tag{2.93}$$

Substituting above equations into (2.88), we obtain

$$k_d = k_{opt}\left(\frac{1}{\mu+g}\right)\left(\mu + \frac{g}{(1-g)\xi_{opt}^{\ 2}}\right) \tag{2.94}$$

The main contribution is done by the first term of (2.88), while the second term is almost negligible. Because the responses of y and x have approximately 90° phase difference between the two, which causes the numerator of the second term almost zero. In addition to this, the magnitude of response x with respect to y is relatively small, depending on the mass ratio, so that the passive optimum stiffness specified by (2.88) is very close to the original passive TMD optimum stiffness. This is the physical explanation why the active control force is relatively smaller for a hybrid system than is required for a full active system, which was numerically predicted and reported by several papers [15],[16],[17]. We must be consistent with the type of disturbance, which is the white noise excitation, to obtain the optimum passive stiffness k_d. Hence (2.42) is substituted into (2.94) and we obtain

$$k_d = \left(\frac{2+\mu+\mu g}{(1-g)(2+\mu-g)}\right)k_{opt} \tag{2.95}$$

If the tuning adjustment is optimized with respect to velocity $\dot{x}$ instead of displacement x, the optimum passive stiffness is obtained by substituting (2.47) into (2.94). The final formula is given by

$$k_d = \frac{1}{1-g}k_{opt} \tag{2.96}$$

According to either (2.95) or (2.96), the optimum active stiffness is negative rather than positive, which is expected from the configuration of transfer function of control force versus disturbance force shown in Figure 2.4, where the peak of control force in the high frequency region is higher than the other peak in the lower frequency zone. This implies that the passive stiffness is so selected as to shift the tuning to a higher frequency, which is specified by the second term of (2.88). Hence the optimum active stiffness is to be generated by the actuator, which is given by

$$g_d = k_{opt} - k_d \tag{2.97}$$

It is natural to wonder if there is another way to optimize the passive damping factor exactly in the same manner as the passive stiffness. In fact, equation (2.86) is also a quadratic form in terms of c_d as well as k_d so that the alternative definition of the passive damping factor can be obtained by

$$c_d = -\frac{m_d E\left[\dot{Y}\ddot{X}\right]}{E\left[(\dot{Y})^2\right]} \tag{2.98}$$

According to the definition above, the passive optimum damping is so selected as to minimize control force rather than control power. Hence there are two different definitions available for optimizing the passive damping factor. Equation (2.98) can be evaluated in the same manner as before and given by

$$c_d = \frac{\mu}{\mu + g} c_{opt} \tag{2.99}$$

Surprisingly, this final result is incidentally identical to the previously obtained optimum passive damping value given by (2.80). Hence it is concluded that if the passive damping c_d is adjusted to (2.80), the control power and force are simultaneously optimized under a white noise disturbance. Moreover, this equation is also identical to (2.30), which is obtained under a harmonic excitation. Hence, three different definitions for the optimum damping factor incidentally yield the same answer to this problem.

2.9 Parameter Optimization under Earthquake Disturbance

So far, we have discussed the optimization of the active TMD under a wind blow disturbance, which is either harmonic or random white noise. According to the acceleration feedback method, the external disturbance effect on the control performance is directly considered and treated in an explicit manner. In fact, the supposed excitation is a harmonic disturbance acting on the primal structure just like a harmonic wind blow inducing the vibration of the building structure, or the stationary random excitation which maybe a better substitution for the actual wind blow disturbances. Hence if the excitation is not like a wind gust but an earthquake that excites the TMD motion as well as the primal system, there arises a suspect that the same control algorithm might be less effective for ground motion disturbance. In this section, earthquake disturbances are considered to examine the difference between the two types of typical external disturbances. The final result ascertains that the same control algorithm works favorably for earthquakes as well as wind blows. Developed below is the equation of motion of the active TMD shown in Figure 2.5 where a harmonic ground motion is acting on the whole system.

$$\begin{cases} m_d(\ddot{y}+\ddot{x}) + c_d\dot{y} + k_d y - u(t) = -m_d\ddot{x}_G & (2.100) \\ m\ddot{x} + kx - c_d\dot{y} - k_d y + u(t) = -m\ddot{x}_G & (2.101) \end{cases}$$

Absolute motion of the primal system response is

$$z = x + x_G \tag{2.102}$$

Substitution of (2.102) into (2.100),(2.101) yields

$$\begin{cases} m_d\ddot{y} + c_d\dot{y} + k_d y = -m_d\ddot{z} + u(t) & (2.103) \\ m\ddot{z} + kz - c_d\dot{y} - k_d y = kx_G - u(t) & (2.104) \end{cases}$$

Supposed that the ground motion x_G is a harmonic excitation given by

$$x_G(t) = F e^{i\omega t} \tag{2.105}$$

Then, the equivalent control algorithm is modified from (2.4) to

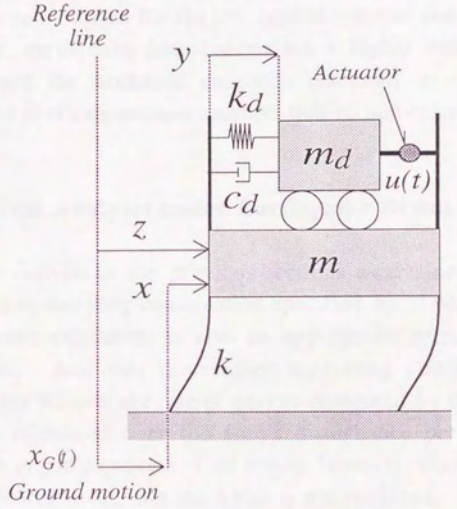

Figure 2.5 Active TMD under a Harmonic Ground Motion

$$u(t) = -g\,m\,\ddot{z} = -g\,m\,(\ddot{x} + \ddot{x}_G) \tag{2.106}$$

If the absolute acceleration of the primal system is employed for the feedback signal, the whole optimization procedure is identical to what is conducted in the previous sections under a harmonic wind blow or a stationary white noise excitation. Hence the optimum parameters obtained so far are also valid for earthquake disturbances as well, which is a significant advantage from a practical point of view. Because neither the sensing equipment nor the control algorithm is to be modified for the two typical types of disturbance excitations.

However, earthquake disturbances are a highly non-stationary random excitation. Hence the stochastic approach discussed in case of white noise excitation in the previous sections must be studied numerically.

2.10 Numerical Analysis under Earthquake Disturbance

The stochastic analysis in the previous sections ascertained that the optimum passive and active damping combination specified by (2.30), which is obtained under a harmonic excitation, is also an appropriate selection under a white noise excitation. And this is a rather surprising result because the final formula indicates the average rate of energy dissipated by the active device will be zero when calculated over the entire disturbance period, if the random excitation is an ergodic process. This result, however, does not imply that the instantaneous power to activate the TMD is not required. As a matter of fact, according to the definition of the power spectral density function in an ergodic sense, we have to take infinitely long period of time for averaging the responses to evaluate them in the real world. In other words, there is always some amount of power that is necessary for activating the mechanism because of the fluctuation of disturbance input.

In this section, several numerical analyses are conducted to evaluate the energy dissipation due to the actuator, whose feedback gain and TMD parameters are optimized according to the formulae developed in this chapter. The parameters and other specifications are all indicated in Table 2.2, where the optimum damping (both active and passive), the tuning frequency, the

feedback gain and the mass ratio are all given. Formulae (2.21), (2.22), (2.94), (2.99) are used for this calculation. The ground excitations are El Centro (NS), Taft (NS), and Hachinohe (NS), whose peak accelerations are all normalized to 100 cm/sec^2. The feedback gain g is set to 0.03, while the mass ratio μ is set to 0.01. As for the numerical computation, the fourth-order Runge-Kutta method was employed with a time increment of 0.01 second. The resulting time histories are shown in Figures 2.6, 2.7, and 2.8, which are corresponding to El Centro, Taft, and Hachinohe excitation, respectively.

As is expected from the analytical study, the control energy dissipation converges to zero under any ground disturbance excitation. This numerical result means that (2.56) is actually satisfied not only under stationary random processes but also under non-stationary random disturbances such as earthquakes. Hence it can be concluded that the optimization of the passive damping factor in a stochastic sense is empirically proved to be valid for application problems in a deterministic sense as well. This conclusion is significantly important, because it is possible to determine the optimum selection of passive devices even before we know the entire process of the earthquake disturbances and wind blows, which explicitly influence the actuator requirement and capacity in a deterministic sense. Therefore, we can design the optimum vibration controller without knowing the disturbances before their occurrence. Judging from Figures 2.6~2.8, it is also understood that the control force is not so much influenced by the selection of passive stiffness, while the selection of passive damping factor is seen to be a sensitive factor that heavily changes the controller's requirement especially control power.

The results of the numerical analyses with respect to the control force, power and energy dissipated by the actuator are also shown in Figures 2.6 ~ 2.8. There are two case studies conducted to compare the selection of passive and active parameters. The optimum tuning frequency and the total damping coefficient are exactly the same for both cases, but the contribution by the active control force is different. Hence the both cases have the same vibration control effect and reduce the primal system response exactly the same amount. It is, however, noted that there is a substantial difference with respect to the active power and energy requirement between the two cases. This significant discrepancy is caused by the intentional miss-selection of passive damping and stiffness, or c_d and k_d, so that it is quantitatively shown to be important for the active TMD to select the passive parameters.

Table 2.2 Numerical Study Cases with Parameters and Gains

	Parameters and Optimum Values		CASE-1 Optimum	CASE-2 Semi-Optimum
Primal System	Mass	m (kg)	9.800×10^5	
	Stiffness	k (N/m)	3.865×10^7	
	Freq.	ω_o (rad/s)	6.280	
Auxiliary System	Mass	m_d (kg)	9.800×10^3	
	Ratio	μ	0.01	
	Gain	g	0.03	
	Opt. Freq. Ratio	ξ_{opt}	0.975	
	Opt. freq.	ω_{opt} (rad/sec)	6.124	
	Opt. Stiffness	k_{opt} (N/m)	3.68×10^5	
	Passive Stiffness	k_d (N/m)	3.91×10^5	3.68×10^5
	Active Stiffness	g_d (N/m)	-0.23×10^5	0.0
	Opt.Damp. Ratio	η_{opt}	0.1219	
	Opt.Damp. Coeff.	c_{opt} (N sec/m)	1.46×10^4	
	Passive damp.	c_d (N sec/m)	0.365×10^4	0.0
	Active Damp.	g_v (N sec/m)	1.095×10^4	1.46×10^4

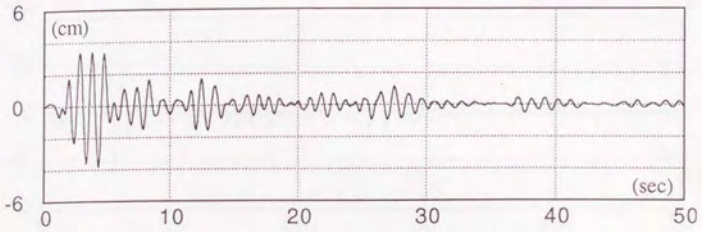

Figure 2.6.a Primal sys. disp. (CASE1) [El Centro (NS) 100gal]

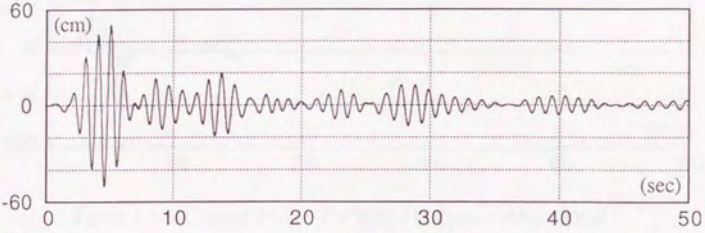

Figure 2.6.b Auxiliary sys. disp. (CASE1) [El Centro (NS) 100gal]

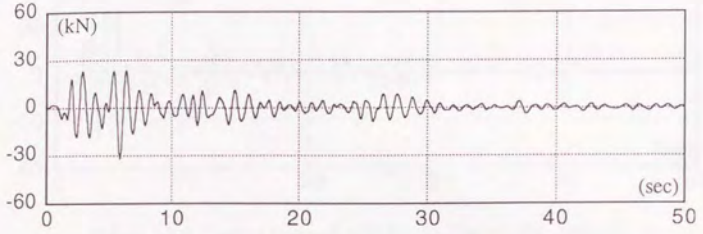

Figure 2.6.c Control Force (CASE1) [El Centro (NS) 100gal]

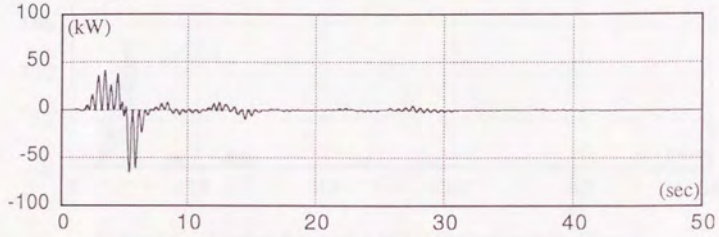

Figure 2.6.d Control Power (CASE1) [El Centro (NS) 100gal]

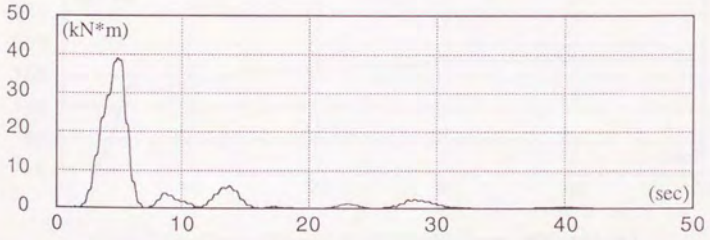

Figure 2.6.e Control Energy (CASE1) [El Centro (NS) 100gal]

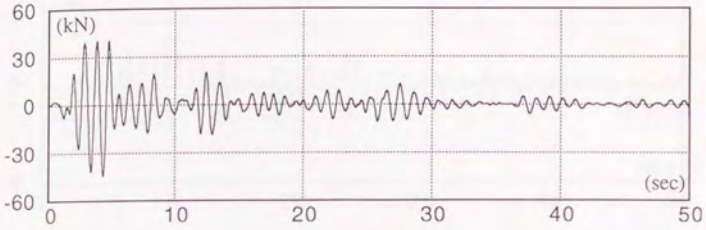

Figure 2.6.f Control Force (CASE2) [El Centro (NS) 100gal]

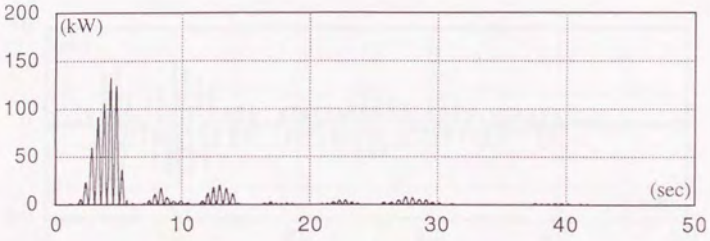

Figure 2.6.g Control Power (CASE2) [El Centro (NS) 100gal]

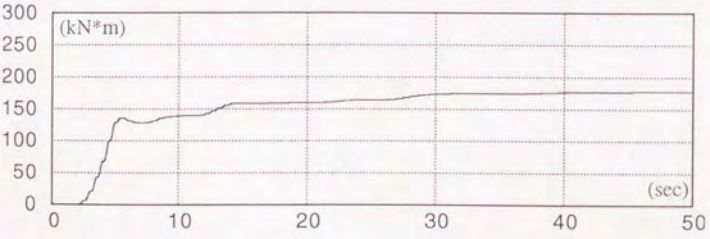

Figure 2.6.h Control Energy (CASE2) [El Centro (NS) 100gal]

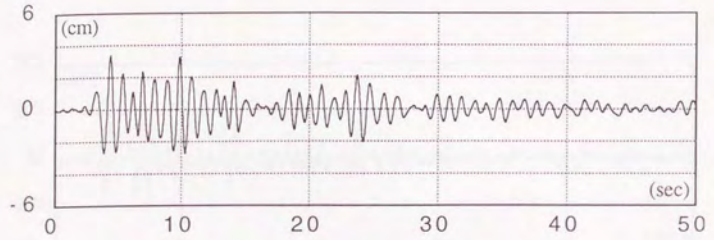

Figure 2.7.a Primal sys. disp. (CASE1) [Taft (NS) 100gal]

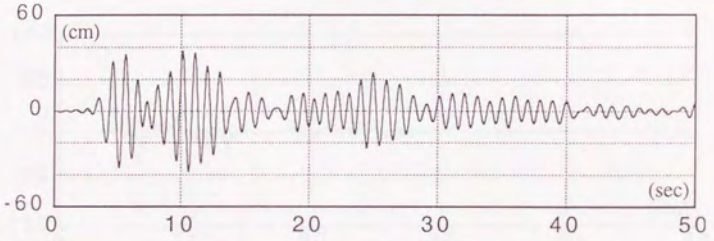

Figure 2.7.b Auxiliary sys. stroke (CASE1) [Taft (NS) 100gal]

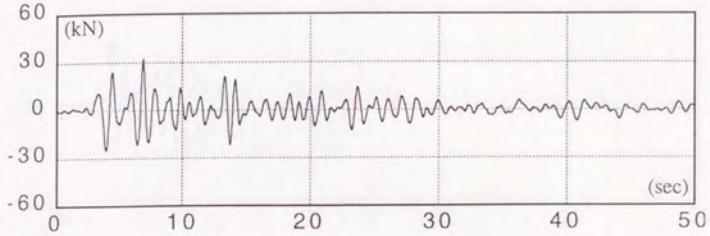

Figure 2.7.c Control Force (CASE1) [Taft (NS) 100gal]

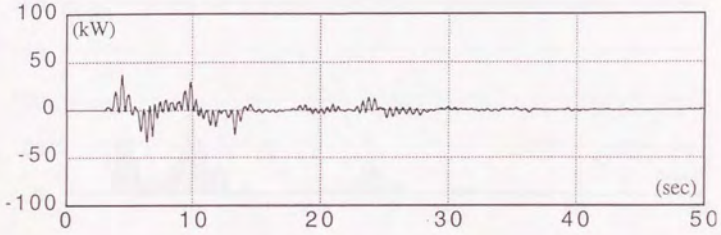

Figure 2.7.d Control Power (CASE 1) [Taft (NS) 100gal]

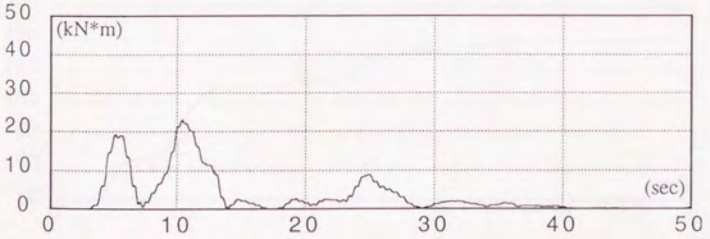

Figure 2.7.e Control Energy (CASE1) [Taft (NS) 100gal]

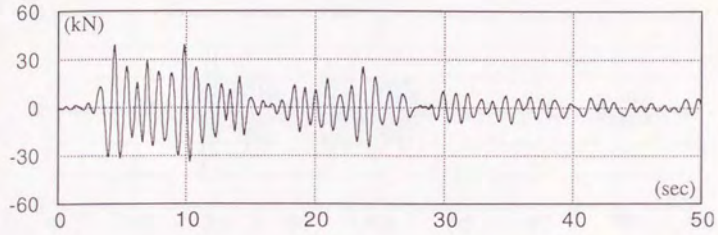

Figure 2.7.f Control Force (CASE2) [Taft (NS) 100gal]

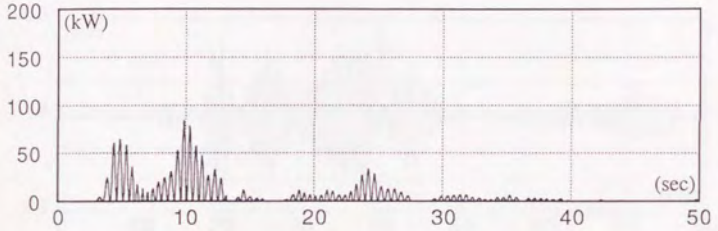

Figure 2.7.g Control Power (CASE2) [Taft (NS) 100gal]

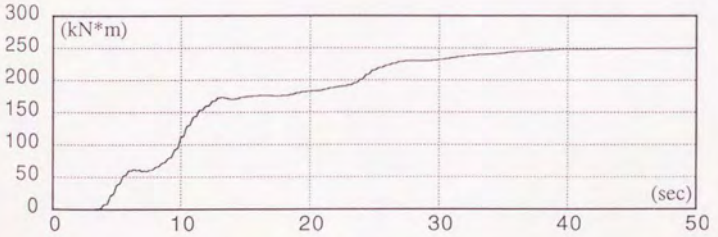

Figure 2.7.h Control Energy (CASE2) [Taft (NS) 100gal]

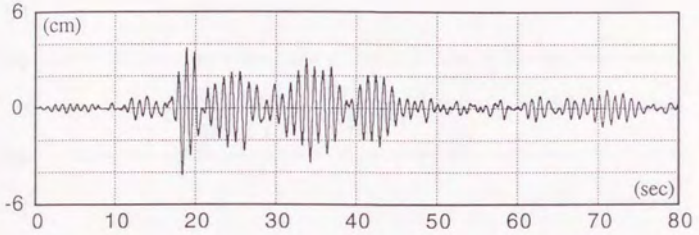

Figure 2.8.a Primal sys. disp. (CASE1) [Hachinohe (NS) 100gal]

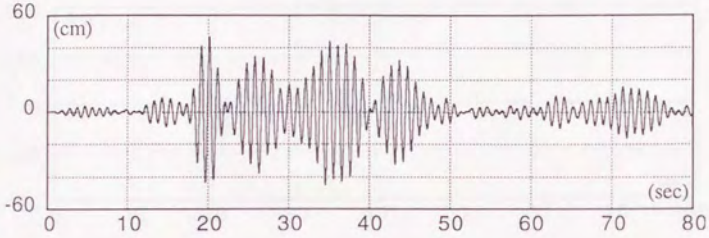

Figure 2.8.b Auxiliary sys. stroke (CASE1) [Hachinohe (NS) 100gal]

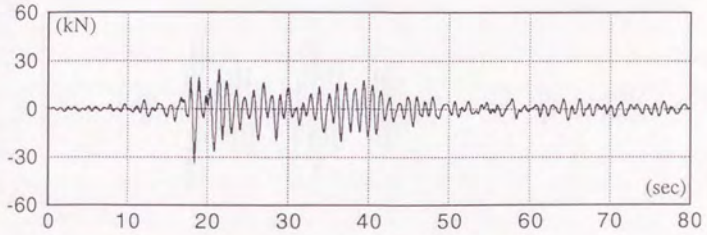

Figure 2.8.c Control Force (CASE1) [Hachinohe (NS) 100gal]

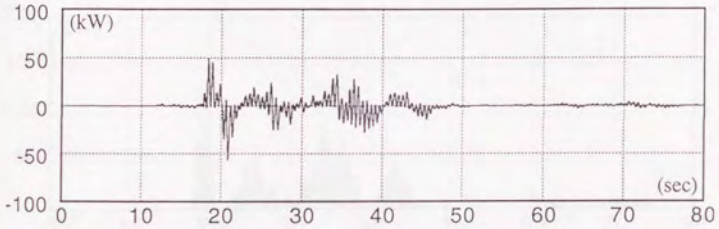

Figure 2.8.d Control Power (CASE1) [Hachinohe (NS) 100gal]

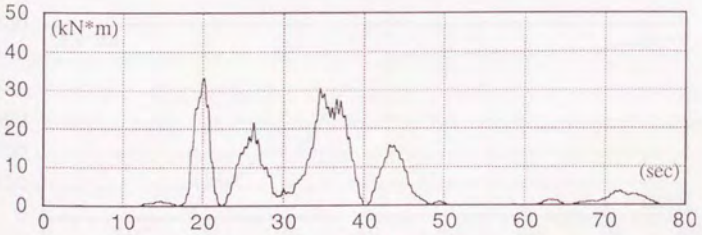

Figure 2.8.e Control Energy (CASE1) [Hachinohe (NS) 100gal]

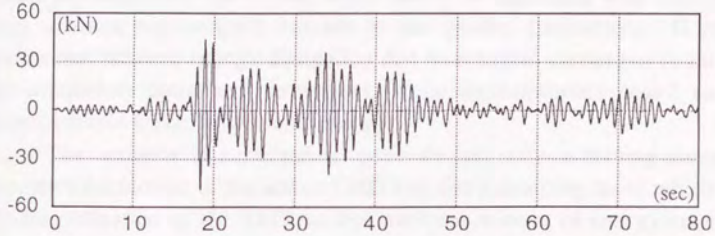

Figure 2.8.f Control Force (CASE2) [Hachinohe (NS) 100gal]

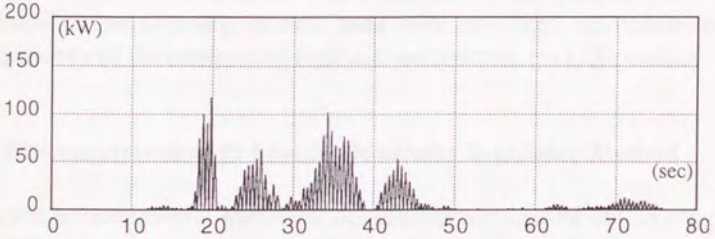

Figure 2.8.g Control Power (CASE2) [Hachinohe (NS) 100gal]

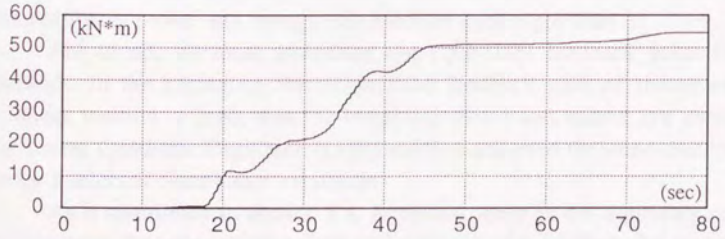

Figure 2.8.h Control Energy (CASE2) [Hachinohe (NS) 100gal]

All the active and passive optimum parameters are selected for case-1 study, while the tuning adjustment is completely due to the passive stiffness and all the damping effect is generated by active TMD for case-2 study. In other words, case-1 is completely optimized, while case-2 is optimized with respect to the total stiffness and damping but not to the passive parameters. It is clearly shown that the total energy dissipation due to actuator converges to zero under the completely optimized parameters, while semi-optimum case-2 requires a larger control force, power and energy.

The actuator is supposed to generate not only a driving force which increases the motion of the active TMD but also a damping force which reduces the free vibration of the TMD so that the total amount of energy required for the active TMD is just for nothing. Because the power required for the actuator switches and changes the sign and the total integral is apt to converge to zero with reasonable expectation. The rest of the problem to consider for the acceleration feedback method is the quantitative comparison with the LQR method. The following section deals with this topic and makes clear the superiority of the acceleration feedback method over the LQR method.

2.11 Comparison with Linear Quadratic Regulator Method

In this section, several numerical calculations are carried out to compare the vibration control performance of the acceleration feedback method with that of the linear quadratic regulator method. There are two factors taken into consideration for evaluating the control performance of both methods: the vibration reduction achieved by each method, and the active cost such as control force, power and energy required for each algorithm.

Fist of all, we must determine the equivalent feedback gains for both methods. In the beginning, the normalized feedback gain of the acceleration feedback method is fixed, then the weighting factor and matrix are varied until the Linear Quadratic Regulator (LQR) method achieved the same control effect under a selected disturbance excitation.

As is mentioned in section 1.5, however, there is not a guiding principle to determine the appropriate values of k_d and c_d, if we follow the conventional LQR method. It is necessary to predetermine the passive parameters before starting the try-and-error method to decide the feedback gains for LQR

method. Many people used the optimum stiffness and damping factor of the passive TMD as the initial values for the recursive calculation to solve the Algebraic Riccati Equation. In this section's study, the passive TMD optimum parameters are selected for the LQR method just like other previous studies.

Another factor to be considered for is the feedback quantity. In the previous section, it is pointed out that the absolute acceleration response is the appropriate feedback quantity for the acceleration feedback method under earthquake disturbances. It is also aimed that the absolute response of building structures under earthquake excitations should be reduced as much as possible. Hence, the absolute displacement and velocity are used as the feedback quantities for the LQR method. The notations of the response values of the primal system are to be referred to Figure 2.5. From the view point of sensing equipment, the absolute displacement and velocity are also the appropriate candidates for the LQR method. Because the relative response values of the primal system with respect to the ground motion are difficult to observe and at lease it necessitates additional sensors placed on the ground level to detect the earthquake motion.

It is also important to select the earthquake excitation carefully in case of the comparison calculation. The spectrum of the disturbance excitation has a significant impact on the response motion of the auxiliary mass system. Because the acceleration response of the primal system contains rather high frequency component while the displacement response has a large amount of low frequency component, when the total system is subjected to earthquake excitation. Hence, the analysis under an earthquake disturbance is favorable for the LQR method than for the acceleration feedback method. On the contrary, wind pressures contain a low frequency component which naturally necessities the drifting motion for the auxiliary system more than required for the acceleration feedback method. In this section, Hachinohe (NS) Earthquake record with the peak acceleration of 100 cm/sec^2 is used for the numerical analysis. Because the advantage is intentionally given to the LQR method for the purpose of this study.

The parameters and feedback gains for both methods are shown in Table 2.3. The normalized feedback gain for the absolute acceleration feedback method is selected to 0.20. Then, the weighting matrix and factor are varied until we obtain the equivalent control effect by means of the corresponding LQR method. The final weighting matrix and factor are also indicated below

Table 2.3. The passive parameters are optimized according to the formulae (2.21), (2.25), (2.30) and (2.94) for the acceleration feedback method. The passive stiffness and damping factor for LQR method are determined according to the passive optimum values according to (1.14) and (1.15).

The numerical results are shown in Figure .2.9 where the primal system absolute acceleration responses are indicated for both algorithms under Hachinohe Earthquake (NS). The vibration control effect due to LQR method is equivalent to that of the acceleration feedback method. There is, however, a discernible difference between the auxiliary system responses as shown in Figure 2.10. The feedback quantity of the LQR algorithm contains a low frequency component, which results in that drifting motion of the auxiliary mass which has no contribution to control effect. This low frequency motion becomes more conspicuous under wind pressure disturbances, because they are basically a static load acting on one side of building structures. Hence, the unnecessary motion of the auxiliary mass is inevitable for LQR method. This is an inherent problem associated with the LQR method applied to active TMD algorithm. This means that the control signal commands the auxiliary mass to generate the low frequency force by means of the mass inertia. On the contrary, the acceleration feedback signal contains only that information necessary for reducing the dynamic motion.

The control device requirements are also indicated in Figures 2.11 ~ 2.13, where the control force, power, and energy are compared for both algorithms. It is obvious that the acceleration feedback has favorable results over the LQR method with respect to each item. Especially, the control energy necessary for the LQR method has a cumulative trend, while there is a convergence at the end of the earthquake for the acceleration feedback method. This characteristic is numerically evaluated for many parameter cases under several earthquakes in the following chapter.

Table 2.3 Parameters and Feedback Gains for LQR method and AF method

Notations	Acceleration Feedback Method	Linear Quadratic Regulator
m (kg)	9.80 x 10^5	
k (N/m)	3.865 x 10^7	
ω_o (rad/s)	6.28 x 10^5	
m_d (kg)	9.80 x 10^3	9.80 x 10^3
k_d (N/m)	4.745 x 10^5	3.79 x 10^5
c_d (Ns/m)	1.67 x 10^3	8.58 x 10^3
μ	0.01	0.01
ξ_{opt}	0.886	---
ω_{opt} (rad/s)	5.561	---
k_{opt} (N/m)	3.031 x 10^3	---
η_{opt}	0.257	---
c_{opt} (Ns/m)	3.51 x 10^4	---
Feedback Algorithm	$u(t) = -mg\ddot{x} - g_v\dot{y} - g_d y$	$u(t) = -g_1 y - g_2 x - g_3\dot{y} - g_4\dot{x}$
Feedback Gains	g = 0.20 g_v = 3.34 x 10^4 g_d = - 1.714 x 10^5	g_1 = 0.00 x 10^5 g_2 = - 9.62 x 10^6 g_3 = 3.53 x 10^4 g_4 = 0.00 x 10^5

where weighting matrix is : $Q = \begin{bmatrix} 0 & 0 & 0 & 0 \\ 0 & 1.0\,E+8 & 0 & 0 \\ 0 & 0 & 0 & 0 \\ 0 & 0 & 0 & 0 \end{bmatrix}$

weighting factor is : R = 1.0 E-6

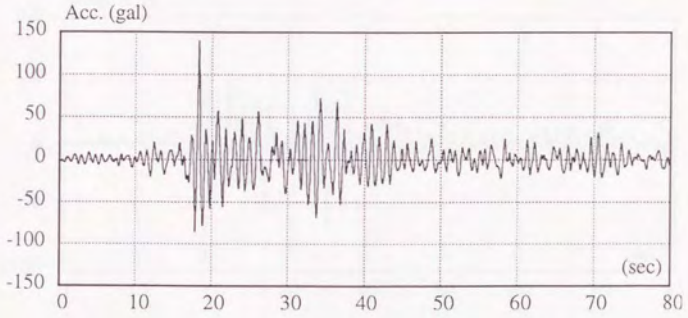

Fig.2.9.a Absolute Acceleration of the Primal System
with Acceleration Feedback Method [Hachinohe (NS) 100gal]

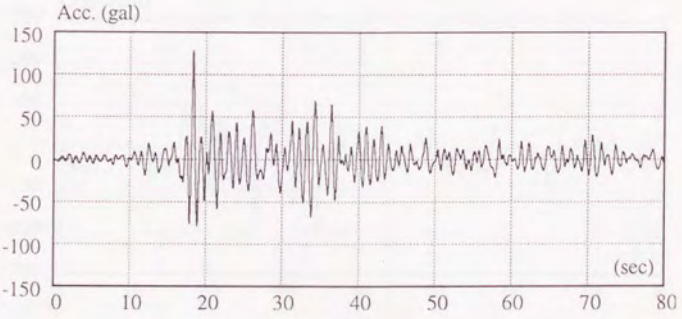

Fig.2.9.b Absolute Acceleration of the Primal System
with Linear Quadratic Regulator Method [Hachinohe (NS) 100gla]

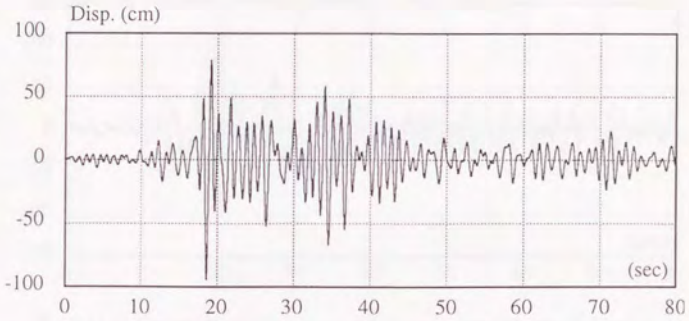

Fig.2.10.a Stroke of the Auxiliary System
with Acceleration Feedback Method [Hachinohe (NS) 100gal]

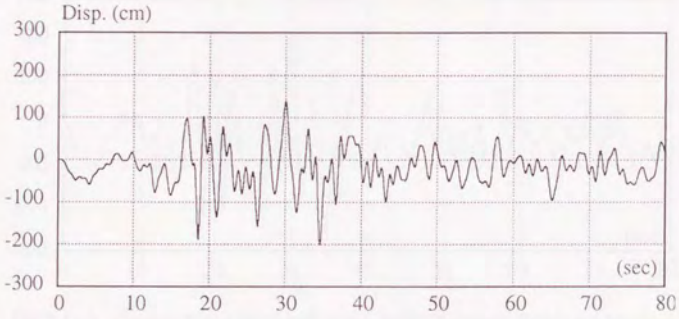

Fig.2.10.b Stroke of the Auxiliary System
with Linear Quadratic Regulator Method [Hachinohe (NS) 100gal]

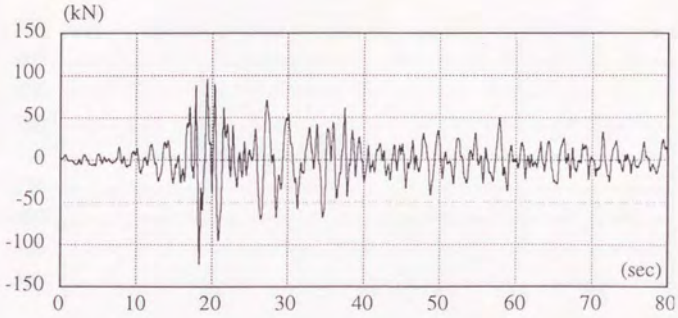

Fig.2.11.a Control Force Response with Acceleration Feedback Method
[Hachinohe (NS) 100gal]

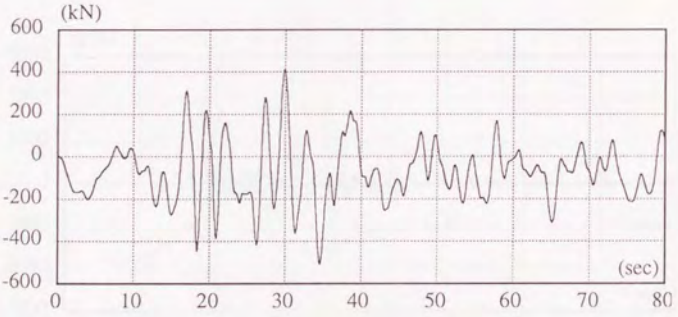

Fig.2.11.b Control Force Response with Linear Quadratic Regulator Method
[Hachinohe (NS) 100gal]

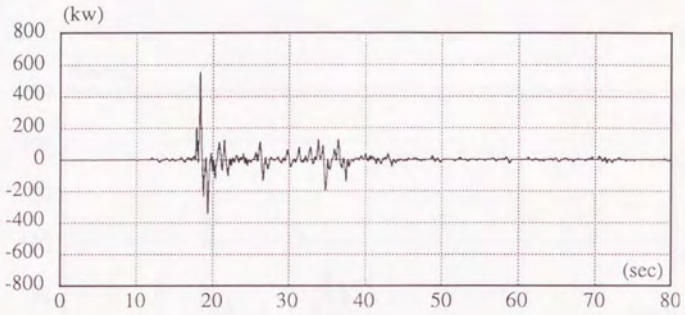

Fig.2.12.a Control Power Response with Acceleration Feedback Method
[Hachinohe (NS) 100gal]

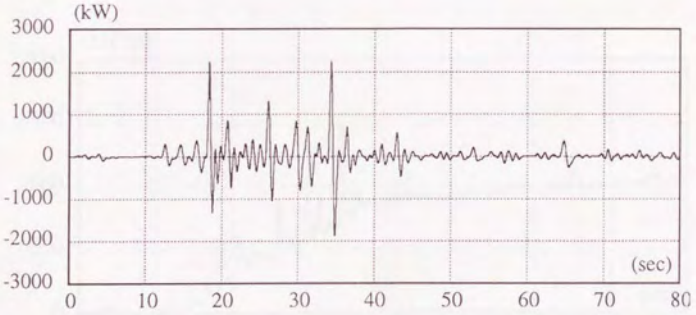

Fig.2.12.b Control Power Response with Linear Quadratic Regulator Method
[Hachinohe (NS) 100gal]

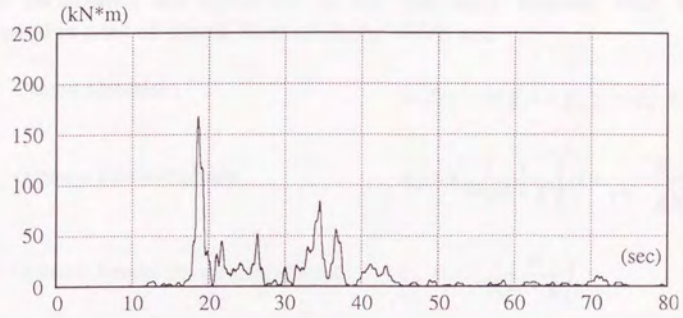

Fig.2.13.a Control Energy Response with Acceleration Feedback Method
[Hachinohe (NS) 100gal]

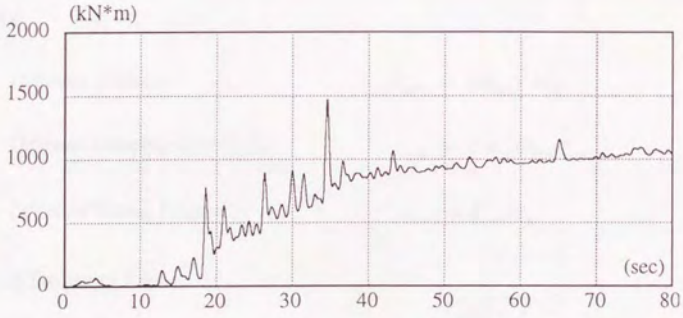

Fig.2.13.b Control Energy Response with Linear Quadratic Regulator Method
[Hachinohe (NS) 100gal]

2.11 Summary of the Formulae

A new control algorithm to improve the TMD performance is proposed and the proposed algorithm is physically explained. Both the feedback gain and the TMD parameters are optimized in the frequency domain, then they are expressed in a set of closed form solutions which are:

Control Algorithm : $$u(t) = -m g \ddot{x} - g_v \dot{y} - g_d y$$

Optimum Passive Stiffness : $$k_d = k_{opt}\left(\frac{1}{\mu + g}\right)\left(\mu + \frac{g}{(1-g)\xi_{opt}^2}\right)$$

Optimum Passive Damping Coefficient : $$c_d = c_{opt}\left(\frac{\mu}{\mu + g}\right)$$

Optimum Displacement Feedback Gain : $$g_d = k_{opt} - k_d$$

Optimum Velocity Feedback Gain : $$g_v = c_{opt} - c_d$$

where

Optimum Stiffness : $$k_{opt} = (\omega_{opt})^2 m_d$$

Optimum Damping Coefficient : $$c_{opt} = 2 m_d \omega_{opt} \eta_{opt}$$

Optimum Tuning Frequency : $$\omega_{opt} = \xi_{opt} \omega_o$$

Optimum Frequency Ratio :

Harmonic Excitation : $$\xi_{opt} = \frac{\sqrt{1-g}}{1+\mu}$$

White Noise Excitation

with respect to displacement : $$\xi_{opt} = \frac{1}{\mu + 1}\sqrt{\frac{2+\mu-g}{2}}$$

White Noise Excitation

with respect to velocity : $$\xi_{opt} = \sqrt{\frac{1}{\mu + 1}}$$

Optimum Damping Factor :

Harmonic Excitation : $$\eta_{opt} = \sqrt{\frac{3(\mu+g)}{8(1+\mu)}}$$

White Noise Excitation

with respect to displacement : $$\eta_{opt} = \sqrt{\frac{(4+3\mu-g)(\mu+g)}{8(1+\mu)(2+\mu-g)}}$$

White Noise Excitation

with respect to velocity : $$\eta_{opt} = \frac{1}{2}\sqrt{\frac{\mu+g}{1-g}}$$

as a result of this optimization, we obtain

Maximum Frequency Response of

the Primal System : $$\alpha_{max} = \sqrt{\frac{2+\mu-g}{\mu+g}}$$

Maximum Frequency Response of

the Auxiliary System : $$\beta_{max} = \frac{\mu+1}{\mu}$$

under a harmonic excitation.

And the average control power is expected to be zero in the ensemble sense, and the control force is minimized under a stationary white noise excitation. It is also noted that the cumulative control energy dissipated by the actuator is converging to zero as the time goes to infinity after the event of random disturbance.

Chapter 3

Numerical Analysis of the Acceleration Feedback Method under Earthquake Disturbance

We have discussed the control performance of the proposed algorithm or the acceleration feedback method from the analytical point of view. Several unique features associated with the new approach have been discovered and theoretically expected. In this chapter, the analytically predicted control performance is numerically evaluated under earthquake disturbances. The real disturbances coming into building structures will be non-stationary random excitations rather than stationary random white noises. Typical examples are earthquakes and wind pressures. Therefore, it is important to distinguish between what is predicted from stochastic analysis and what is expected to happen in a real world. In this chapter, the control performance and device requirement of the acceleration feedback method are evaluated by the deterministic approach under several earthquake disturbances. Most of the numerical results are assessed and explained in terms of energy response spectrum.

3.1 Energy Equilibrium under Earthquake Disturbance

The cumulative control work done by the actuator can be neutralized in an average sense by adjusting the passive damping factor in such a manner that the total energy dissipated by the damper and the total energy brought by the disturbance input are equalized and balanced during the entire period of disturbance excitation. This optimum passive damping factor can be found by a stochastic approach (See chapter 2.). This result, however, does not mean that the actuator requires no power at all. In fact, it should generate the adequate control force according to the current motion of the active TMD, which needs either increase or decrease of the mass speed. Hence the sign of the actuator power is not constant but fluctuating according to the relative motion of the auxiliary system to the primal system. More precisely, when the

primal system vibration is relatively large and the auxiliary system response is small, the actuator should generate acceleration force to drive the TMD. When the primal system response is reduced but the TMD still continues its free vibration, then the generated control force is mainly a damping effect on the auxiliary system. Therefore, it is naturally expected that the total energy dissipated by the actuator will converge to zero over the entire period of excitation even under a highly non-stationary random disturbance.

In this section, the energy equilibrium of the system under an earthquake disturbance is obtained and studied for the purpose of verifying the stochastic prediction. In addition to this, the control performance and device requirement can be clarified in terms of energy response spectrum. As the first step, the energy integral is defined and the energy equilibrium is obtained. The equations of motion of the active TMD under an earthquake disturbance are given by

$$\begin{cases} m_d(\ddot{x}+\ddot{y}+\ddot{x}_G)+c_d\dot{y}+k_d y-u(t)=0 & (3.1) \\ m(\ddot{x}+\ddot{x}_G)+kx+m_d(\ddot{x}+\ddot{y}+\ddot{x}_G)=0 & (3.2) \end{cases}$$

where all the notations are referred to Figure 2.5. The energy equilibrium is obtained by multiplying the velocity vector in the same manner as (2.51), and the final result is shown by

$$\begin{aligned} &\frac{1}{2}m(\dot{x})^2+\frac{1}{2}k\,x^2+\frac{1}{2}m_d(\dot{x}+\dot{y})^2+\frac{1}{2}k_d y^2+\int_0^t c_d(\dot{y})^2 d\tau \\ &\qquad=\int_0^t \dot{y}\,u(\tau)\,d\tau-\int_0^t\left[(m+m_d)\dot{x}+m_d\dot{y}\right]\ddot{x}_G\,d\tau \end{aligned} \tag{3.3}$$

We introduce the following definitions for each term of (3.3).

$$E_s=\frac{1}{2}m\left[\dot{x}(t)\right]^2+\frac{1}{2}k\left[x(t)\right]^2 \tag{3.4}$$

$$E_t=\frac{1}{2}m_d\left[\dot{x}(t)+\dot{y}(t)\right]^2+\frac{1}{2}k_d\left[y(t)\right]^2 \tag{3.5}$$

$$E_d = \int_0^t c_d \left[\dot{y}(\tau)\right]^2 d\tau \tag{3.6}$$

$$E_c = \int_0^t \dot{y}(\tau)\, u(\tau)\, d\tau \tag{3.7}$$

$$E_i = -\int_0^t \left[(m + m_d)\dot{x}(\tau) + m_d \dot{y}(\tau)\right] \ddot{x}_G(\tau)\, d\tau \tag{3.8}$$

where E_s (t) : Structure energy
E_t (t) : TMD energy
E_d (t) : Energy dissipated by the passive damper
E_c (t) : Control energy
E_i (t) : Input energy brought by the disturbance excitation

There are several factors that influence those energy response values: the mass of the primal system m, the mass ratio μ, the feedback gain g, the natural frequency ω_o, and the disturbance input $\ddot{x}_G$. The other parameters are set to the optimum values according to the formulae in chapter 2. Obviously, the energy response increases in proportion to the mass m so that we are interested in the energy per unit weight of the primal system. Although there are five factors to be determined, what we could select in the process of design are only μ and g. Because ω_o is a given parameter associated with a target structure, and we do not know the earthquake disturbance $\ddot{x}_G$ until an actual event takes place. Hence we should examine the energy response spectrum for the variation of μ and g.

Finally, the energy equilibrium is obtained as

$$E_s + E_t + E_d = E_c + E_i \tag{3.9}$$

It is noted that this equilibrium is not only satisfied at the end of disturbance excitation but also at any instant time t during the transient state of the response. By definition, the structure energy E_s, the TMD energy E_t, and the damping energy E_d are all positive so that the summation of the control

energy E_c and the input energy E_i always takes positive value during any disturbance excitation.

It is better to show an example calculation of the energy response time history than to go into further discussion of this equilibrium equation. Shown in Figure 3.1 is the energy response time history whose parameters and feedback gains are shown in Table 3.1. The parameters selected for this study are exactly the same values as employed in section 2.10 in the previous chapter. The disturbance earthquake is Hachinohe (NS) whose peak acceleration is scaled to 100 cm/sec^2. With a purpose of clarifying the equilibrium of these five terms of (3.9), the left hand side of (3.9) is shown in the upper hemisphere of the Figure 3.1 while the right hand is in the lower side of the figure. All the energy responses take positive values or zero.

It is also noted that the E_s and E_t are converging to zero as the time goes to infinity, because the system is asymptotically stable. And E_c is supposed to be converging to zero, which is theoretically proved under a stationary random white noise disturbance and is actually observed in case of an actual earthquake disturbance. Hence the damping energy and the input energy are expected to be reaching the same value as the time goes to infinity.

In the forthcoming sections, the above statements are numerically studied so that the control performance and the device requirement are clarified in terms of energy response spectrum.

Table 3.1 Parameters and Gains for an Example Study

	Mass Data	Damping Data	Stiffness Data
Primal System	m = 980 ton	*	k = 3.865 x 10^7 N/m ω_o = 6.28 rad/s
Auxiliary System	m_d = 9.8 ton μ = 0.01 g = 0.03	η_{opt} = 0.1219 c_{opt} = 1.46x10^4 Ns/m c_d = 0.365x10^4 Ns/m g_v = 1.095 x10^4 Ns/m	ξ_{opt} = 0.975 ω_{opt} = 6.124 rad/s k_{opt} = 3.68 x10^5 N/m k_d = 3.91 x10^5 N/m g_d = - 0.23 x10^5 N/m

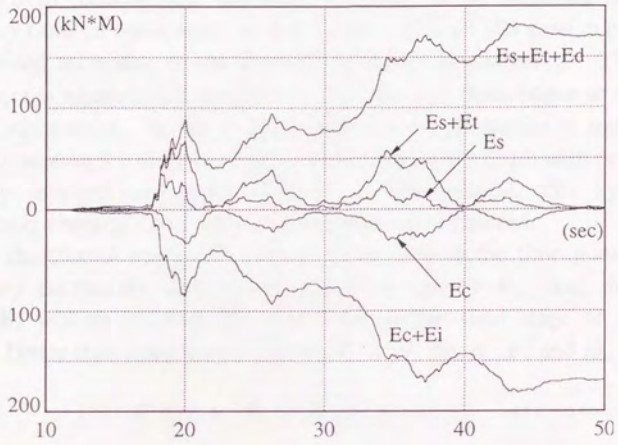

Figure 3.1 Energy Response Equilibrium

[Hachinohe (NS) 100gal $m = 980$ ton , $\omega_o = 6.28$ rad/s , $\mu = 0.01$, $g = 0.03$]

3.2 Control Energy Ec, Input Energy E_i and Damping Energy E_d

We have several good reasons to believe that the control energy defined by (3.7) under any earthquake disturbance will be converging to zero as the time goes to infinity, which is expressed as

$$E_c(\mu, g, \omega_o) = 0 \quad as\ t \to \infty \qquad \text{for any } \mu \text{ and } g \qquad (3.10)$$

As is proved theoretically, the control energy in an ensemble sense under stationary random white noise is exactly zero, if the TMD passive parameter c_d is optimized according to the formula specified in chapter 2. The question raised here is whether it is possible to treat the real disturbance as a stationary random white noise. So far as those several example studies in section 2.10 as well as in section 3.1 are concerned, all of them satisfy (3.10) with respect to the arbitrary selected earthquake records. In this section, this hypothesis is numerically checked under various earthquake disturbances.

If the control energy E_c converges to zero as the time goes to infinity under any earthquake disturbance, the input energy E_i and the damping energy E_d will be reaching the same value at the final stage of disturbance period. Hence next equation is to be satisfied for any μ, g, and ω_o.

$$E_d(\mu, g, \omega_o) = E_i(\mu, g, \omega_o) \qquad as\ t \to \infty \qquad (3.11)$$

Conversely, if this equation is satisfied, the control energy E_c is proved to be zero as the time goes to infinity. Hence the above control energy equilibrium is to be examined under various earthquake disturbances with respect to numerous optimum parameters. The damping energy is a simply increasing function but the input energy might take the maximum value not at the end of excitation but at a certain time during the earthquake event. Therefore, the above equilibrium is evaluated after the system response is well subdued.

It is to be noted that the input energy increases as the weight of the primal system becomes large, which is self evident from the definition. Hence the energy response should be evaluated per unit weight of the primal system. One conventional method commonly used for expressing energy response spectra for this purpose is to substitute the energy response by the equivalent velocity response [37], whose definitions are

$$V_d(\mu, g, \omega_o) = \lim_{t \to \infty} \sqrt{\frac{2E_d(\mu, g, \omega_o)}{m}} \tag{3.12}$$

$$V_i(\mu, g, \omega_o) = \lim_{t \to \infty} \sqrt{\frac{2E_i(\mu, g, \omega_o)}{m}} \tag{3.13}$$

where V_d is the damping energy response spectrum and V_i is the input energy response spectrum expressed in terms of velocity. It is noted that all the above responses are the final integral values. We are interested in the above energy response spectra with respect to the natural period of the primal system or T_o ($= 2\pi / \omega_o$) under actual earthquake disturbances. Because it is empirically known that the response values are considerably affected by the natural period of the primal system. The selected earthquake disturbances are : El Centro (NS), Taft (EW) and Hachinohe (NS). The peak acceleration is scaled to 100 cm/sec^2 for all the earthquakes.

The resulting V_d and V_i are shown and compared in Figure 3.2 ~ 3.7, where the x-axis is the natural period T_o ($= 2\pi / \omega_o$) while the y-axis is the energy response in terms of velocity. Interestingly V_i and V_d take the same value over the entire range of natural frequency of the primal system with reasonably small deviation from each other. In fact, both of them are seen to be identical in all of the figures over the whole range of period. At lease for these example studies, there is no discernible discrepancy between V_d and V_i. Whatever the feedback gain and the mass ratio are, this equilibrium is always satisfied at least under these earthquake records used for this study. Hence it is concluded that the control energy E_c is expected to converge to zero at the end of any random disturbance excitations.

In the previous chapter, there are proposed three different definitions for searching the optimum passive damping coefficient c_d. Surprisingly, they yielded exactly the same answer to this optimum problem. Again, we have come to the same result that this optimum formula (cf. Section 2.11) is not only valid for stationary random disturbances but also for non-stationary earthquakes. The remarkable coincidence between the damping energy response spectrum V_d and the input energy response spectrum V_i certifies that the control energy response E_c be zero at the final stage of any random disturbances.

Another important aspect of this study is the qualitative evaluation of the damping energy response. Because this information is indispensable to specify the damping device energy dissipation capacity. Although there are only three earthquake records examined so far, it could be said that the input energy or the damping energy in terms of velocity is almost less than 80 cm/sec for middle size earthquake motions whose peak acceleration is about 100 cm/sec^2. When interpreted into a more familiar unit, the total energy brought by a middle size earthquake into a building structure (the total weight is 10,000 ton with an active TMD) is about 2000 kcal. Hence, the increase of the damping material temperature after the event of an earthquake should be considered as one of the important criteria for designing the damping device.

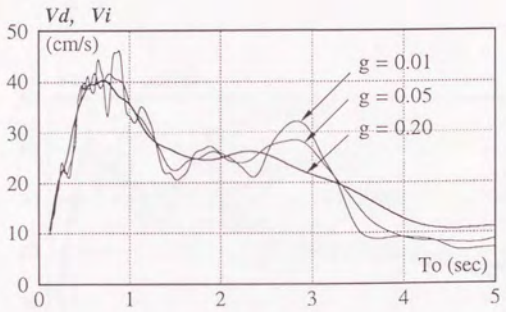

Figure 3.2 Damping Energy Response Spectrum Vd
and Input Energy Response Spectrum Vi
[El Centro (NS) 100gal $\mu = 0.01$]

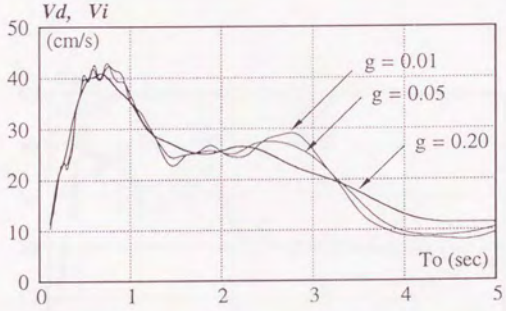

Figure 3.3 Damping Energy Response Spectrum Vd
and Input Energy Response Spectrum Vi
[El Centro (NS) 100gal $\mu = 0.05$]

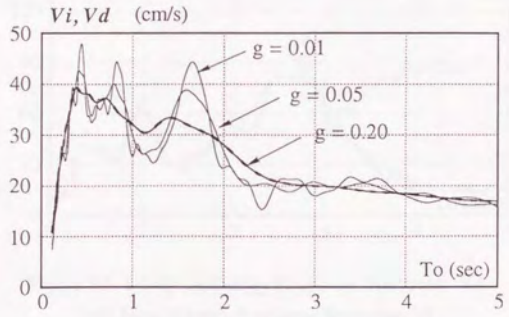

Figure 3.4 Damping Energy Response Spectrum ***Vd***
and Input Energy Response Spectrum *Vi*
[Taft (EW) 100gal μ = 0.01]

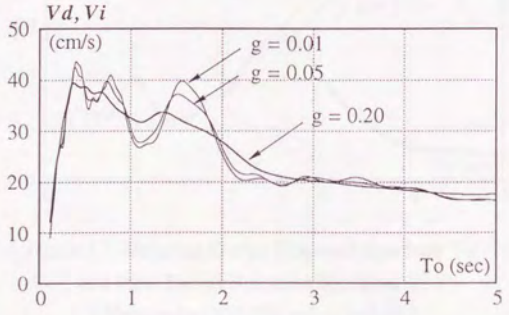

Figure 3.5 Damping Energy Response Spectrum *Vd*
and Input Energy Respons Spectrum *Vi*
[Taft (EW) 100 gal μ = 0.05]

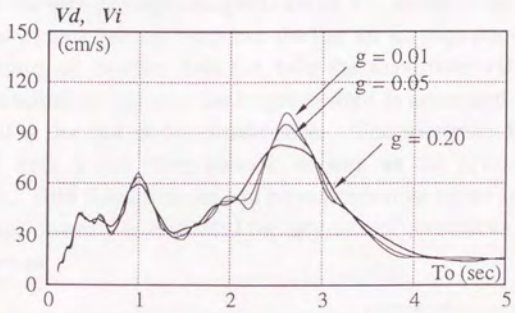

Figure 3.6 Damping Energy Response Spectrum *Vd*
and Input Energy Response Spectrum *Vi*
[Hachinohe (NS) 100gal $\mu = 0.01$]

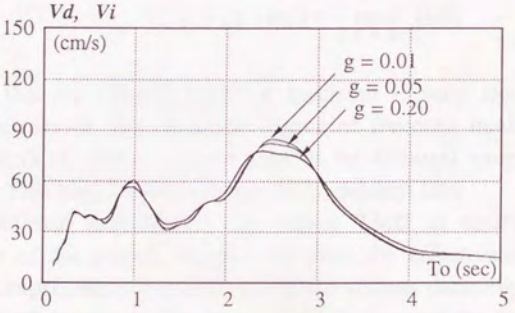

Figure 3.7 Damping Energy Response Spectrum *Vd*
and Input Energy Response Spectrum *Vi*
[Hachinohe (NS) 100 gal $\mu = 0.05$]

3.3 Control Performance under Earthquake Disturbance

In this section, the control performance of the acceleration feedback method is evaluated by the energy response spectrum of V_s, which is the maximum value of the primal system energy response during an earthquake disturbance. This energy response, of course, does not take the maximum value at the end of disturbance excitation, because the target system is asymptotically stable and it comes to halt at the end of the disturbance. The spectrum V_s is affected by the feedback gain g and mass ratio μ as well as the primal system natural frequency ω_o. And this spectrum can be expressed in terms of velocity so that the normalized quantity is evaluated for any size of structures. The definition of V_s is given as

$$V_{s,1}(\mu, g, \omega_o) = \max_{0 \le t \le \infty} \sqrt{\frac{2E_s(\mu, g, \omega_o)}{m}} \tag{3.14}$$

On the other hand, the conventional velocity response spectrum of the primal system according to the ordinary definition is

$$V_{s,2}(\mu, g, \omega_o) = \max_{0 \le t \le \infty} |\dot{x}(t)| \tag{3.15}$$

It is known that the velocity response spectrum is very close to the energy response spectrum in case of single degree of freedom model. Hence, it is expected that (3.14) and (3.15) are seen to be identical except a very small difference. This supposition is numerically checked later.

The physical meaning of the active TMD is clearly the damping augmentation of the primal system. In fact, the effectiveness of the active TMD can be expressed in terms of equivalent viscous damping factor. Hence, the control performance of the active TMD is assessed by means of response spectra of the primal system, while the ordinary response spectra (single degree of freedom model) are used for estimating the equivalent damping factor for a TMD with a given μ and g. Again the same three earthquake disturbances are used for this numerical study.

First, the control performance of the active TMD is substituted by the equivalent passive TMD whose mass ratio is defined to be μ_e. The optimization process in chapter 2 certifies that the resonance peak of the primal system with

the active TMD is to be equalized by the equivalent passive TMD with a mass ratio μ_e . Recalling (1.16) and (2.19), we can expect the same control performance from the passive TMD with the mass ratio μ_e as from the active TMD with μ and g . The equivalent mass ratio is defined by

$$\mu_e = \frac{\mu + g}{1 - g} \tag{3.16}$$

The control performance of the active TMD is simply estimated by the equivalent mass ratio μ_e defined above. This quantity can easily specify the TMD performance in terms of mass ratio. The rest of the task to be done is to make clear the relation between the mass ratio of the passive TMD and the viscous damping factor, which is studied by means of response spectrum.

First, the response energy spectrum V_s with respect to the passive TMD is evaluated for earthquake disturbances. The resulting response energy spectra are shown in Figure 3.8.a ~ 3.10.a. Then, the velocity response spectra associated with the same passive TMD is evaluated for the same earthquake disturbances. They are shown in Figure 3.8.b ~ 3.10.b, which have a good agreement with Figure 3.8.a ~ 3.10.a. As the mass ratio increases, V_s spectrum becomes smaller for most of the frequency zone. On the other hand, the response energy spectra for a single-degree-of-freedom model with various viscous damping factors are indicated in Figure 3.8.c ~ 3.10.c. Comparing these response spectra, we can estimate the equivalent damping factor η_e related to the equivalent mass ratio μ_e . The following is the proposed equivalent damping factor expressed in terms of μ_e .

$$\eta_e = \frac{1}{3}\sqrt{\frac{\mu_e}{\mu_e + 2}} \tag{3.17}$$

It is also important to clarify the response of the auxiliary mass system. Just like the primal system energy response spectrum, we can obtain the energy response spectrum of the active TMD under the same earthquake records as before. This response spectrum is useful for evaluating the device requirement. It is obvious that there is a limitation for the active TMD displacement, which is determined according to the space availability for each project. Hence, the

maximum response value of the auxiliary mass should be evaluated for many earthquake records to clarify the active TMD device requirement. With this purpose, the energy response spectrum for the TMD is defined as

$$V_{t,1}(\mu, g, \omega_o) = \max_{0 \le t \le \infty} \sqrt{\frac{2E_t(\mu, g, \omega_o)}{m_d}} \tag{3.18}$$

where $V_{t,1}$ is obtained for the auxiliary mass m_d instead of m. By definition, the energy response E_t is always positive so that $V_{t,1}$ spectrum is certified to exist for all frequency range. On the other hand, the TMD velocity response spectrum is defined and given by

$$V_{t,2}(\mu, g, \omega_o) = \max_{0 \le t \le \infty} |\dot{y}(t)| \tag{3.19}$$

It is expected that these two response spectra are very close to each other, because the energy does not change significantly for a short amount of time. According to the above definitions, $V_{t,1}$ and $V_{t,2}$ spectra are obtained for the same three earthquake records as before and shown in Figure 3.11 ~ 3.13.

Referring to these response spectra, it is possible to estimate the device capability and the stroke limitation.

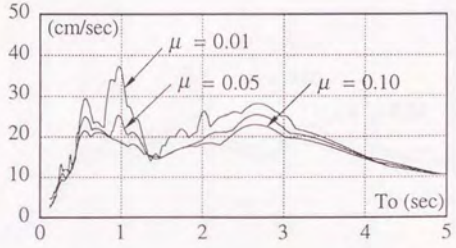

Figure 3.8.a Energy Response Spectrum $V_{s,1}$
[El Centro (NS) 100 gal (Passive TMD)]

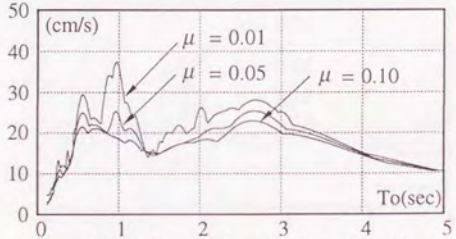

Figure 3.8.b Velocity Response Spectrum $V_{s,2}$
[El Centro (NS) 100gal (Passive TMD)]

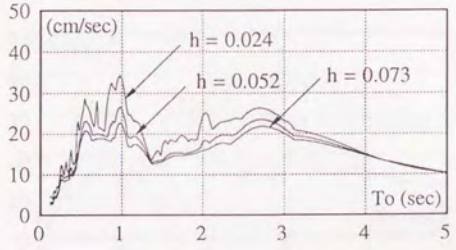

Figure 3.8.c Velocity Response Spectrum Vs
[El Centro (NS) 100gal]

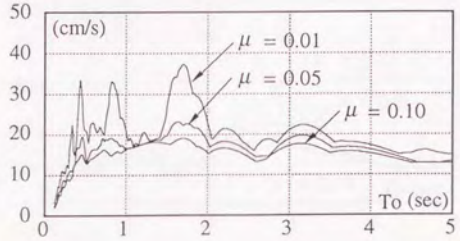

Figure 3.9.a Energy Response Spectrum $V_{s,1}$
[Taft (EW) 100gal (Passive TMD)]

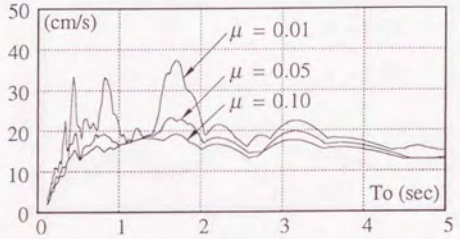

Figure 3.9.b Velocity Response Spectrum $V_{s,2}$
[Taft (EW) 100gal (Passive TMD)]

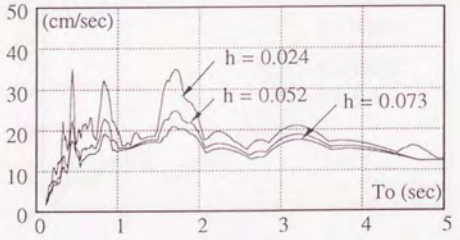

Figure 3.9.c Velocity Response Spectrum *Vs*
[Taft (EW) 100gal (Passive TMD)]

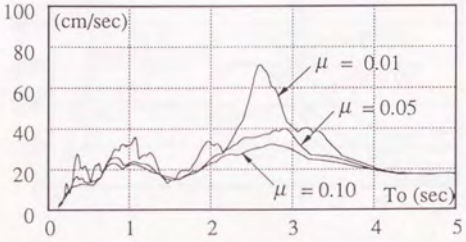

Figure 3.10.a Energy Response Spectrum $V_{s,1}$
[Hachinohe (NS) 100gal (Passive TMD)]

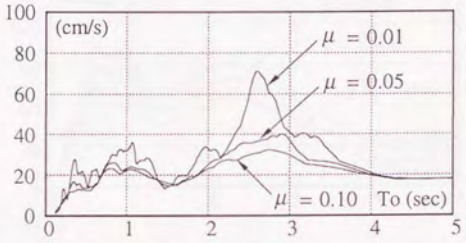

Figure 3.10.b Velocity Response Spectrum $V_{s,2}$
[Hachinohe (NS) 100gal (Passive TMD)]

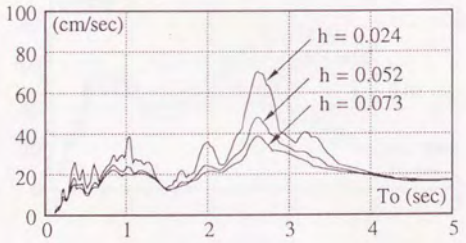

Figure 3.10.c Velocity Response Spectrum *Vs*
[Hachinohe (NS) 100gal]

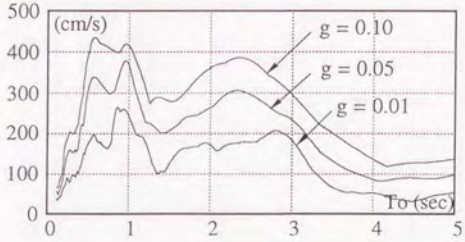

Figure 3.11.a Energy Response Spectrum Vt,1
[El Centro (NS) 100gal μ = 0.01]

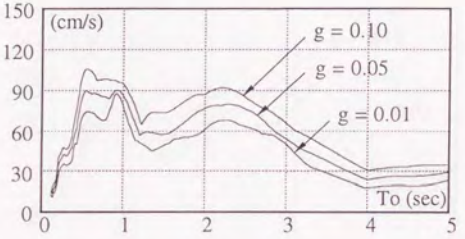

Figure 3.11.b Energy Response Spectrum Vt,1
[El Centro (NS) 100gal μ = 0.05]

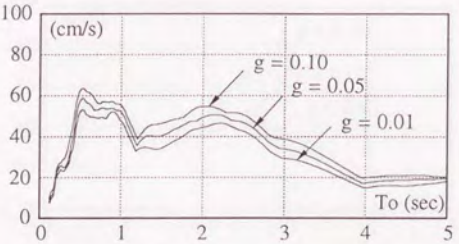

Figure 3.11.c Energy Response Spectrum Vt,1
[El Centro (NS) 100gal μ = 0.10]

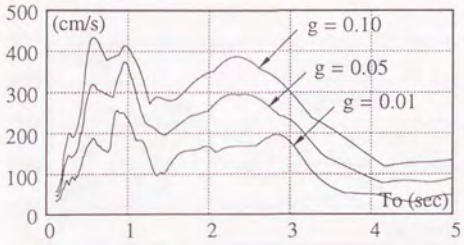

Figure 3.11.d Velocity Response Spectrum Vt,2
[El Centro (NS) 100gal μ = 0.01]

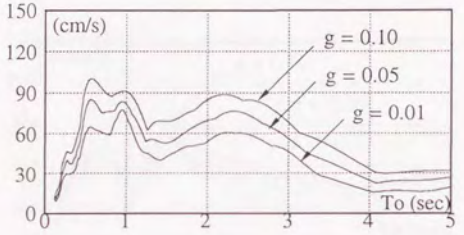

Figure 3.11.e Velocity Response Spectrum Vt,2
[El Centro (NS) 100gal μ = 0.05]

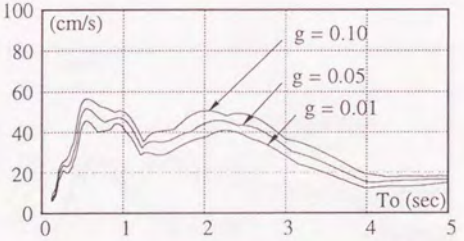

Figure 3.11.f Velocity Response Spectrum Vt,2
[El Centro (NS) 100gal μ = 0.10]

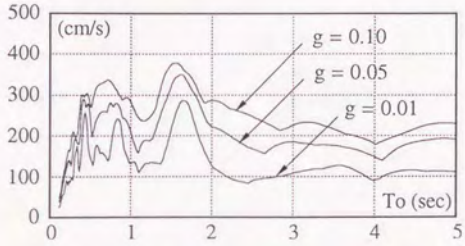

Figure 3.12.a Energy Response Spectrum Vt,1
[Taft (EW) 100gal μ = 0.01]

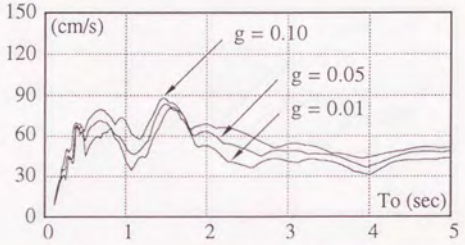

Figure 3.12.b Energy Response Spectrum Vt,1
[Taft (EW) 100gal μ = 0.05]

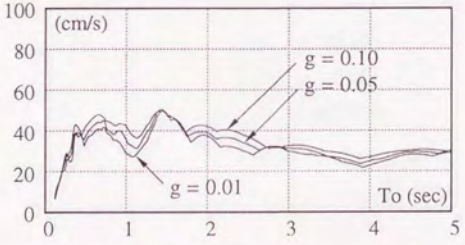

Figure 3.12.c Energy Response Spectrum Vt,1
[Taft (EW) 100gal μ = 0.10]

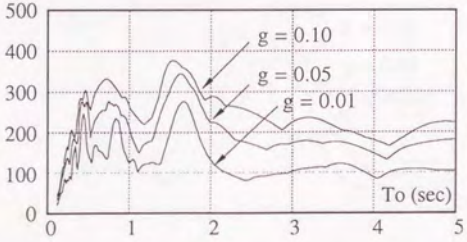

Figure 3.12.d Velocitry Response Spectrum Vt,2
[Taft (EW) 100gal μ = 0.01]

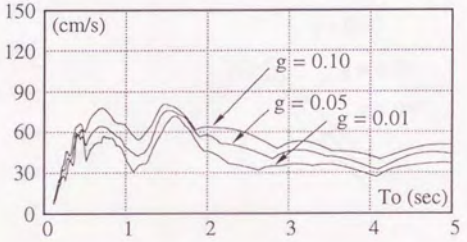

Figure 3.12.e Velocitry Response Spectrum Vt,2
[Taft (EW) 100gal μ = 0.05]

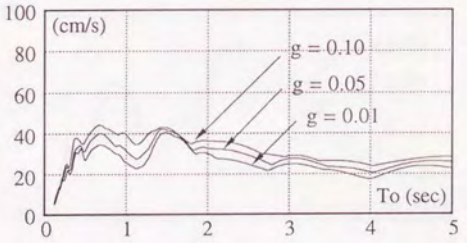

Figure 3.12.f Velocity Response Spectrum Vt,2
[Taft (EW) 100gal μ = 0.10]

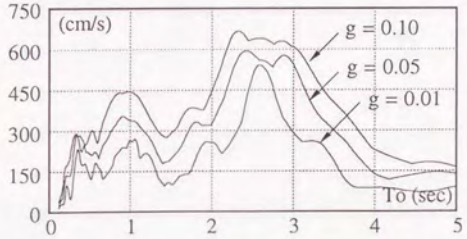

Figure 3.13.a Energy Response Spectrum Vt,1
[Hachinohe (NS) 100gal μ = 0.01]

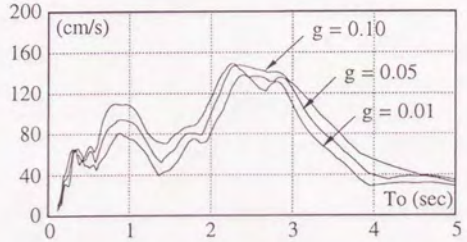

Figure 3.13.b Energy Response Spectrum Vt,1
[Hachinohe (NS) 100gal μ = 0.05]

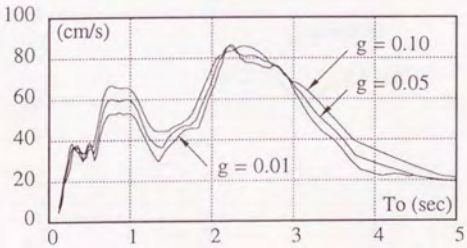

Figure 3.13.c Energy Response Spectrum Vt,1
[Hachinohe (NS) 100gal μ = 0.10]

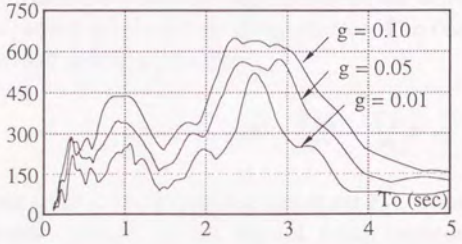

Figure 3.13.d Velocity Response Spectrum Vt,2
[Hachinohe (NS) 100gal μ = 0.01]

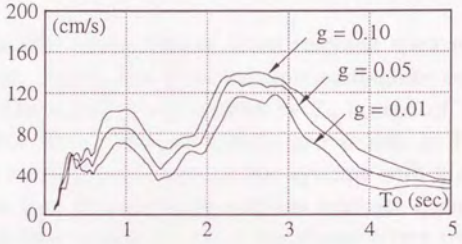

Figure 3.13.e Velocity Response Spectrum Vt,2
[Hachinohe (NS) 100gal μ = 0.05]

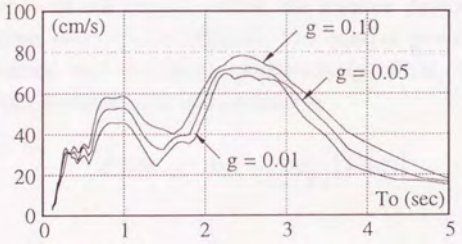

Figure 3.13.f Velocity Response Spectrum Vt,2
[Hachinohe (NS) 100gal μ = 0.10]

3.4 Control Force and Power Requirement

One of the important active device requirement is the control force necessary for the actuator which drives the auxiliary mass. The control force per unit weight of the primal system is given by

$$u(t) = -g\ddot{x} - \frac{g_v}{m}\dot{y} - \frac{g_d}{m}y \tag{3.20}$$

We introduce the control force response spectrum F_c , whose definition is such that the maximum response of the control force recorded under a certain earthquake disturbance is plotted for a system with a given set of μ and g with respect to a variable ω_o. The statement above is interpreted to

$$F_c(\mu, g, \omega_o) = \max_{0 \le t \le \infty} |u(t)| \tag{3.21}$$

Apparently, the unit of the control force response spectrum F_c is cm/sec^2 or acceleration unit. Again, the three example earthquake records are used for this analysis. The x-axis is represented by T_o instead of ω_o as usual. The resulting control force response spectra are shown in Figure 3.14 ~ 3.16. Obviously, the control force required for systems with high feedback gain is relatively larger than those systems with low feedback quantity. The natural period of the primal system T_o has a significant effect on the control force requirement. As T_o becomes longer, the required control force decreases sharply. Hence, it can be said that it is easier to reduce tall building vibration rather than low rise building response that is normally high frequency.

It is pointed out that the energy in a cumulative sense does not matter for the active member of the device, while the passive device design is strictly restrained by those energy accumulation. The control power necessary for the actuator is obtained and discussed quantitatively. First, the control power response spectrum is introduced and defined as

$$P_c(\mu, g, \omega_o) = \max_{0 \le t \le \infty} |\dot{y}\, u(t)| \tag{3.22}$$

where P_c is the maximum power recorded during an earthquake disturbance. The unit of this response spectrum is (cm^2/s^3). Therefore, it is not influenced by the weight of the primal structure.

Again, the same three earthquake records are used for this study to obtain the power response spectra which are shown in Figure 3.17 ~ 3.19. The peak value is significantly influenced by the feedback gain and the mass ratio. If the same control performance is aimed, it is far better to increase the mass ratio rather than the feedback gain. Because the power requirement is much higher for a high feedback system with a small TMD than for a low feedback system with a larger TMD.

One of the important criteria for the design of an active TMD is the power requirement. Even if the control force requirement is large, there is a way to reduce it by means of a lever. Yet, there is no way to reduce the power requirement. If we wish to make an active TMD for seismic response control of a building structure, the power capacity of the device would be the most important criterion.

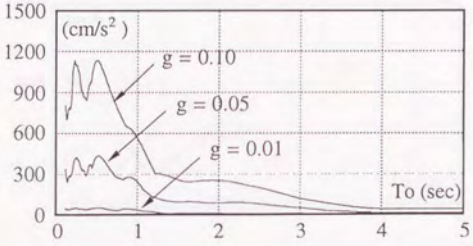

Figure 3.14.a Control Force Response Spectrum Fc
[El Centro (NS) 100gal μ = 0.01]

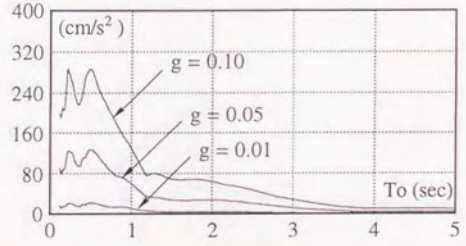

Figure 3.14.b Control Force Response Spectrum Fc
[El Centro (NS) 100gal μ = 0.05]

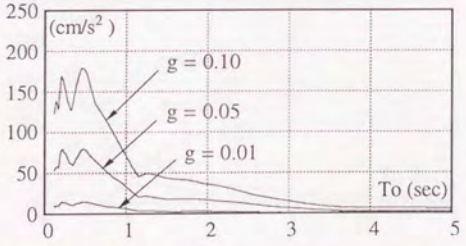

Figure 3.14.c Control Force Response Spectrum Fc
[El Centro (NS) 100gal μ = 0.10]

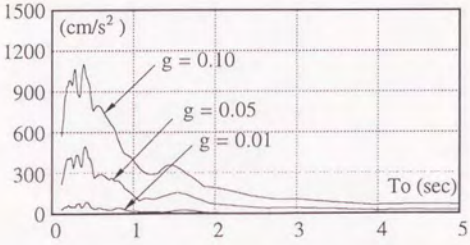

Figure 3.15.a Control Force Response Spectrum Fc
[Taft (EW) 100gal μ = 0.01]

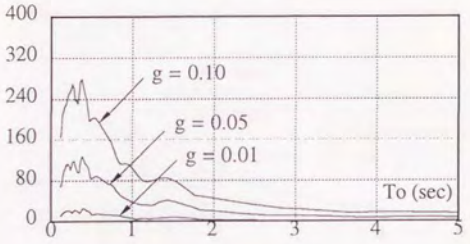

Figure 3.15.b Control Force Response Spectrum Fc
[Taft (EW) 100gal μ = 0.05]

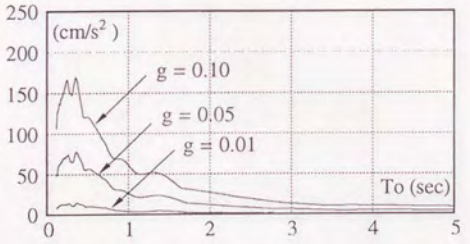

Figure 3.15.c Control Force Response Spectrum Fc
[Taft (EW) 100gal μ = 0.10]

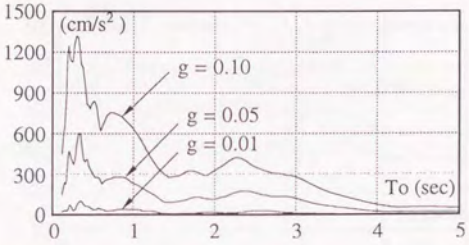

Figure 3.16.a Control Force Response Spectrum Fc
[Hachinohe (NS) 100gal μ = 0.01]

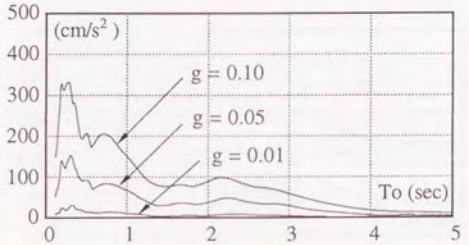

Figure 3.16.b Control Force Response Spectrum Fc
[Hachinohe (NS) 100gal μ = 0.05]

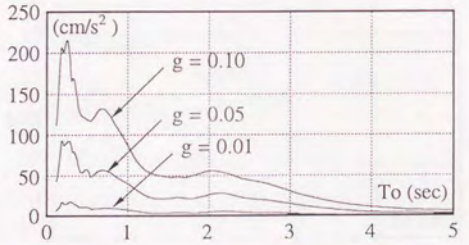

Figure 3.16.c Control Force Response Spectrum Fc
[Hachinohe (NS) 100gal μ = 0.10]

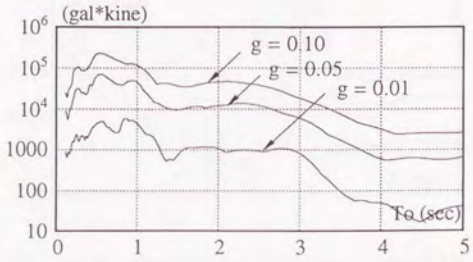

Figure 3.17.a Control Power Response Spectrum Pc
[El Centro (NS) 100gal μ = 0.01]

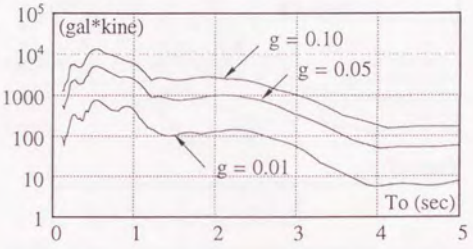

Figure 3.17.b Control Power Response Spectrum Pc
[El Centro (NS) 100gal μ = 0.05]

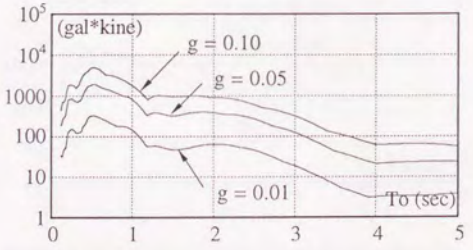

Figure 3.17.c Control Power Response Spectrum Pc
[El Centro (NS) 100gal μ = 0.10]

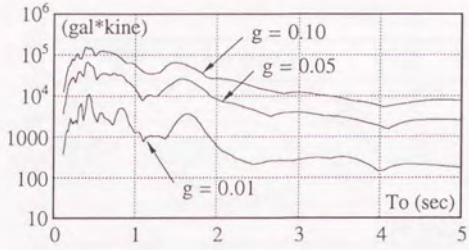

Figure 3.18.a Control Power Response Spectrum Pc
[Taft (EW) 100gal μ = 0.01]

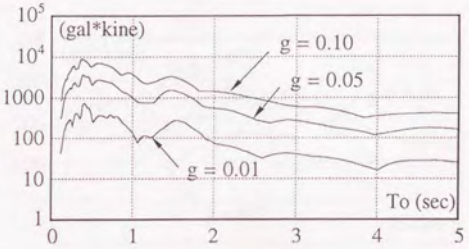

Figure 3.18.b Control Power Response Spectrum Pc
[Taft (EW) 100gal μ = 0.05]

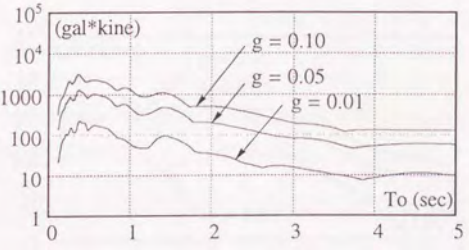

Figure 3.18.c Control Power Response Spectrum Pc
[Taft (EW) 100gal μ = 0.10]

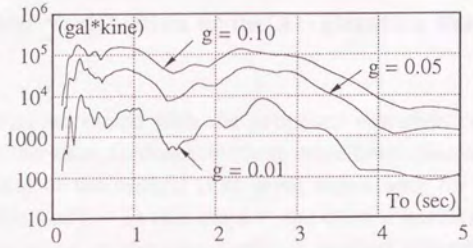

Figure 3.19.a Control Power Response Spectrum Pc
[Hachinohe (NS) 100gal μ = 0.01]

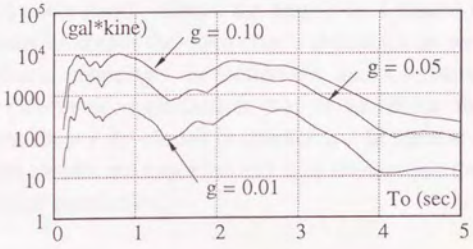

Figure 3.19.b Control Power Response Spectrum Pc
[Hachinohe (NS) 100gal μ = 0.05]

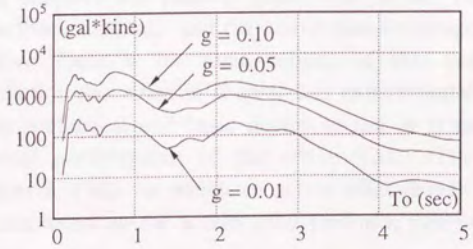

Figure 3.19.c Control Power Response Spectrum Pc
[Hachinohe (NS) 100gal μ = 0.10]

Chapter 4

Experimental Verification of the Acceleration Feedback Method

Numerous merits associated with the proposed vibration control strategy, or the absolute acceleration feedback method, have been theoretically made clear. But the feasibility of the method is of great importance for application, which is the goal of this study. In this chapter, the control performance of the active TMD according to the acceleration feedback method is experimentally studied. The general description of the experimental study is given in the first section. The verification of the theoretical study counts on the precision of the experiment, especially the system identification, because it would be impossible to verify the control algorithm unless the dynamic properties of the specimen devices are well understood. Hence the emphasis is placed on the preliminary identification tests to obtain the controller's dynamics as well as the specimen structure's dynamic property. In section 4.5 and 4.6, there are reported the results of the parameter optimization that is based on the obtained device dynamics and the theory developed in chapter 2. In the end of this chapter, the shaking table test results are reported and it is shown that they are well agreed with the theoretical prediction.

4.1 Scope of Experiment

There are three different types of vibration absorbing devices which are studied in this chapter: the passive TMD, the active TMD based on the acceleration feedback method, and the active passive composite TMD (Figure 4.1). The active TMD is the main subject of this experiment, and the theoretical prediction described in chapter 2 is experimentally observed. The passive TMD is a classical and basic device so that it is used as an index to assess the control performance of the active TMD. The composite TMD consists of a passive TMD on which an active mass driver (AMD) is placed. The control force based on the acceleration feedback method is created by the

reaction force of an actuator, while the necessary control force for the composite TMD is generated by the inertia force of the AMD.

This unique device is an invention by Toshikazu Yamada [22]. The paper was submitted to Japan Patent Bureau in 1986 to claim for its license permission. Yet, the appropriate control algorithm had been unknown until the absolute acceleration feedback method was discovered by the author [18] in 1992 followed by the successive papers [19],[20]. This device has several superiority to the direct-drive active TMD when applied to large structures. For example, there is no mechanical noise vibration that is induced and transferred to the building structure by the active mass driver (AMD), because the actuator is not directly attached to the structure. Hence the motion of the active device (AMD) is more stable and free from high frequency noise contamination. A second merit is that the passive portion can be used as the passive TMD when the active portion does not move in case of emergency power failure. Therefore, the fail safe mechanism is automatically achieved without any additional complexity. Moreover, the active portion mass is extremely small as compared with the bulk weight of the primal structure so that the feasibility of the active TMD methodology is increased significantly by means of this invention. Finally, the active control force necessary for this device is reduced substantially because the size of the AMD is quite small.

These three different control devices are tested by a shaking table (See Photo 4.1) which can generate both harmonic and random excitations. Prior to the shaking table test, there are conducted several identification tests to obtain the dynamic properties of the control devices and the specimen structure. Attention is paid to the system identification phase of the experiment. Because the precision of the identification influences the control performance, the device requirement, and the agreement between the experimental observation and the theoretical prediction. After the system identification is conducted, the aforementioned three devices are numerically studied to determine the parameters according to the theory in chapter 2. Then, each device is excited on the shaking table to verify the control performance both under harmonic and random excitation. In the end of this chapter, there are also several numerical analyses carried out to compare the experimental result with the theoretical prediction. As a result, the feasibility and practicability of the control methodology associated with the theory developed in chapter 2 are verified experimentally.

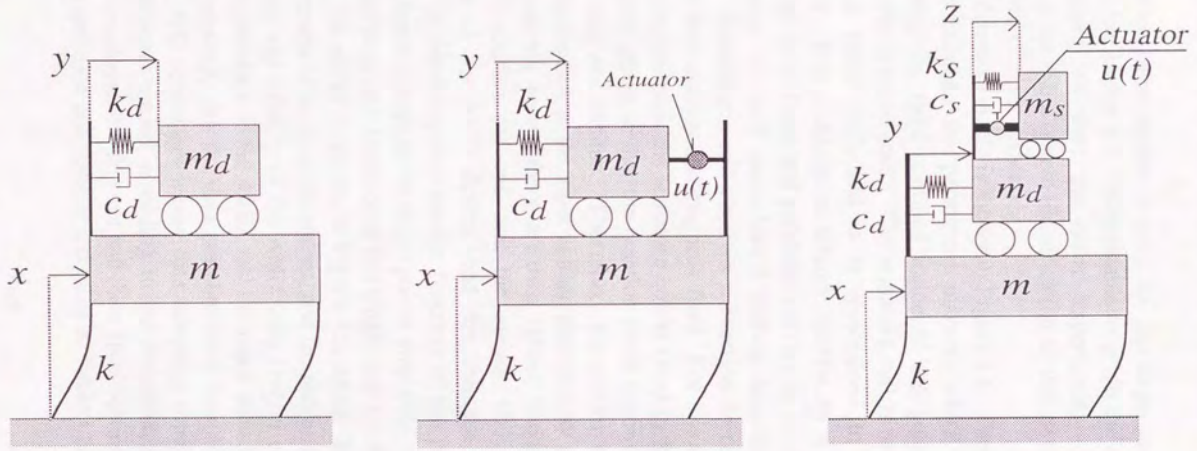

Passive TMD

Active TMD

Composite TMD

Figure 4.1 Specimen Devices Employed for the Experiment

4.2 Identification of the Active Mass Driver

An electro-magnetic excitor is used for this experimental study as an active control device. Hence it is indispensable to grasp the dynamic property of the excitor before we start the entire experiment. The objective of this preliminary test is the system identification of this device, which is referred to as Active Mass Driver (AMD).

The details of AMD is shown in Figure 4.2. There is a moving armature coil placed between the permanent magnets which generate a strong and uniform magnetic field confined inside of the yoke that is enclosed by a housing frame made of steel. The armature coil is mechanically supported by two sliding linear rails and it is constrained to move within 15.0 cm horizontally. It is provided an electric current by a power amplifier, which takes voltage as an input and produces current as an output. Under ordinary circumstances, this coil starts lateral motion according to the input voltage linearly. Because the coil receives a reaction force which is linear to the intensity of both current and magnetic field. For this specific test set up shown in Figure 4.3, however, the armature coil is fixed to the reaction floor by way of the support plates so that the reaction force is converted into the motion of the whole magnetic excitor. Therefore, the excitor body, which weighs 37.8 kg, moves according to the input voltage provided by the power amplifier. As for the restoring force, there are two rubber bands placed parallel to the magnets to connect the coil and the excitor body. This is the general description of the AMD device used for this test. The identification is completed by obtaining the transfer function of the response of AMD weight versus the input voltage given to the power amplifier. As a result, we come to know the stiffness and damping of this single-degree-of oscillator.

The test set up is shown in Figure 4.3, which illustrates the signal flow, the arrangement of sensing equipment, and the measuring system. The relative displacement and velocity of the AMD with respect to the reaction floor, the absolute acceleration of the AMD, and the input sinusoidal signal are measured all simultaneously. All the data are converted into digital sequential numbers by way of A/D converters whose data sampling time and measuring duration are appropriately varied according to the excitation frequency. The sensing equipment employed for this test and their specifications are given in Table 4.1. The data acquisition condition is indicated in Table 4.2, where the test results

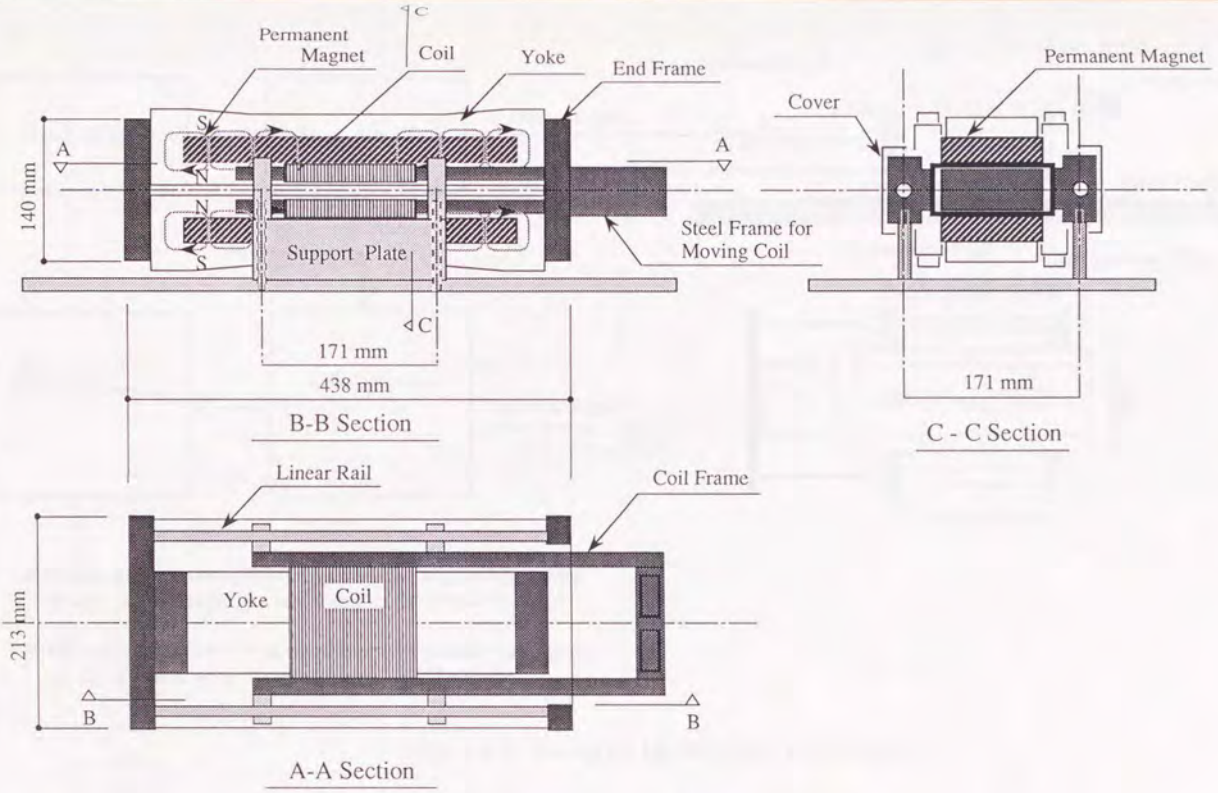

Figure 4. 2 Active Mass Driver (AMD)

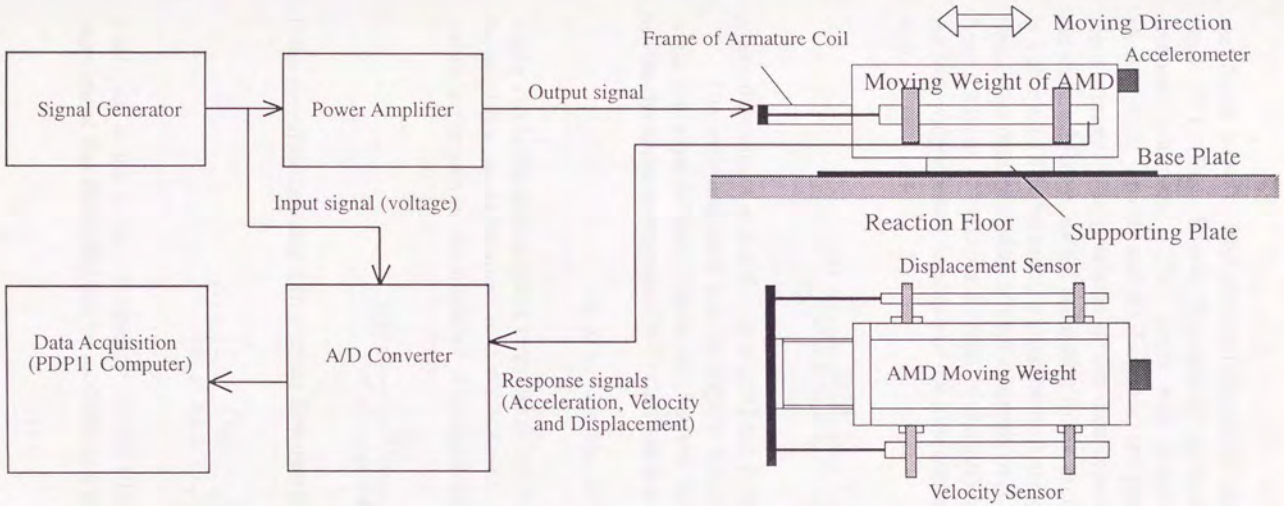

* Frame of amarture coil is fixed to the supporting plate which is then rigidly connected to the reaction floor.

* The velocity sensor and displacement sensor can move in accordance with the motion of AMD weight.

Figure 4. 3 Set Up of Identification Test of AMD

are shown as well. The obtained sequential digital data are processed by the usual FFT (Fast Fourie Transform) procedure and converted into the frequency domain. The phase and magnitude of the three responses (acceleration, velocity and displacement) are plotted in Figure 4.4-4.9 versus the input voltage. The precision of the data depends on the length of measuring duration, which is varied according to the excitation frequency as is indicated in Table 4.2. The harmonic excitation tests are repeated as many as plot points. Hence the data precision is kept constant over the entire range of frequency from 0.2 Hz to 15.0 Hz. As a result of the curve fitting, we eventually obtained the following transfer function of the displacement $x(s)$ versus the input voltage $v(s)$.

$$x(s) = \left(\frac{0.65}{s^2 + 6.5s + 32.0}\right)\left(\frac{94.2}{s + 94.2}\right)v(s) \tag{4.1}$$

where the units of $x(s)$ and $v(s)$ are [m] and [voltage], respectively.

The indicated solid lines in Figure 4.4~4.9 are in accordance with (4.1), while the experimental results are marked by 'o'. Suppose that the AMD system dynamics is expressed in a relatively low frequency range by

$$m_s\ddot{x} + c_s\dot{x} + k_s x = G_a\, v(t) \tag{4.2}$$

where $x(t)$ is the displacement response of the AMD, $v(t)$ is the input voltage to the amplifier, m_s is the mass, c_s is the damping, k_s is the stiffness of the AMD, and G_a is the gain of the amplifier. The input-output relation is expressed by

$$x(s) = \frac{G_a}{m_s s^2 + c_s s + k_s}\, v(s) \tag{4.3}$$

If the amplifier contains a first order low pass filter, (4.3) is modified into

$$x(s) = \left(\frac{G_a}{m_s s^2 + c_s s + k_s}\right)\left(\frac{\omega_c}{s + \omega_c}\right)v(s) \tag{4.4}$$

where ω_c is the corner frequency of the filter. It is understood from the experiment that the AMD can be modeled as a second order oscillator coupled

Table 4.1 Test Equipment

Item	Type	Specification
Accelerometer	Japan Air Electric Inc. Model MA101-10	Sensitivity : 0.5vol/G Limit : 10.0G
Velocity Sensor	Cheavitz LVT Model 7L10 VT-Z	Sensitivity : 8.0mm/s per mV Stroke Limit : 250mm
Displacement sensor	Kyowa Co. LVDT Model DLT-100BS	Sensitivity : 0.0267 vol/mm (with Linear Amplifier)
AMD	Acoustic Power System Inc. APS Model 113	Stroke Limit : 15.0 cm Max. Force: 2.45×10^2 N
Power Amplifier	APS Model 114	Max. Input Level : 10vol

Table 4.2 Measuring Condition and Test Results

Frequency	Sampling Time	Sampling Duration	Acceleration		Velocity		Displacement	
(Hz)	(1/sec)	(sec)	Amp. (gal/v)	Phase (deg)	Amp. (kine/v)	Phase (deg)	Amp. (cm/v)	Phase (deg)
0.2	20	400	3.71	-174.9	2.41	95.3	1.92	5.1
0.3	30	267	8.56	166.9	4.18	77.0	2.22	-12.9
0.4	40	200	15.8	151.7	5.99	61.7	2.39	-28.2
0.5	50	160	21.2	135.2	6.64	45.5	2.11	-44.6
0.6	60	134	29.5	122.9	7.76	33.2	2.06	-56.8
0.7	70	115	42.7	111.5	9.73	21.7	2.21	-68.2
0.8	80	100	43.5	98.8	8.70	9.0	1.73	-80.9
0.9	90	89	46.9	88.7	8.41	-1.2	1.48	-90.9
1.0	100	80	61.2	76.5	9.87	-13.4	1.57	-103.2
1.1	110	73	62.1	68.0	9.14	-21.8	1.32	-111.4
1.2	120	67	59.6	62.3	8.07	-27.7	1.07	-117.1
1.5	150	54	63.4	45.2	6.93	-44.7	0.73	-134.3
2.0	200	40	66.6	23.0	5.53	-66.7	0.43	-156.4
2.5	250	32	63.9	10.0	4.32	-79.6	0.27	-169.6
3.0	300	27	61.4	2.2	3.52	-87.5	0.18	-177.4
4.0	400	20	56.3	-9.2	2.54	-98.7	0.10	171.4
5.0	500	16	51.9	-10.8	2.00	-100.8	0.06	172.4
6.0	600	14	48.4	-17.4	1.67	-107.4	0.04	162.5
8.0	800	10	43.3	-25.9	1.32	-115.8	0.02	145.8
10.0	1000	8	37.6	-32.2	1.11	-122.3	0.02	132.7
12.0	1200	6.7	36.3	-37.8	1.06	-127.9	0.02	122.7
15.0	1500	5.3	35.4	-44.4	1.03	-133.7	0.02	114.8

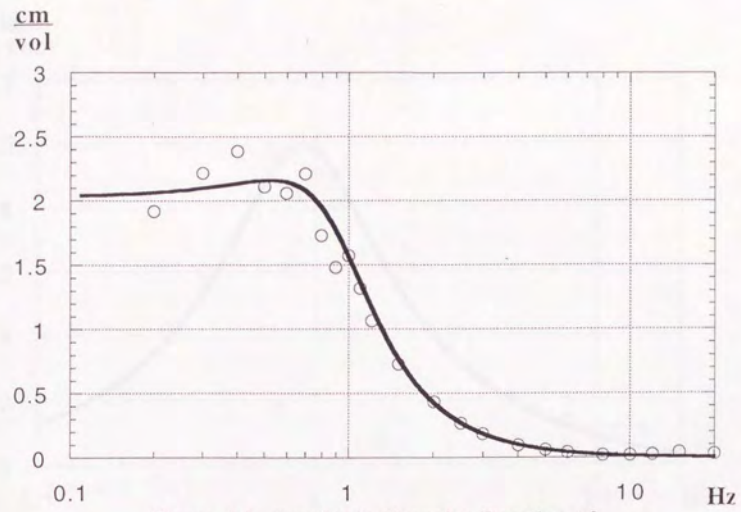

Figure 4.4 Amplitude Transfer Function of
AMD Displacement versus Input Voltage

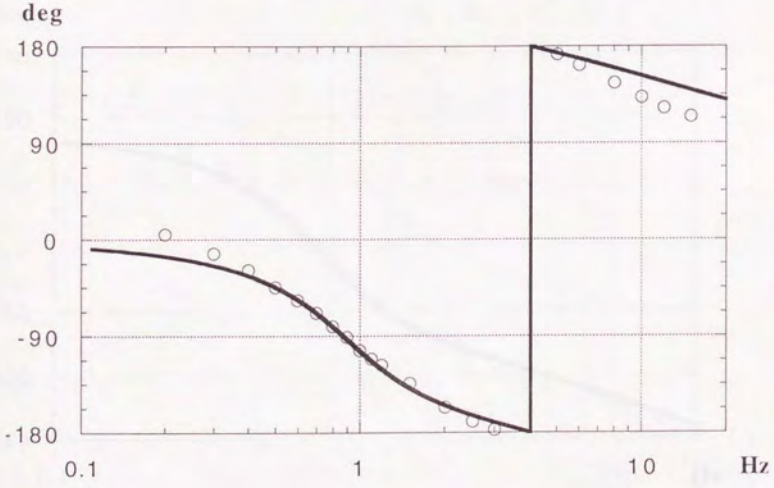

Figure 4.5 Phase Transfer Function of
AMD Displacement versus Input Voltage

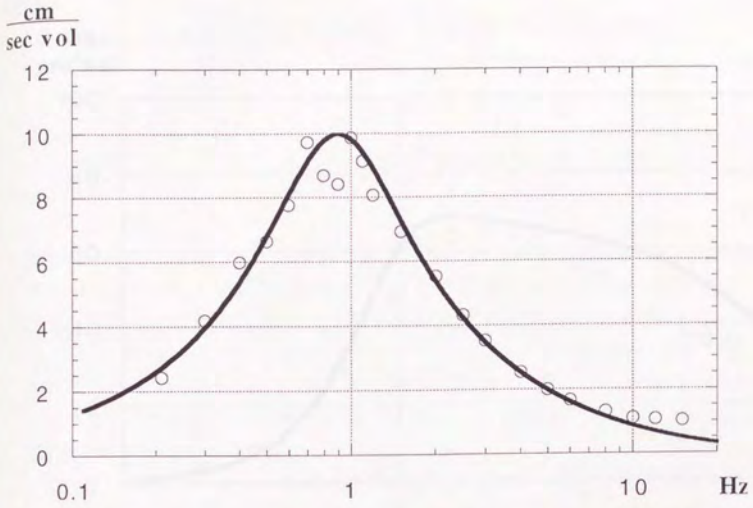

Figure 4.6 Amplitude Transfer Function of AMD Velocity versus Input voltage

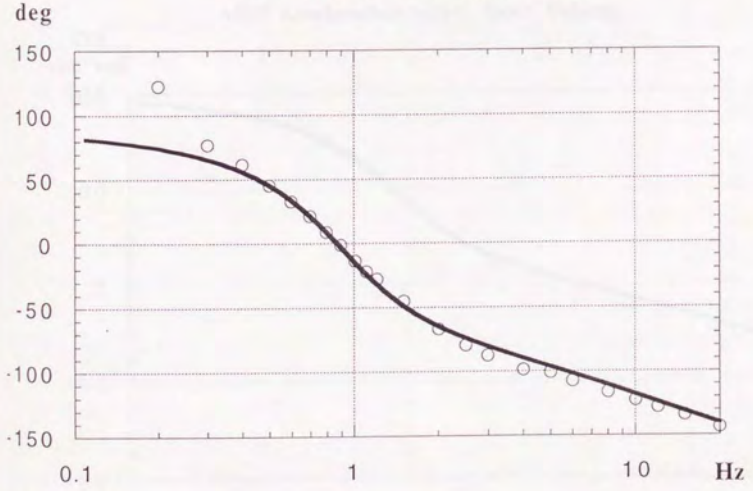

Figure 4.7 Phase Transfer Function of AMD Velocity versus Input Voltage

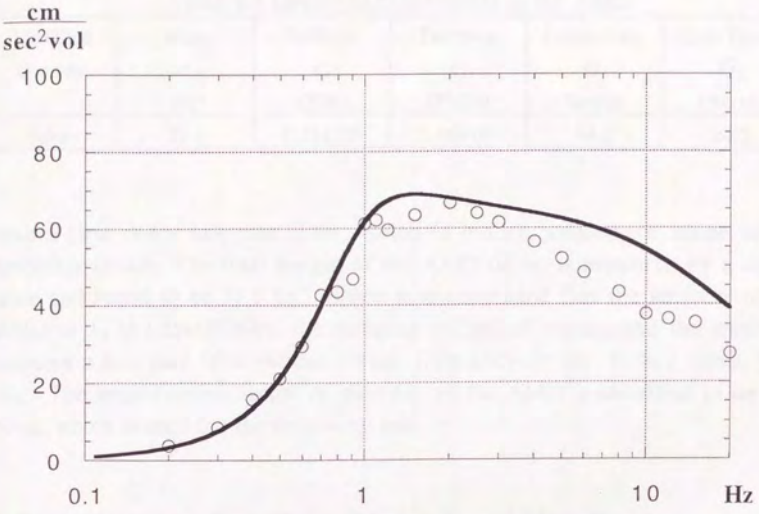

Figure 4.8 Amplitude Transfer Function of AMD Acceleration versus Input Voltage

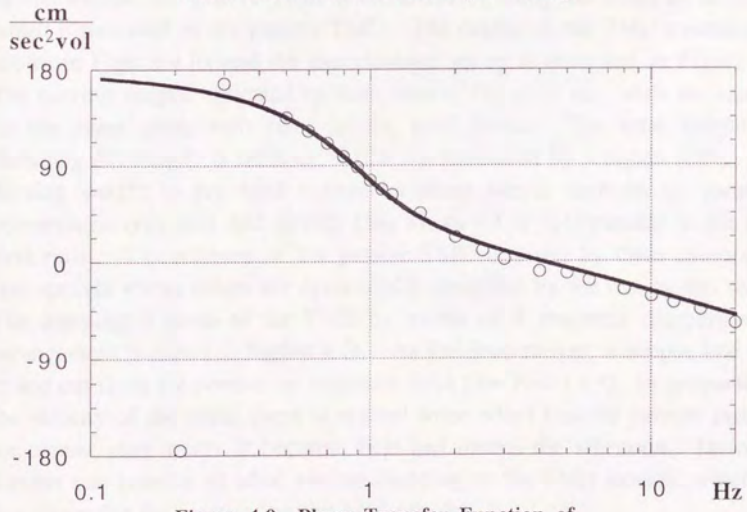

Figure 4.9 Phase Transfer Function of AMD Acceleration versus Input Voltage

Table 4.3 Identified Coefficients of the AMD

Identified Quantity	Mass m_s (kg)	Stiffness k_s (N/m)	Damping c_s (Ns/m)	Corner Frq. ω_c (rad/s)	Gain Factor G_a (N/vol)
Values	37.8	1.21×10^3	2.46×10^2	94.2	24.5

with a first order low pass filter, which is hidden somewhere inside of the amplifier circuit. The total weight of the AMD or m_s is measured by a digital scale and found to be 37.8 kg. Hence it is concluded that the stiffness of the AMD or k_s is 1.21×10^3 N/m, the damping is 2.46×10^2 Nsec/m, and the amplifier contains a low pass filter whose corner frequency or ω_c is 94.2 rad/sec (15.0 Hz). The amplification factor or gain G_a of the AMD is identified to be 24.5 N/vol, which is used for the following test.

4.3 Identification Test of the Passive Tuned Mass Damper

In this section, the passive TMD is identified by using the AMD as an excitor which is mounted on the passive TMD. The details of the TMD mechanism is shown in Figure 4.10, and the experimental set up is indicated in Figure 4.11. The moving weight, indicated by slash lines in Fig. 4.10, can slide uni-laterally on the linear guide rails fixed to the steel frame. The total weight (not including AC motor) is 388.6 kg, which was measured by a digital scale. This moving weight is provided a predetermined lateral stiffness by means of compression type steel coil springs (See Photo 4.3 or 4.4) parallel to the linear steel rails. The stiffness of the passive TMD is given by these compression type springs whose values are dynamically identified by the test in this section. The damping is given to the TMD by means of 4 magnetic dampers whose arrangement is shown in Figure 4.10. As the mass moves, a copper late slides in and out from the permanent magnetic field (See Photo 4.3). In proportion to the velocity of the mass, there is created some whirl flow of current inside of the copper plate where it becomes heat and damps the vibration. Hence this damper can provide an ideal viscous damping to the TMD motion, which is a key factor for the verification test of the theory.

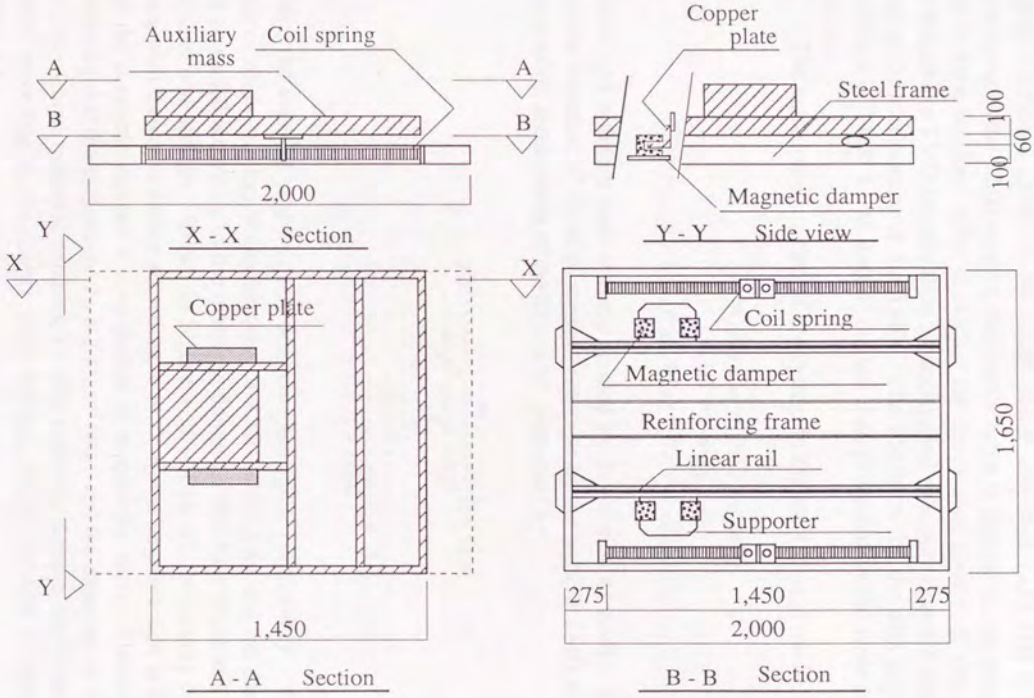

Figure 4.10 Passive TMD Specimen

The test set up is shown in Figure 4.11, whose model is shown in Figure 4.12. The data acquisition flow is also indicated in Figure 4.11. The AMD is placed on the passive TMD and the signal generator is used to provide the input signal (sinusoidal signal) to the AMD power amplifier (APS 114) to excite it. According to the AMD motion, the inertia force is applied to the passive TMD and it starts motion. After it reaches the steady state condition, the responses of the passive TMD (acceleration , velocity, and displacement) are measured as well as the acceleration of the AMD. The condition for the data acquisition is indicated in Table 4.5 as well as the test data processed in the same manner as before.

The equation of motion of the system in Figure 4.12 is given below.

$$\begin{cases} m_s(\ddot{z}+\ddot{y})+c_s\dot{z}+k_s z = u(t) \\ u_e(t) = -m_s(\ddot{y}+\ddot{z}) \\ m_d\ddot{y}+c_d\dot{y}+k_d y = u_e(t) \end{cases} \tag{4.5}$$

where $u_e(t)$ is the net control force created by the motion of AMD. Hence the transfer function of the displacement response of the passive TMD $y(t)$ versus the absolute acceleration of AMD can be expressed by

$$y(s) = \frac{-m_s}{m_d s^2 + c_d s + k_d}(\ddot{z}+\ddot{y})(s) \tag{4.6}$$

$$y(s) = \frac{-0.0973}{s^2 + 0.75s + 68.0}(\ddot{z}+\ddot{y})(s) \tag{4.7}$$

where the units of y and $(\ddot{x}+\ddot{y})$ are [cm] and [gal], respectively. The AMD mass or m_s is 37.8 kg, while the mass of TMD is 388.6 kg and the damping, c_d can be varied according to the magnetic damper. But k_d is fixed and given by the steel coil springs. Shown in Figure 4.13 ~ 4.18 are the results of the test along with the curve fitting according to (4.7), whose negative sign is taken off, and the magnetic damper's contribution is supposedly zero. Therefore, it is concluded that the stiffness or k_d is 2.65×10^4 N/m , and the damping is 2.7×10^2 N s/m (4% without magnetic damping). The magnetic damper coefficient can be varied according to the copper plate margin, whose relation is identified in section 4.4.

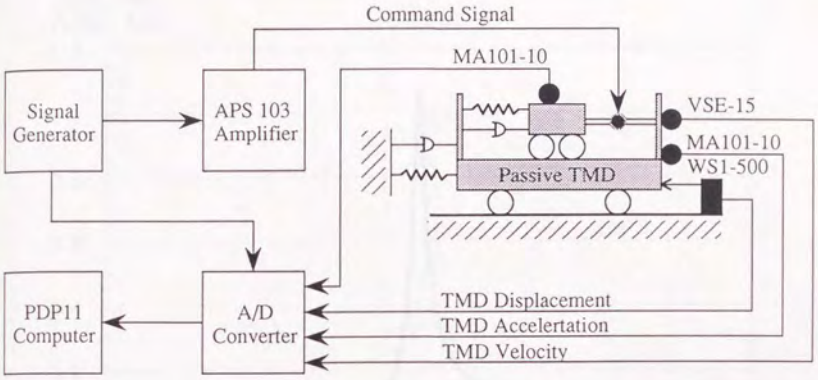

Figure 4.11 Set Up of the Passive TMD Identification Test

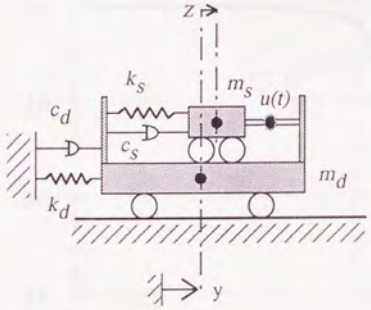

ms : Mass of the AMD
cs : Damping of the AMD
ks : Stiffness of the AMD
md : Mass of the Passive TMD
cd : Damping of the Passive TMD
kd : Stiffness of the Passive TMD
u(t) : Control Force of the AMD
z : Response Displacement of the AMD
y : Response Displacement of the TMD

Figure 4.12 Model of the Identification Test

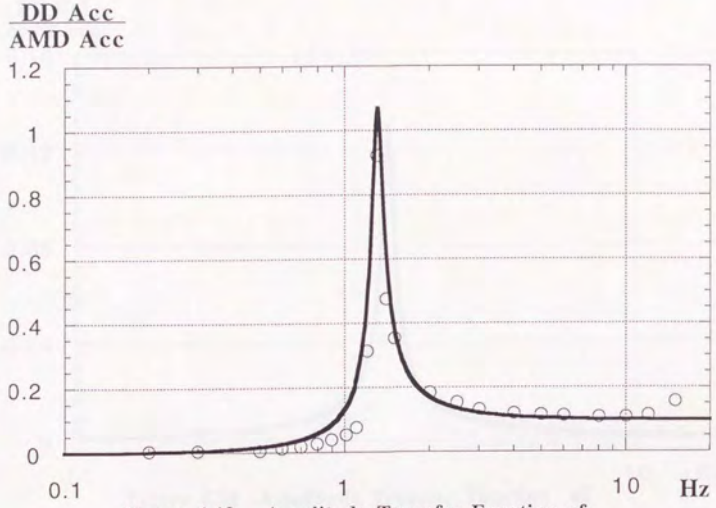

Figure 4.13 Amplitude Transfer Function of DD Acceleration versus AMD Acceleration

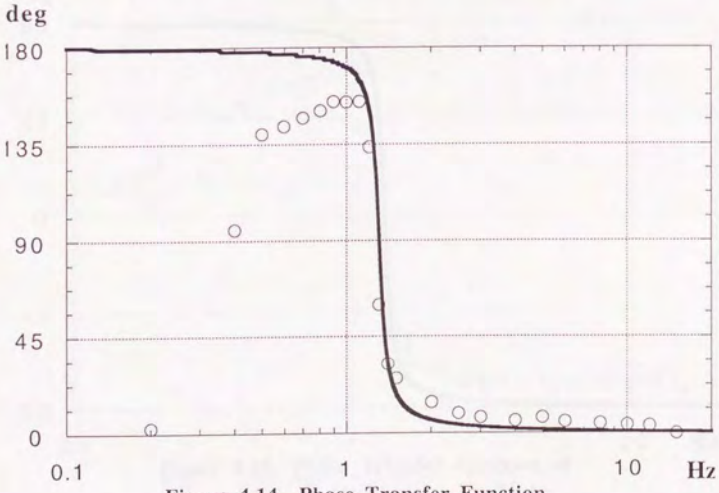

Figure 4.14 Phase Transfer Function of DD Acceleration versus AMD Acceleration

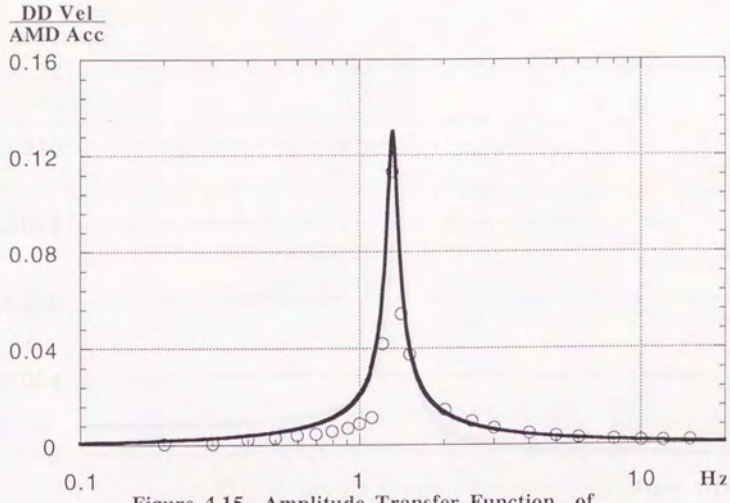

Figure 4.15 Amplitude Transfer Function of DD Velocity versus AMD Acceleration

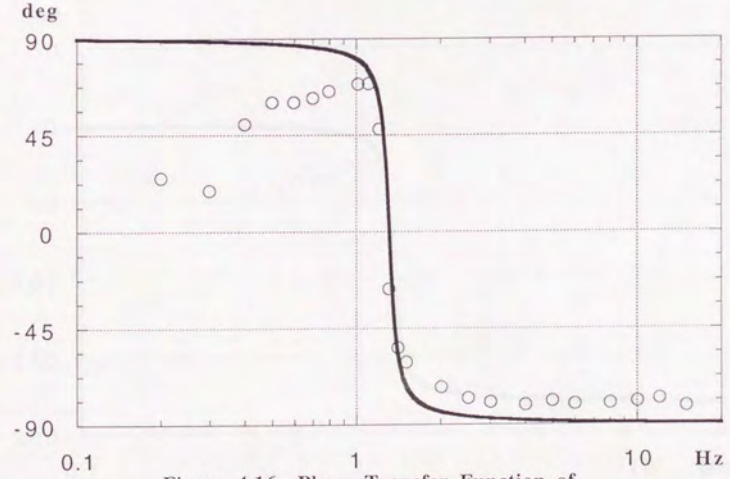

Figure 4.16 Phase Transfer Function of DD Velocity versus AMD Acceleration

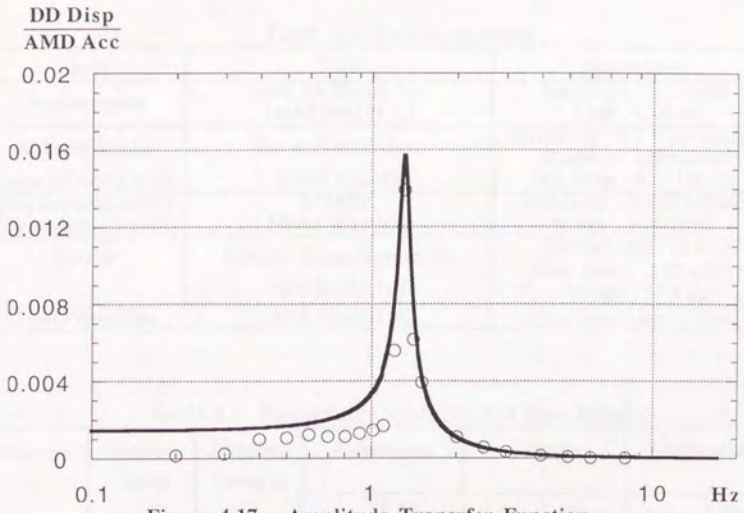

Figure 4.17 Amplitude Transrfer Function
of DD Displacement versus AMD Acceleration

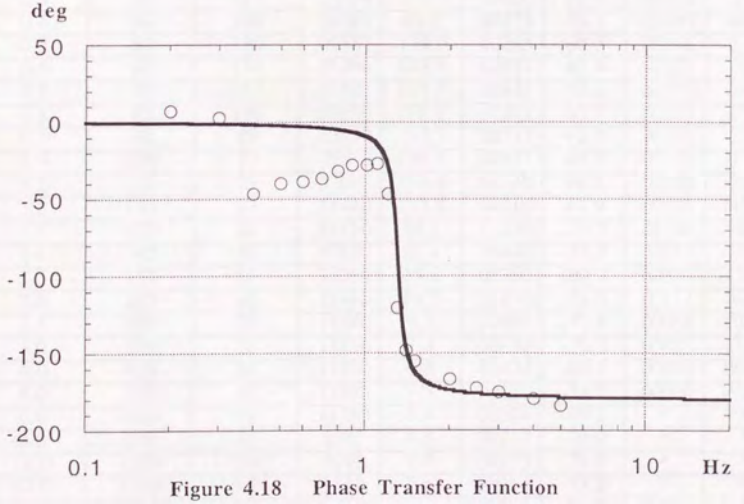

Figure 4.18 Phase Transfer Function
of DD Displacement versus AMD Acceleration

Table 4.4 Test Equipment

Item	Type	Specification
Accelerometer	Japan Air Electric Inc. Model MA101-10	Sensitivity : 0.5 vol/G Limit : 10.0 G
Velocity Sensor (none reference type)	Tokyo Sokusin Inc. Model VSE-15	Sensitivity : 0.1 V per cm/sec Range: +- 100 cm/sec Frq. range : 0.1~100 Hz
Displacement sensor (wire disp. sensor)	ASM Co. Model WS1-500	Sensitivity : 0.002 vol/mm Range : 0~500 mm
Excitor	Acoustic Power System Inc. APS Model 113	Stroke Limit : 15.0 cm Max. Force: 2.45 x10^2 N Weight : 37.8 kg
Power Amplifier	APS Model 114	Max. Input Level : 10vol

Table 4.5 Measuring Condition and Test Results

Frequency	Sampling Time	Sampling Duration	Acceleration		Velocity		Displacement	
(Hz)	(1/sec)	(sec)	Amp. (gal/gal)	Phase (deg)	Amp. kine/gal	Phase (deg)	Amp. (cm/gal)	Phase (deg)
0.2	20	400	.00526	2.8	.00065	25.2	.00016	7.2
0.3	30	267	.00559	177.9	.00066	19.3	.00026	2.7
0.4	40	200	.00289	95.2	.00235	50.1	.00099	-46.7
0.5	50	160	.00587	139.9	.00295	60.5	.00106	-39.8
0.6	60	134	.01246	143.3	.00412	60.4	.00121	-38.7
0.7	70	115	.01841	147.3	.00471	62.5	.00113	-36.7
0.8	80	100	.02650	150.7	.00571	65.7	.00113	-31.9
0.9	90	89	.03870	154.7	.00713	92.5	.00129	-28.0
1.0	100	80	.05410	154.6	.00887	68.9	.00146	-27.9
1.1	110	73	.07690	154.9	.01140	69.1	.00168	-26.9
1.2	120	67	.31440	133.8	.04210	47.9	.00560	-46.6
1.3	130	62	.92150	59.7	.11330	-26.5	.01390	-120.5
1.4	140	58	.47650	32.4	.05440	-53.9	.00617	-148.0
1.5	150	54	.35380	25.6	.03760	-60.7	.00395	-154.9
2.0	200	40	.18440	14.3	.01470	-72.3	.00111	-166.7
2.5	250	32	.15380	9.2	.00980	-77.5	.00058	-172.5
3.0	300	28	.13150	7.4	.00699	-79.3	.00033	-175.1
4.0	400	20	.11860	5.9	.00474	-80.6	.00016	180.6
5.0	500	16	.11590	7.3	.00371	-78.7	.00009	176.2
6.0	600	14	.11250	5.5	.00301	-80.1	*	*
8.0	800	10	.1083	4.5	.00217	-79.9	*	*
10.0	1000	8.0	.1091	3.9	.00175	-78.9	*	*
12.0	1200	6.7	.1141	3.6	.00154	-77.8	*	*
15.0	1500	5.3	*	*	.00169	-81.2	*	*

Table 4.6 Mass, Stiffness and Damping of the Passive TMD

Mass (kg)	Damping (N sec/m)	Stiffness (N/m)
388.6	270.0 (4%)	2.65×10^4 N/m (1.27 Hz)

4.4 Identification of the Active Tuned Mass Damper

In this section, the system dynamics of the active TMD with an AC servo motor is identified. The AC servo motor can generate torque which is linear to the input signal or voltage, however, the inertia of the motor axis has some influence on the final dynamics so that the effective mass of the active TMD is different from the total weight of the TMD. The compensation for this rotational inertia is conducted as follows. The equation of motion in Figure 4.19.a is given below.

$$\begin{cases} m_d\ddot{x} = -c_d\dot{x} - k_d x + R_t \\ I_d\ddot{\theta} = -R_t r + M_t \\ x = \theta r \end{cases} \tag{4.8}$$

where x is the displacement response of the weight, θ is the rotation of the A/C motor, m_d is the mass, k_d is the stiffness, c_d is the damping of the active TMD, R_t is the reaction force, r is the equivalent radius of the motor axis, I_d is the equivalent rotational inertia associated with the motor torque, and M_t is the motor torque.

Equation (4.8) is reduced to

$$\left(m_d + \frac{I_d}{r^2}\right)\ddot{x} + c_d\dot{x} + k_d x = \frac{M_t}{r} \tag{4.9}$$

The motor torque is supposed to be linear to the input voltage, because the AC motor's physical principle is exactly the same as the AMD excitor. For this specific device, there is a servo amplifier matched to the motor, however, the circuits information is not precisely available. Hence we suppose that the

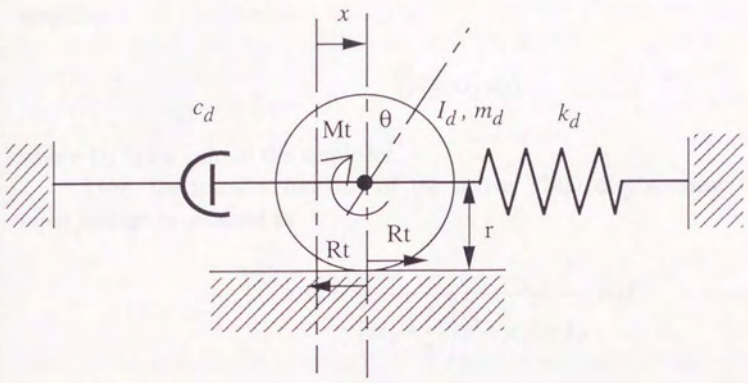

Figure 4.19 Active TMD with AC Servo Motor

torque generated from the motor is linear to the input voltage to the servo amplifier.

$$\frac{M_t}{r} = G_d\, v(t) \tag{4.10}$$

where G_d is the gain of the amplifier.

Then, the transfer function of the active TMD displacement from the input voltage is obtained as

$$x(s) = \frac{G_d}{\left(m_d + \frac{I_d}{r^2}\right)s^2 + c_d s + k_d}\, v(s) \tag{4.11}$$

Thought the system dynamics is expressed in (4.11), the effective inertia force acting on the primal specimen structure is associated with the mass m_d. Hence (4.11) is converted into

$$\begin{aligned} x(s) &= \frac{G_e}{m_d s^2 + c_e s + k_e}\, v(s) \\ &= \frac{\gamma G_d}{m_d s^2 + \gamma c_d s + \gamma k_d}\, v(s) \\ \gamma &= \frac{m_d}{\left(m_d + \frac{I_d}{r^2}\right)} \end{aligned} \tag{4.12}$$

where k_e is the effective stiffness, c_e is the effective damping coefficient, G_e is the effective gain factor, and γ is the compensation factor. Equation (4.12) can be substituted for the ordinary second order system with a force control actuator.

The test set up is shown in Photo 4.2, where the damping due to the magnetic damper is set to zero. In other words, c_d is provided by the self inductance of the motor coil not by the magnetic dampers. But the stiffness is given by the steel coil springs whose coefficient k_d is already identified by the

previous test, which is 27.0 kgf/cm or 2.65×10^4 N/m. The total weight is 441.6 kg which contains the additional weight of the A/C motor (53 kg). Neither the gain factor nor the motor inertia is known until the identification test is conducted. Therefore, the objective of this identification test is to obtain the compensation factor γ and the gain factor G_e. The measuring condition for data acquisition and the test results are shown in Table 4.7 and Figures 4.20 ~ 4.22. The final resulting transfer function of the active TMD response versus the input voltage is given by

$$x(s) = \left(\frac{0.84}{s^2 + 3.5s + 56}\right)\left(\frac{4000}{s^2 + 15s + 4000}\right)v(s) \qquad (4.13)$$

where the units of x and v are [m] and [voltage], respectively. Obviously, there is a second order low pass filter inside of the power amplifier. Finally, the identified coefficients are all given in Table 4.8.

Table 4.7 Measuring Condition and Test Results

Frequency	Sampling Time	Sampling Duration	Acceleration		Velocity		Displacement	
(Hz)	(1/sec)	(sec)	Amp. (gal/vol)	Phase (deg)	Amp. kine/vol	Phase (deg)	Amp. (cm/vol)	Phase (deg)
0.2	20	400	2.41	176.6	1.8	86.6	1.44	-11.6
0.4	40	200	9.94	163.2	4.09	85.6	1.64	-16.8
0.6	60	133	29.24	158.6	7.72	75.4	2.03	-23.1
0.8	80	100	57.93	143.9	11.53	60.2	2.28	-36.5
1.0	100	80	106.4	120.3	16.84	34.5	2.65	-61.1
1.2	120	66.7	178.4	86.1	23.73	0.2	3.12	-94.5
1.6	160	50	118.8	48.0	11.7	-38.4	1.15	-133.2
2.0	200	40	103.0	36.0	8.21	-51.4	0.646	-147.0
3.0	300	26.7	99.9	8.2	5.29	-79.3	0.272	-178.3
4.0	400	20	136.2	-1.0	5.45	-89.6	0.173	178.5
5.0	500	16	110.8	-2.4	4.23	-90.0	0.129	178.4
6.0	600	13.3	131.4	-7.1	3.75	-90.5	0.096	171.1
7.0	700	11.4	140.9	-17.7	4.24	-105.0	0.087	157.7
8.0	800	10	186.3	-35.4	4.42	-120.9	0.086	144.6
9.0	900	8.9	221.8	-38.9	4.96	-125.9	0.089	141.0
10.0	1000	8	278.4	-73.3	5.41	-160.0	0.085	101.2
11.0	1100	7.27	337.7	-87.6	4.83	-174.3	*	*
12.0	1200	6.67	312.2	-120.4	3.26	153.7	*	*
13.0	1300	6.15	229.1	-139.6	2.31	134.4	*	*
14.0	1400	5.71	109.7	-150.1	1.35	122.9	*	*

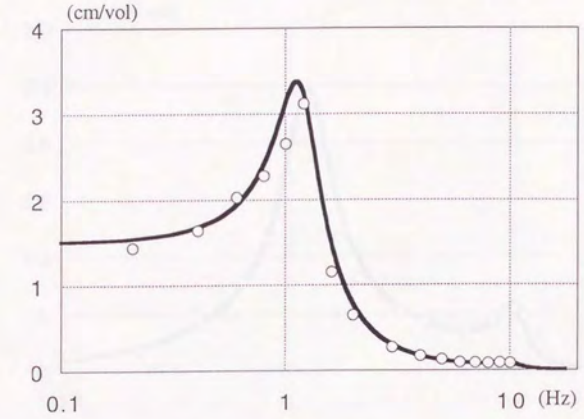

Figure 4.20.a Displacement versus Input Votage (Amplitude)

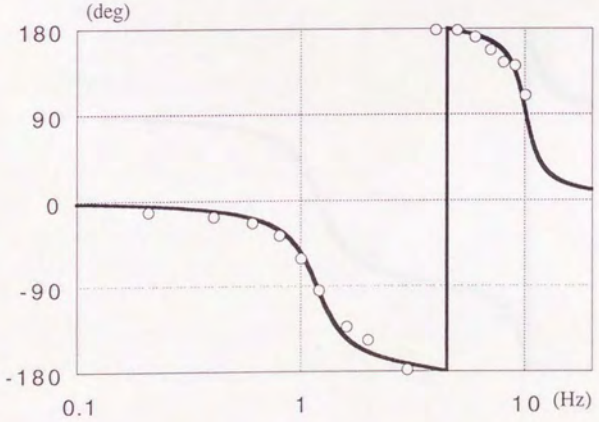

Figure 4.20.b Displacement versus Input Voltage (Phase)

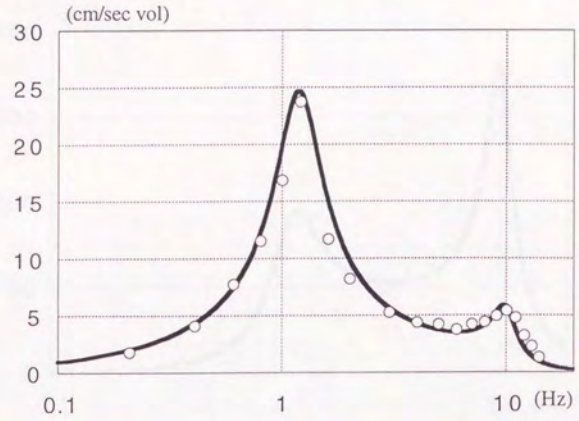

Figure 4.21.a Velocity versus Input Voltage (Amplitude)

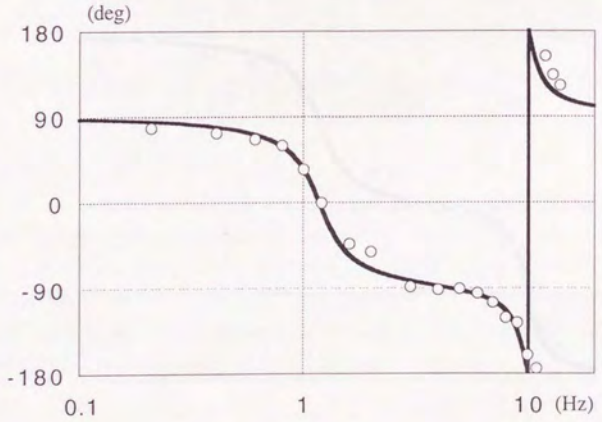

Figure 4.21.b Velocity versus Input Voltage (Phase)

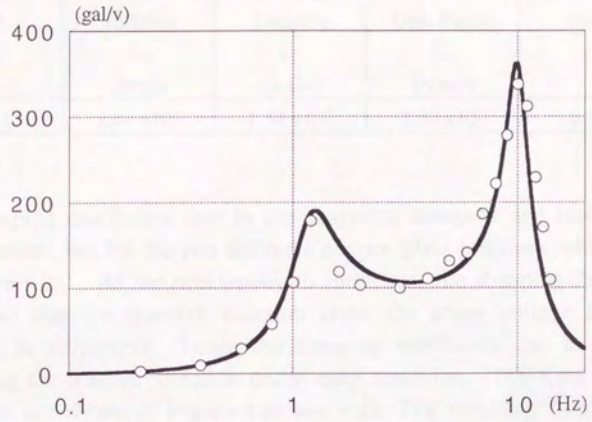

Figure 4.22.a Acceleration versus Input Voltage (Amplitude)

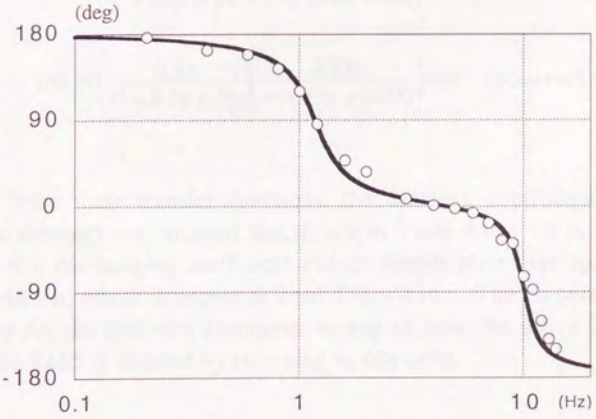

Figure 4.22.b Acceleration versus Input Voltage (Phase)

Table 4.8 Identified Parameters of the Active TMD

Mass md (kg)	Effective Stiffness k_e (N/m)	Effective Damping c_e (N s/m)	Effective Gain Factor G_e (N/vol)	Compensation Factor γ
441.6	2.47×10^4	1.54×10^3	3.70×10^2	0.932

The damping coefficient due to the magnetic dampers are identified by the same method, but for the two different copper plate positions which are shown in Figure 4.23. As the overlap width increases, the damping factor becomes larger so that the transfer function from the input voltage to the output response is influenced. Hence the damping coefficient can be identified by observing the transfer function under each condition. The final results of the two cases are shown in Figure 4.24 and 4.25. The resulting transfer functions are

$$x(s) = \left(\frac{0.84}{s^2 + 6.0s + 56}\right)\left(\frac{4000}{s^2 + 15s + 4000}\right)v(s) \quad \text{(when t = 2.85 cm)} \qquad (4.14)$$

$$x(s) = \left(\frac{0.84}{s^2 + 8.5s + 56}\right)\left(\frac{4000}{s^2 + 15s + 4000}\right)v(s) \quad \text{(when t = 5.0 cm)} \qquad (4.15)$$

Judging from these transfer functions, the damping coefficients due to the magnetic dampers are obtained and shown in Table 4.10. It is fairly safe to estimate that the damping coefficient and the copper plate overlap width have a linear relation, which is expected from Table 4.10. The damping adjustment necessary for the optimum parameter setting of both the active TMD and the composite TMD is realized by referring to this table.

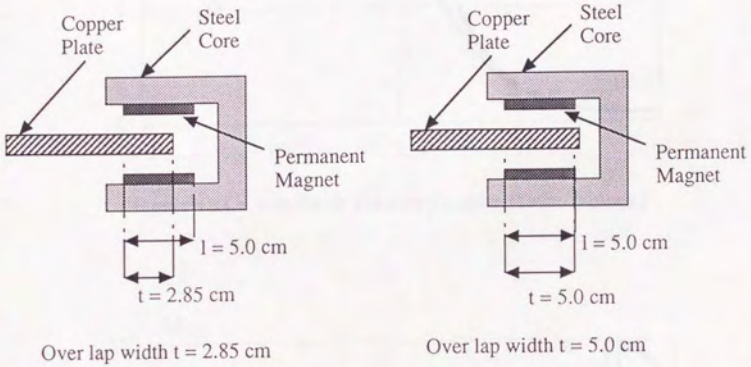

Figure 4.23 Magnetic Damper and Overlap Width

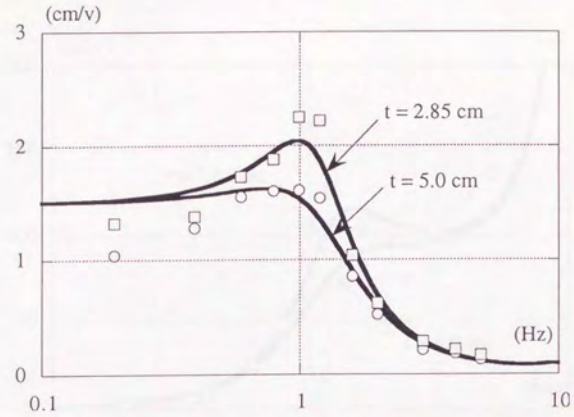

Figure 4.24.a Amplitude Transfer Function (Disp./ Voltage)

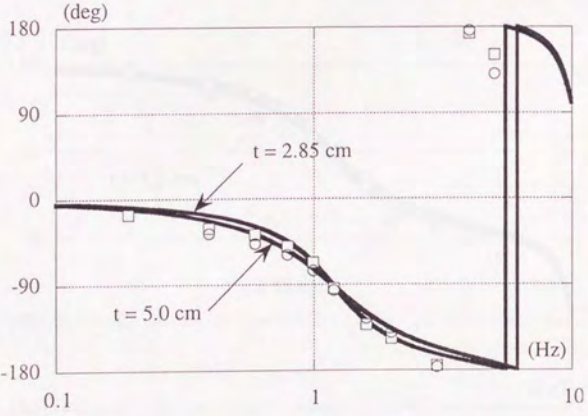

Figure 4.24.b Phase Transfer Function (Disp./Voltage)

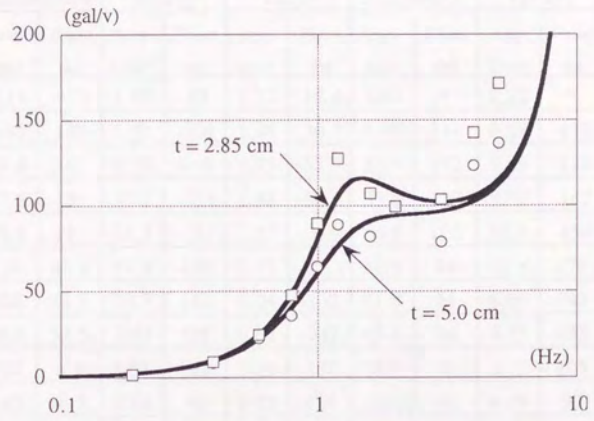

Figure 4.25.a Amplitude Transfer Function (Acc./ Voltage)

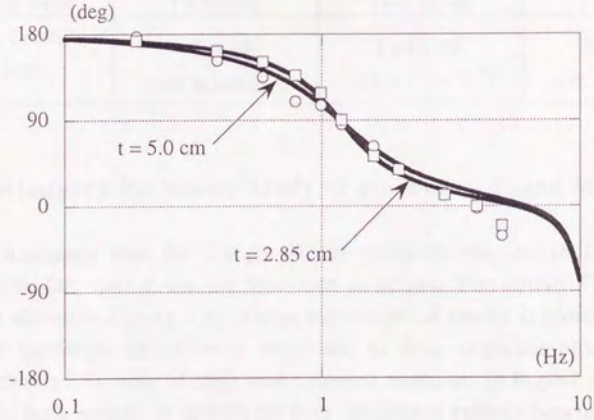

Figure 4.25.b Phase Transfer Function (Acc./ Voltage)

Table 4.9 Test Result of the Damping Identification

Freq. (Hz)	Case 1 (Overlap width = 2.85 cm)						Case 2 (Overlap width = 5.0cm)					
	Acceleration		Velocity		Disp.		Acceleration		Velocity		Disp.	
	Amp. gal/v	Phase deg	Amp. kine/v	Phase deg	Amp. cm/v	Phase deg	Amp. gal/v	Phase deg	Amp. kine/v	Phase deg	Amp. cm/v	Phase deg
0.2	2.11	-179	1.68	-83	1.32	-16.4	1.69	*	1.32	*	1.04	*
0.4	8.84	149	3.52	-108	1.38	-30.7	8.40	144	3.28	-113	1.28	-28
0.6	24.6	142	6.52	-119	1.73	-37.9	22.4	132	5.89	-128	1.55	-45
0.8	47.8	130	9.51	-133	1.88	-50.2	35.6	120	8.02	-142	1.60	-70
1.0	89.8	113	14.3	-151	2.25	-66.9	64.5	105	10.2	-159	1.61	-74
1.2	128	85.8	17.0	-180	2.22	-94.2	88.9	84	11.8	179	1.54	-94
1.6	108	48.1	10.7	142	1.04	-132	81.8	54	8.66	149	0.86	-117
2.0	99.6	33.5	7.93	128	0.62	-147	85.8	40	6.77	133	0.52	-141
3.0	104	4.4	5.51	102	0.29	-176	78.7	4	4.12	105	0.21	-166
4.0	142	-6.5	5.68	90	0.22	174	123.4	-4	4.89	90	0.19	178
5.0	171	-29.1	5.46	69	0.17	151	136.4	*	4.35	60	0.13	149
6.0	192	-59.0	5.09	38	0.13	*	*	*	*	148	*	-125

Table 4.10 Relation of Damping Coefficient and Copper Plate Overlap Width

Overlap width	t = 0.0 cm	t = 2.85 cm	t = 5.0 cm
Damping Coefficient (N sec/m)	1.54×10^3 (self inductance)	2.64×10^3 ($\Delta\eta = 1.1 \times 10^3$)	3.74×10^3 ($\Delta\eta = 2.2 \times 10^3$)

4.5 Preliminary Parameter Study of the Active Tuned Mass Damper

All the necessary data for the parameter study for the active TMD has been obtained so far, except for the specimen structure. The active TMD specimen set up is shown in Figure 4.26, whose mathematical model is indicated in Figure 4.1. The specimen structure is composed of four concrete blocks connected with each other by way of steel stub columns as shown in Figure 4.26 and Photo 4.7. This bulk weight is upheld by four laminated rubber bearings, which are used as base isolation materials in these days. These rubber bearings are highly flexible in lateral direction but substantially stiff to sustain vertical load, which

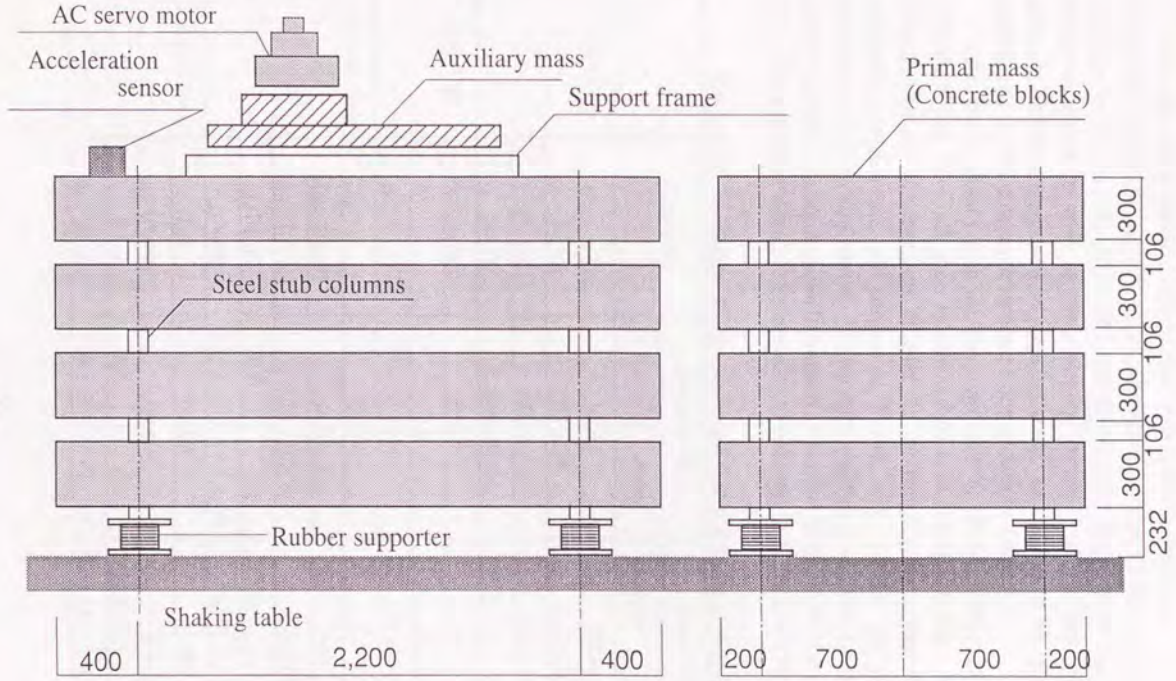

Figure 4.26 Set Up of the Active TMD on the Shaking Table

can make an ideal single-degree-of-freedom model. Because the steel stub columns are rigid enough, compared with rubber bearings, it is possible to neglect the second or higher modal vibrations. Prior to the main shaking table test, free vibration tests are conducted to examine the natural frequency of the structure model as well as the damping factor. The total weight of the concrete blocks is measured by a spring scale, and found to be 16274 kg. The parameters of this specimen structure are shown in Table 4.11.

All the necessary data for the optimization of the active TMD have been obtained. The feedback gain is selected to 0.20 for this study. Recalling the formulae in the summary of chapter 2, we can readily obtain the optimum parameters which are all shown in Table 4.11, where the passive TMD parameters are also indicated. Frequency response analysis is carried out in advance so that the control performance is predicted prior to the shaking table test. The resulting simulated responses are shown in Figure 4.27~4.28.

Table 4.11 Optimum Parameters and Gains for the Active TMD

	Notations	Passive TMD		Active TMD	
		Formula	Actual	Formula	Actual
System Data	m [kg]	16274		16274	
	k [N/m]	1.05×10^6		1.05×10^6	
	c [N s/m]	5.2×10^3		5.2×10^3	
	ω_o [rad/s]	8.04 (1.28Hz)		8.04 (1.28Hz)	
Mass Data	m_d [kg]	441.6		441.6	
	g	0.0		0.200	
	μ	0.0271		0.0271	
Stiffness Data	ξ_{opt}	0.974		0.871	
	ω_{opt} [rad/s]	7.83		7.00	
	k_{opt} [N/m]	2.71×10^4		2.16×10^4	
	g_d [N/m]	0.0	0.0	-1.30×10^4	-0.49×10^4
	k_d [N/m]	2.71×10^4	2.65×10^4	3.46×10^4	2.65×10^4
Damping Data	η_{opt}	0.100		0.288	
	c_{opt} [N s/m]	0.69×10^3		1.78×10^3	
	g_v [N s/m]	0.0	0.0	1.57×10^3	1.54×10^3
	c_d [N s/m]	0.69×10^3	0.70×10^3	0.21×10^3	0.24×10^3

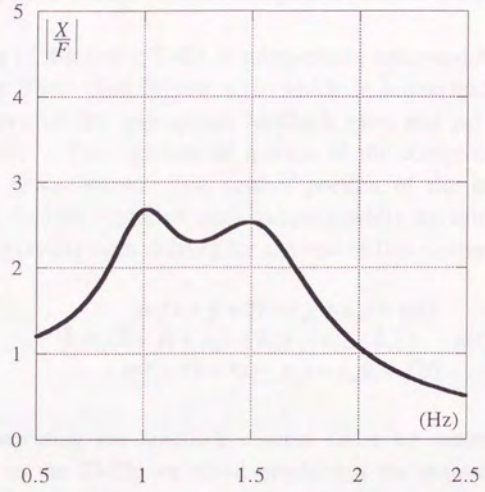

Figure 4.27 Active TMD Preliminary Parametric Study
(Primal System Frequency Response)

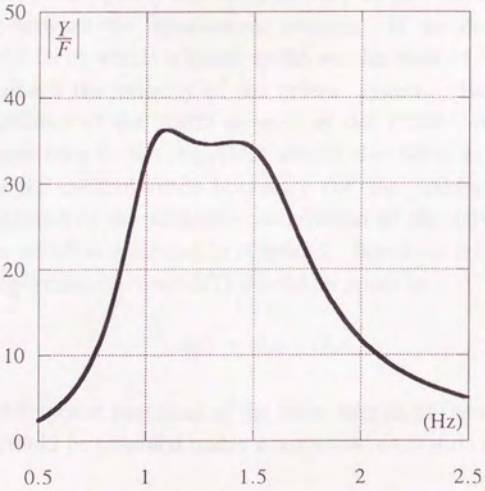

Figure 4.28 Active TMD Preliminary Parametric Study
(Auxiliary System Frequency Response)

4.6 Preliminary Study of the Composite Tuned Mass Damper

The feasibility of the active TMD is substantially enhanced by the invention of the composite TMD (See Figure 4.1), which is numerically studied in this section to determine the appropriate feedback gains and parameters associated with this device. The equation of motion of the composite TMD shown in Figure 4.1 is given below. The passive portion of the composite TMD is referred to as the PMD (passive mass damper), while the active part is referred to as the AMD (active mass driver) for the rest of this section.

$$\left\{ \begin{array}{c} m_s(\ddot{x}+\ddot{y}+\ddot{z}) + c_s\dot{z} + k_s z = u(t) \\ m_d(\ddot{x}+\ddot{y}) + c_d\dot{y} + k_d y - c_s\dot{z} - k_s z = -u(t) \\ m\ddot{x} + c\dot{x} + kx - c_d\dot{y} - k_d y = f(t) \end{array} \right. \tag{4.16}$$

Instead of generating the feedback control force by means of the actuator supplemented to the TMD, we could produce it by activating another small mass, the AMD, attached on the PMD. We should start from reconsidering the feedback strategy because the AMD system dynamics should be taken into account for the optimization process. The basic function of the AMD could be viewed as a differentiator, because the natural frequency of the AMD system is adjusted to the primal system natural frequency so that there is approximately 90° phase lag between the input-output relation. If we desire to obtain the feedback control force which is linear to the acceleration of the primal system, we should feedback the velocity of the primal system. Hence there are the optimum parameters of the AMD as well as the PMD. Another important factor considered here is that the AMD should also work as a damper for the PMD, because the control force necessary for the acceleration feedback is substantially reduced by the adequate combination of the driving force and the damping force, which is discussed in chapter 2. Based on the discussion above, the feedback algorithm for the AMD should be given by

$$u(t) = G_1\dot{x} + G_2 y \tag{4.17}$$

First of all, the response functions of the three degree of freedom model shown in Figure 4.1 should be obtained under a harmonic excitation given by

$$f(t) = F\, m\, (\omega_o)^2 e^{i\omega t} \tag{4.18}$$

Then, the steady state responses of the specimen structure, the PMD, and the AMD are given by (4.19) ~ (4.21), respectively. And the frequency response functions are defined by (4.22), (4.23), and (4.24).

Primal system steady response :	$x(t) = X\, e^{i\omega t}$	(4.19)
PMD system steady response :	$y(t) = Y\, e^{i\omega t}$	(4.20)
AMD system steady response :	$z(t) = Z\, e^{i\omega t}$	(4,21)

Primal system frequency response function :	$\left\lvert \frac{X}{F} \right\rvert (f)$	(4.22)
PMD system frequency response function :	$\left\lvert \frac{Y}{F} \right\rvert (f)$	(4.23)
AMD system frequency response function :	$\left\lvert \frac{Z}{F} \right\rvert (f)$	(4.24)

Utilizing the steady state response functions defined by (4.22), (4.23), and (4.24), a parameter study is carried out. The objective of this study is to investigate the physical meaning of the individual parameter. The mass ratio for the following parameter study is predetermined and given in Table 4.12, where other parameters are also given. They are consistent with the experimental study which follows this section.

1. Feedback Gain G_1

The physical meaning of this feedback gain is the driving force acting on the PMD. As we increase G_1, we seem to have a large passive TMD as far as the response of the primal system is concerned. The response peak of the PMD system is not influenced by this feedback gain, so we could select it independently from the auxiliary system response. In case of the active TMD in chapter 2, there is a locked point in the response function of the active TMD which is defined as β that depends on the mass ratio only. Therefore, it is also expected that the PMD system might have a locked point, no matter what G_1 may be. Hence we could select this feedback gain only considering the control effect of the device.

2. Feedback Gain G_2

The physical meaning of the second feedback gain is a damping force given to the auxiliary system. As we increase G_1 , we should increase G_2 as well. Because the optimum damping necessary for the auxiliary system is to be raised as the acceleration feedback gain increases (c.f. chapter 2). So there should be an optimum feedback gain G_2 , which is linked with the value of G_1 .

3. Stiffness of the PMD

According to the classical passive TMD optimization, it is necessary to adjust the stiffness of the PMD system for balancing the two peaks of the response curve of the primal system. Hence, there should be an optimum stiffness for the PMD which depends on the feedback gain G_1 . The location of these locked points is less influenced by the selection of G_2 , because of the analogy of the active TMD. Hence, after selecting G_1 and G_2 , we could adjust the stiffness of the PMD only paying attention to the response curve of the primal system.

4. Damping of the PMD

As is mentioned before, the passive damping of the PMD will be very small. Because the combination of the driving force due to G_1 and the active damping due to G_2 will shrink at the tuning frequency. This prediction will be verified later. More precisely, the mass ratio between the primal and auxiliary systems determines the optimum combination of the active and passive damping factors. Under ordinary cases the mass ratio is very small (less than 0.01). Therefore, the passive damping factor is also small. (cf. chapter 2) If we desire some amount of passive damping installed to the device for the safety guaranty, we should decrease the feedback gain G_2 . But the response of the AMD will be increased because the cancellation of the driving force is not expected.

5 Stiffness of the AMD

The natural frequency of the AMD system should be tuned to the primal system, because it must work as a differentiator as is explained before. It is also expected that there is the optimum tuning frequency of the AMD system which is influenced by the natural frequencies of the primal and auxiliary systems. But the deviation from the optimum stiffness will have a small influence on the control performance, because the damping installed to this

small oscillator is very large so that the phase response curve does not sharply change around the tuning frequency of the AMD.

6. Damping of the AMD

The damping factor necessary for the AMD system will be very large. The phase response curve should not change radically around the tuning frequency of the AMD system, because it should differentiate the feedback signals and also should damp the free vibration of itself. It should be noted that this damping force is to be created by the actuator rather than a passive damper. Because the inertia force and the spring force will diminish each other at the natural frequency of the primal system and the control force will be smaller than otherwise. This phenomenon is similar to the situation of the acceleration feedback control force which is reduced by combining the driving force and damping force (Figure 2.5).

7 Example

There are three example case studies shown in Figure 4.29 ~ 2.31, where there are only two parameters G_2 and c_d, which are varied. As the combination of the passive and active damping is gradually changed, the response curves of the AMD system are significantly influenced while the other two system responses are not significantly disturbed. Obviously the case 2 optimizes the response of the AMD system under a given feedback gain G_1.

Table 4.12 Parameters for Preliminary Study of Composite TMD

Parameters	Case 1	Case 2	Case 3
m	16274 kg		
c	5.20×10^3 Ns/m		
k	1.05×10^6 N/m		
m_d	388.6 kg		
c_d	9.80×10^2 N s/m	5.29×10^2 N s/m	1.96×10^2 N s/m
k_d	2.65×10^4 N/m		
m_s	37.8 kg		
c_s	1.47×10^3 N s/m		
k_s	2.25×10^3 N/m		
G_1	1.47×10^4 N s/m		
G_2	0.0	1.42×10^4 N/m	2.45×10^4 N/m

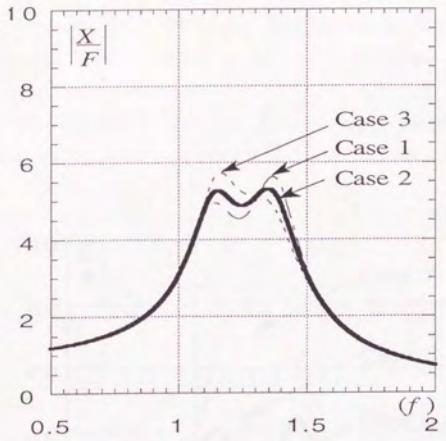

Figure 4.29 Primal System Frequency Response

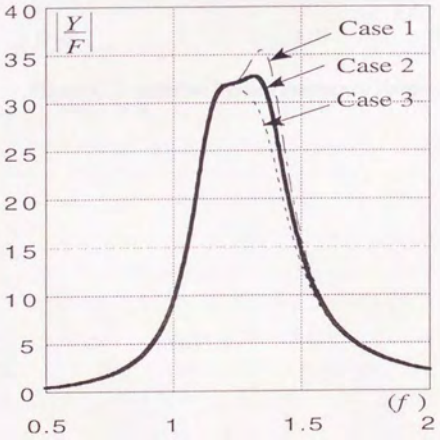

Figure 4.30 Primal System Frequency Response

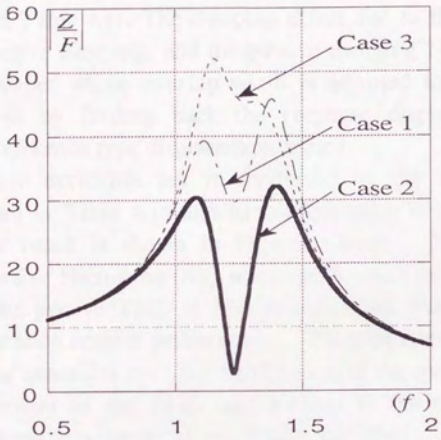

Figure 4.31 Satellite System Frequency Response

4.7 Excitation Test of the Active Tuned Mass Damper

The active and passive TMD parameters are all set to the values given in Table 4.11. The passive TMD weight is not 388.6 kg but 441.6 kg, because the additional weight of the AC motor, 53.0 kg , is counted, of course it does not move in case of the passive TMD test. The passive damping coefficient is set to 700 N s/m or 10 % by means of the magnetic dampers whose overlap width of the copper plates is adjusted to 1.8 cm.

According to the optimum formulae, the parameters of the active TMD are also given in Table 4.11. The damping effect due to the self inductance is assumed to be active damping, and the passive damping 240 N s/m is given by the magnetic damper whose overlap width is adjusted to 5 mm. The active stiffness is given by feeding back the response displacement which was measured by a reference type displacement sensor.

The random excitation test is conducted by the shaking table whose capacity is shown in Table 4.13 and its configuration is shown in Photo 4.1. The typical test result is shown in Figure 4.32~39. The excitation is the earthquake record of Hachinohe (NS) whose peak acceleration is normalized to 20 cm/sec^2. The passive TMD is also tested under the same excitation to compare the vibration control performance. The data sampling time is 0.01 sec and the measured quantities are : the acceleration of the specimen structure, the relative displacement of the TMD with respect to the top of the specimen structure, the absolute velocity of the TMD, the absolute acceleration of the shaking table.

The experimentally obtained results are simulated by using the observed shaking table acceleration for numerical calculation. The identified parameters of the test specimen and the control devices were used for this part of the analysis. The simulated results of the time history responses of the specimen structure, the TMD, and the AMD under Hachinohe earthquake excitation are shown in Figure 4.32 ~ 4.39, they are in a good accordance with the simulation.

It is clear that the control effect is achieved as much as expected analytically. Comparing the acceleration responses of the passive and active TMDs, the amplitude of the active TMD is augmented in general but the free vibration is not conspicuous where the passive one lingers even after the disturbance excitation recedes from the main structure, for example, from 10 to 14 second in Figure 4.36 and 4.38. It is true that the peak of the resonance

Table 4.13 Specification of the Shaking Table Facilities

Shaking Table Configuration	4.0 m x 4.0 m, aluminum, weight :8.5 ton
Capacity of the specimen weight	20.0 ton
Maximum output force	3.92×10^5 N (lateral), 9.8×10^5 N (vertical)
Capacity of stroke	150 mm (lateral); 75 mm (vertical)
Maximum output acceleration	1.2 G (lateral); 3.0 G (vertical)
Frequency range	0 ~ 30 Hz
Input signal type	random, sinusoidal, rectangle (both lateral and vertical)
Capacity of overturning moment	1.1×10^6 N m
Natural frequency of the system (including the hydraulic system)	none load :24 Hz (lateral); 55 Hz(vertical) 10 ton : 17 Hz(lateral); 40 Hz(vertical) 20 ton : 13 Hz (lateral); 30 Hz(vertical)
Hydraulic system	Oil volume : 416 l/min Pressure : 210 kg/cm2

curve of the auxiliary system of the active TMD is as much as the passive one, but the band width of the response function is widen as a result of the acceleration feedback so that the motion of the active TMD is larger than the passive one under random disturbances such as earthquakes. It is also noted that the peak response of the auxiliary mass motion was recorded earlier in case of active than passive. (Compare Figure 4.36 with Figure 4.38.)

As a conclusion of this shaking table test, it can be said that the control device worked as exactly as designed and the control performance was achieved as much as expected from the theoretical prediction. Therefore, the advantages of the acceleration feedback method compared with the passive TMD are actually observed so that the theoretically promised superiority of the proposed methodology is empirically proved to exist in a real world.

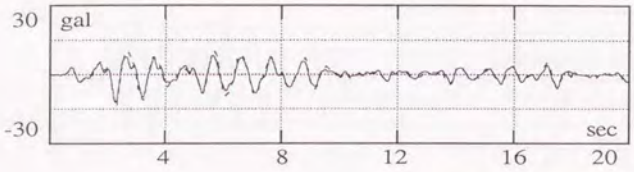

Figure 4.32 Response Acceleration of Specimen Structure ------ : Analysis
(Acceleration Feedback Control) —— : Experiment

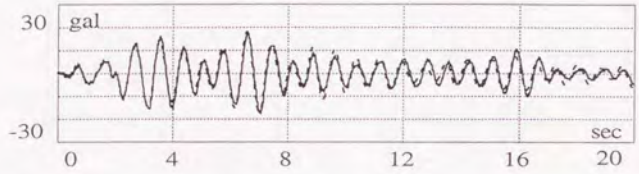

Figure 4.33 Response Acceleration of Specimen Structure ------ : Analysis
(Passive TMD Control) —— : Experiment

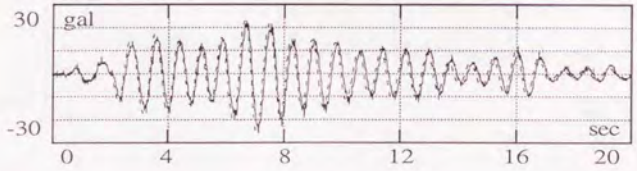

Figure 4.34 Response Acceleration of Specimen Structure ------ : Analysis
(Without Control) —— : Experiment

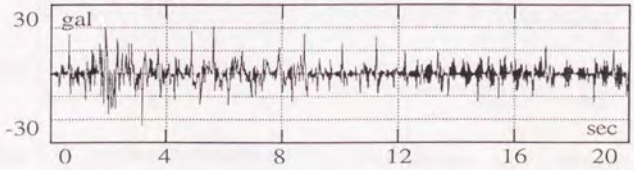

Figure 4.35 Shaking Table Acceleration —— : Measured

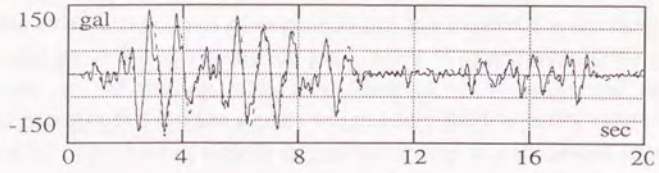

Figure 4.36 Response Acceleration of TMD ------ : Analysis
(Acceleration Feedback Control) —— : Experiment

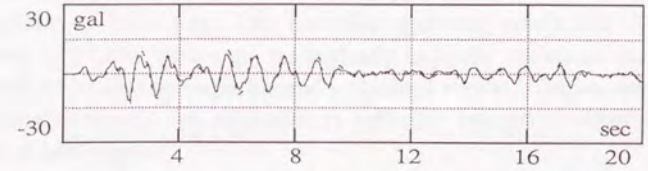

Figure 4.37 Response Acceleration of Specimen Structure ------ : Analysis
(Acceleration Feddback Control) —— : Experiment

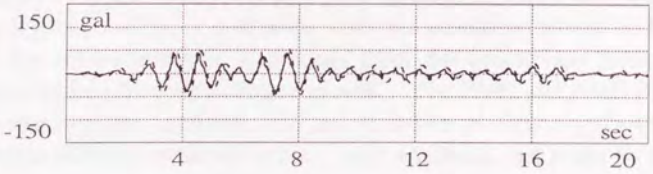

Figure 4.38 Response Acceleration of TMD ------ : Analysis
(Passive TMD Control) —— : Experiment

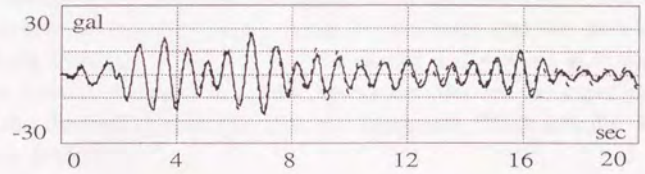

Figure 4.39 Response Acceleration of Specimen Structure ------ : Analysis
(Passive TMD Control) —— : Experiment

4.8 Excitation Test of the Composite Tuned Mass Damper

In this section, two types of excitation test are reported: a harmonic excitation test, and an earthquake excitation test. After the composite TMD is fabricated and set on the shaking table (See Photo 4.5.), it is excited according to numerous sinusoidal wave signals which cover the frequency range from 0.5 Hz to 2.0 Hz. The shaking table is excited according to a sinusoidal signal of which frequency is specified in Table 4.14. As is reported before, the primal system natural frequency is 1.28 Hz so that the center of the excitation frequency range is aimed around 1.0 Hz. The test procedure is exactly the same as the previous system identification tests, and the data acquisition condition and the test results are shown in Table 4.14. This harmonic excitation results are all indicated in Figure 4.40 ~ 4.45, where the theoretically expected resonance curves are also plotted along with the experimentally obtained results. The agreement between the experiment and the prediction is sufficient enough to obtain the expected control performance.

After the harmonic excitation test was conducted, the same test specimen was subjected to an earthquake excitation, which is the Hachinohe earthquake (NS) whose peak acceleration is scaled to 40 cm/s^2. First, the result of the no-control test is shown in Figure 4.46 and the simulated result is also shown in Figure 4.47. Both of them are in a good agreement. Then the composite TMD case is shown in Figure 4.48 along with the simulation shown in Figure 4.49. The control performance is obvious from the comparison between the two cases, and they are well simulated as well. The PMD and AMD responses are also observed and simulated, they are all shown in Figure 4.50 ~ 4.53. Again, the experimentally obtained data are well simulated, and it can be said that the theoretically expected control performance is actually achieved.

The feasibility of the acceleration feedback method is extremely enhanced by the composite TMD, which also played an important role to verify the validity of the theoretical development of the acceleration feedback method. As a result of this experiment, it can be concluded that the specimen structure with the composite TMD has been fabricated and worked as is designed. It is again noticed that there is a well agreement between the experimental results and the theoretical values so that the composite TMD actually works as the theory prescribes.

The whole experiments including system identification tests for the devices are conducted with much attention paid to the precision and agreement with the theory. Because the purpose of this experiment lies in the verification of the acceleration feedback method which is out of the scope of the modern control method. Now that this unique method is proved to be effective both theoretically and experimentally.

Table 4.14 Results of Harmonic Shaking Table Test of the Composite TMD

Frequency	AMD Acceleration		TMD Acceleration		System Acceleration	
(Hz)	Amp. (gal/gal)	Phase (deg)	Amp. (gal/gal)	Phase (deg)	Amp. (gal/gal)	Phase (deg)
0.50	25.5	24.1	3.75	4.8	0.986	0.9
0.60	27.9	13.1	2.11	0.2	1.080	0.6
0.80	34.3	-17.0	3.47	-16.8	1.44	-1.3
0.85	39.1	-28.0	4.48	-24.1	1.59	-2.5
0.90	41.8	-36.8	5.56	-31.0	1.80	-4.1
0.95	44.1	-56.6	7.79	-43.1	2.08	-7.6
1.00	44.8	-71.7	10.00	-54.6	2.43	-12.0
1.02	45.9	-81.6	11.29	-61.0	2.59	-14.9
1.04	46.2	-92.4	12.81	-67.7	2.78	-17.9
1.06	45.6	-103.2	14.28	-74.8	2.98	-21.5
1.08	44.7	-116.1	15.95	-82.8	3.18	-25.5
1.10	46.4	-128.3	17.69	-90.7	3.41	-30.2
1.12	45.6	-141.7	19.39	-99.2	3.64	-35.3
1.14	44.7	-156.6	21.14	-108.5	3.87	-40.9
1.16	43.3	-172.1	22.69	-118.0	4.08	-47.2
1.17	42.0	-181.3	23.24	-123.4	4.14	-50.8
1.18	39.9	-188.6	23.30	-127.4	4.14	-53.2
1.19	38.9	-196.3	23.84	-131.4	4.22	-55.6
1.20	38.5	-205.5	24.53	-136.3	4.29	-59.0
1.21	37.5	-214.0	25.04	-140.7	4.36	-61.7
1.22	36.7	-223.6	25.49	-145.7	4.43	-65.2
1.23	36.6	-234.4	26.08	-151.0	4.51	-68.9
1.24	36.0	-244.2	26.46	-155.9	4.58	-72.3
1.25	35.9	-254.4	26.80	-161.1	4.63	-76.1
1.26	35.8	-264.8	27.02	-166.5	4.65	-80.0
1.27	35.8	-275.5	27.07	-171.7	4.65	-83.8
1.28	35.7	-286.3	26.97	-177.1	4.65	-87.7
1.29	35.2	-297.1	26.90	-182.0	4.68	-91.1
1.30	35.2	-307.0	26.52	-187.2	4.62	-95.0
1.32	35.7	-326.0	25.66	-197.2	4.49	-102.6
1.34	34.7	-343.6	24.41	-206.5	4.31	-109.9
1.36	37.5	-359.5	23.02	-216.6	4.04	-116.8
1.38	33.7	-373.7	21.18	-223.0	3.82	-122.7
1.40	32.2	-386.4	19.51	-230.0	3.57	-128.2
1.45	29.5	-411.9	15.65	-244.9	2.93	-139.4
1.50	25.9	-429.3	12.62	-254.6	2.40	-146.7

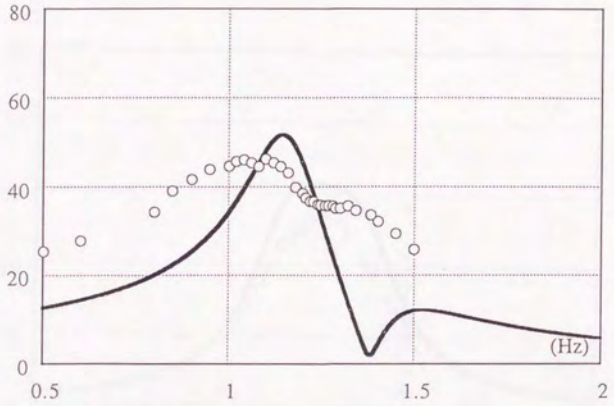

Figure 4.40 Amplitude Transfer Function of AMD
(AMD Acceleration versus Table Acceleration)

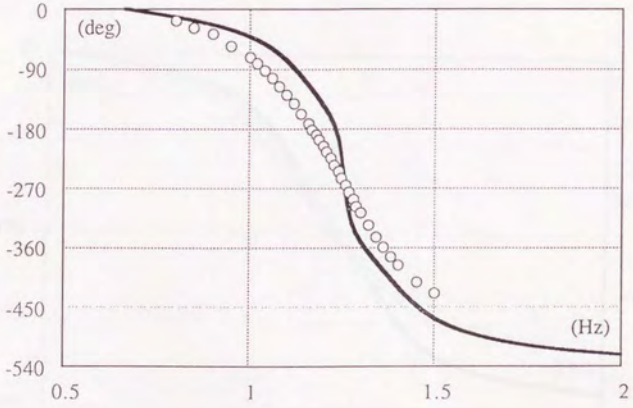

Figure 4.41 Phase Transfer Function of AMD
(AMD Acceleration versus Table Acceleration)

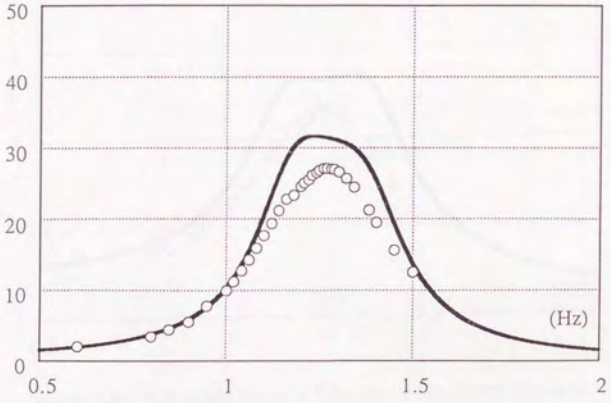

Figure 4.42 Amplitude Transfer Function of PMD
(PMD Acceleration versus Table Acceleration)

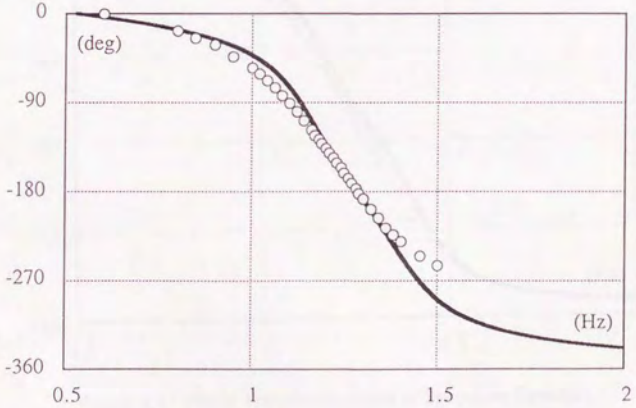

Figure 4.43 Phase Transfer Function of PMD
(PMD Acceleration versus Table Acceleration)

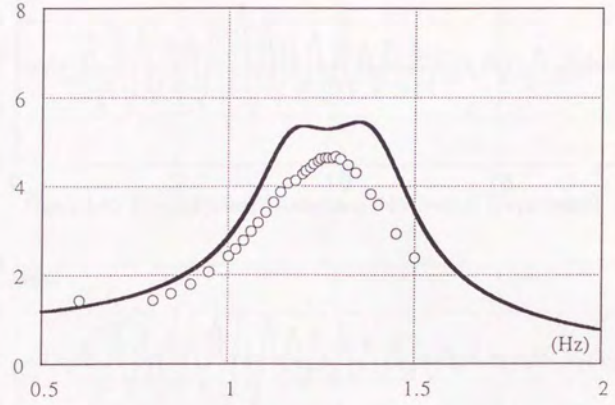

Figure 4.44 Amplitude Transfer Function of Specimen Structure
(Specimen Acceleration versus Table Acceleration)

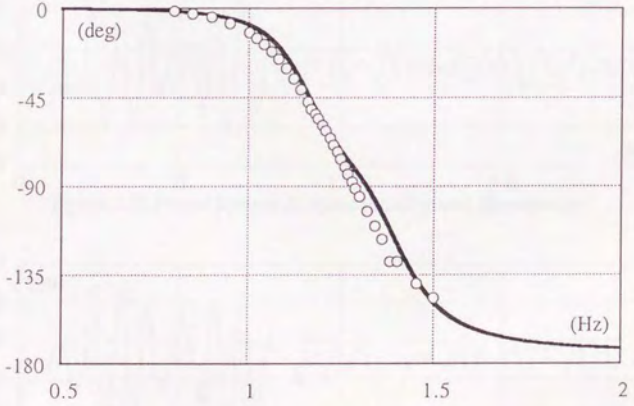

Figure 4.45 Phase Transfer Function of Specimen Structure
(Specimen Acceleration versus Table Acceleration)

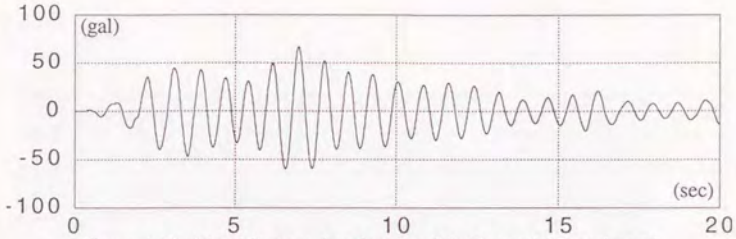

Figure 4.46 Primal System Acceleration (No Control) [Experiment]

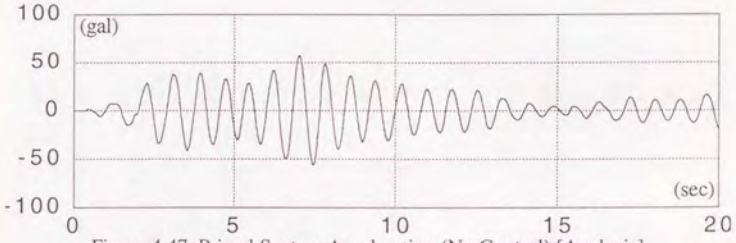

Figure 4.47 Primal System Acceleration (No Control) [Analysis]

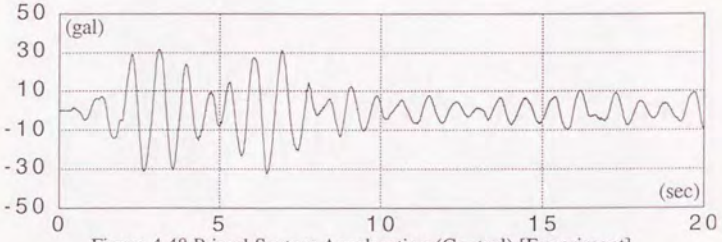

Figure.4.48 Primal System Acceleration (Control) [Experiment]

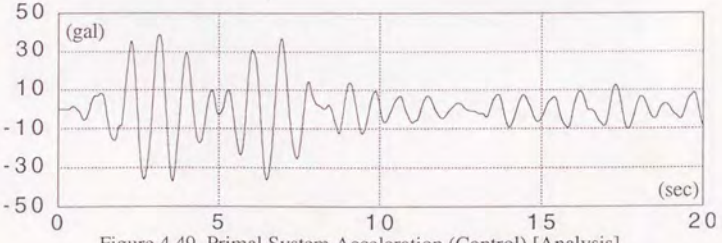

Figure 4.49 Primal System Acceleration (Control) [Analysis]

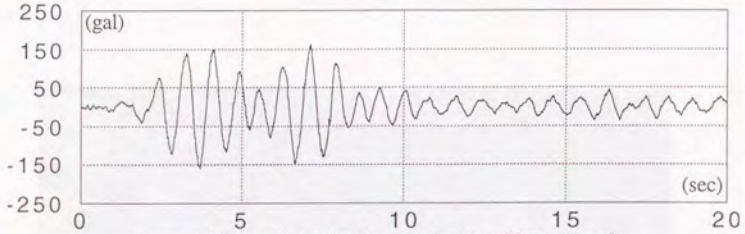

Figure 4.50 Auxiliary System Acceleration [Experiment]

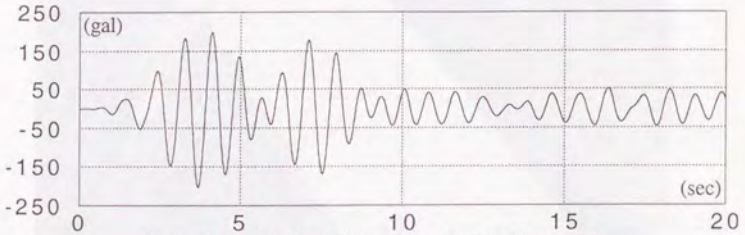

Figure 4.51 Auxiliary System Accelertion [Analysis]

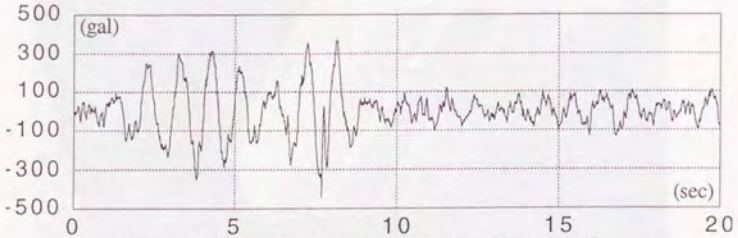

Figure 4.52 Satellite System Acceleration [Experiment]

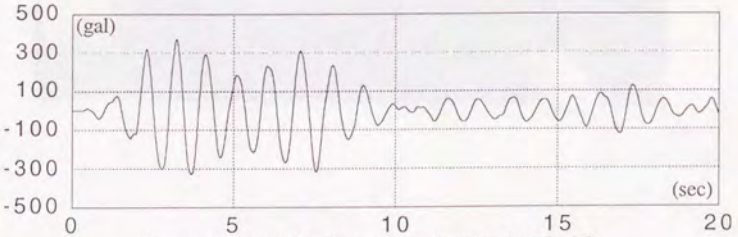

Figure 4.53 Satellite System Acceleration [Analysis]

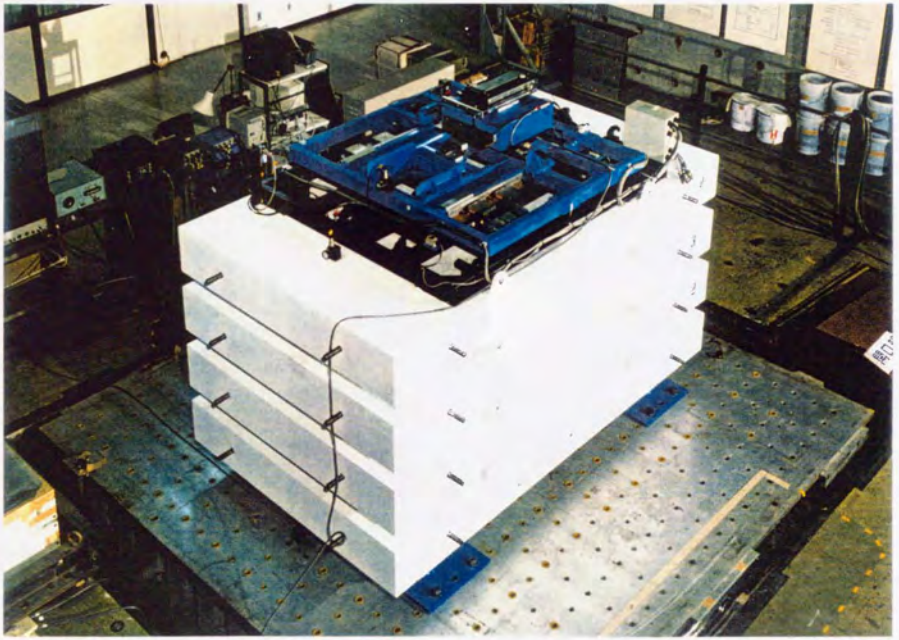

Photo 4.1 Set Up View of the Specimen Structure on the Shaking Table

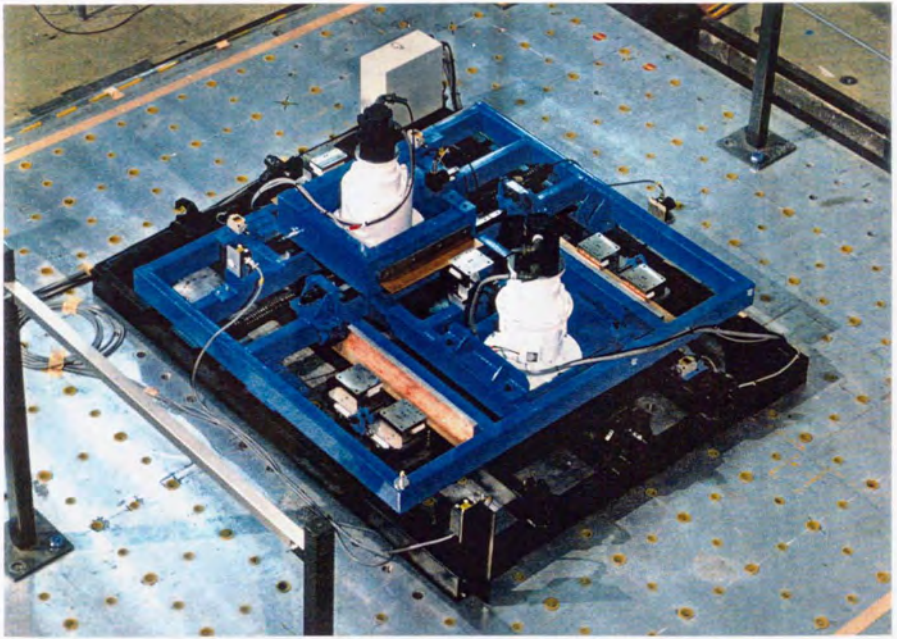

Photo 4.2 Active Tuned Mass Damper

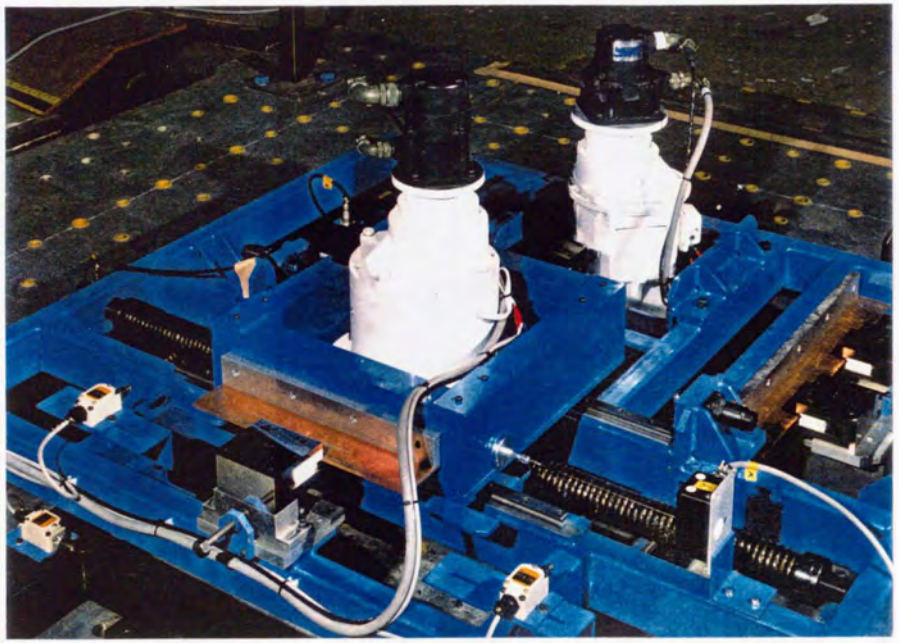

Photo 4.3 Close up of the Active TMD and Magnetic Damper

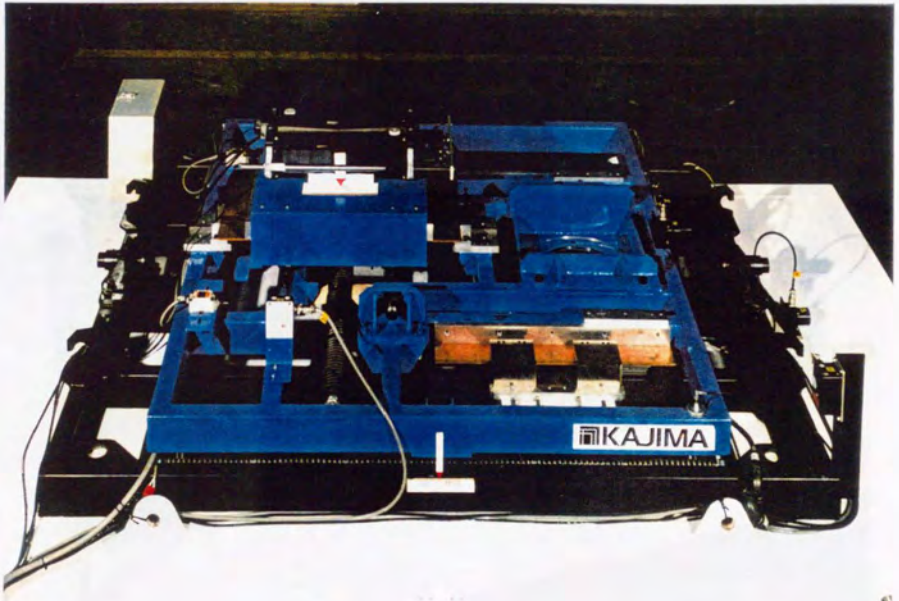

Photo 4.4 Set Up View of the Composite TMD

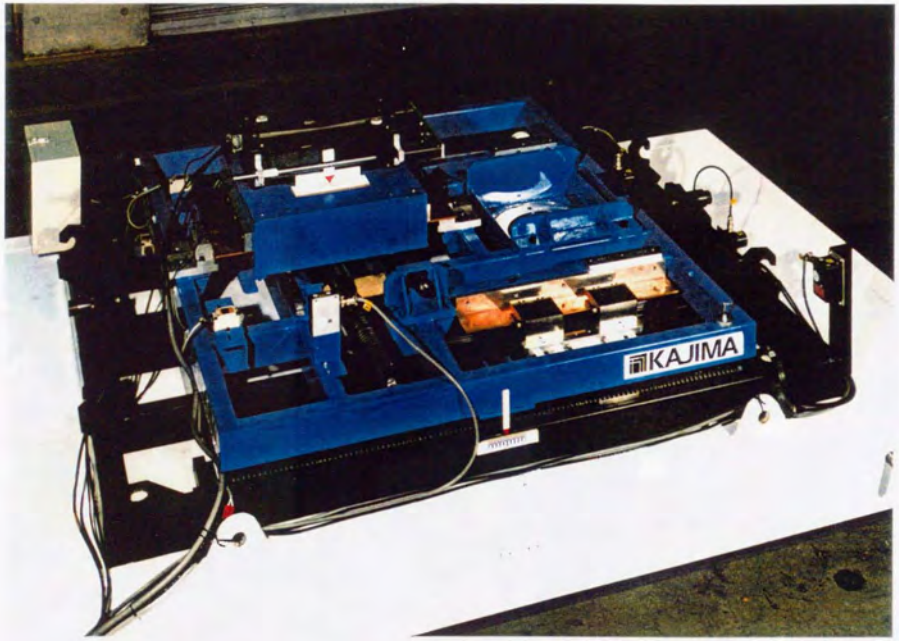

Photo 4.5 Side View of the Composite TMD

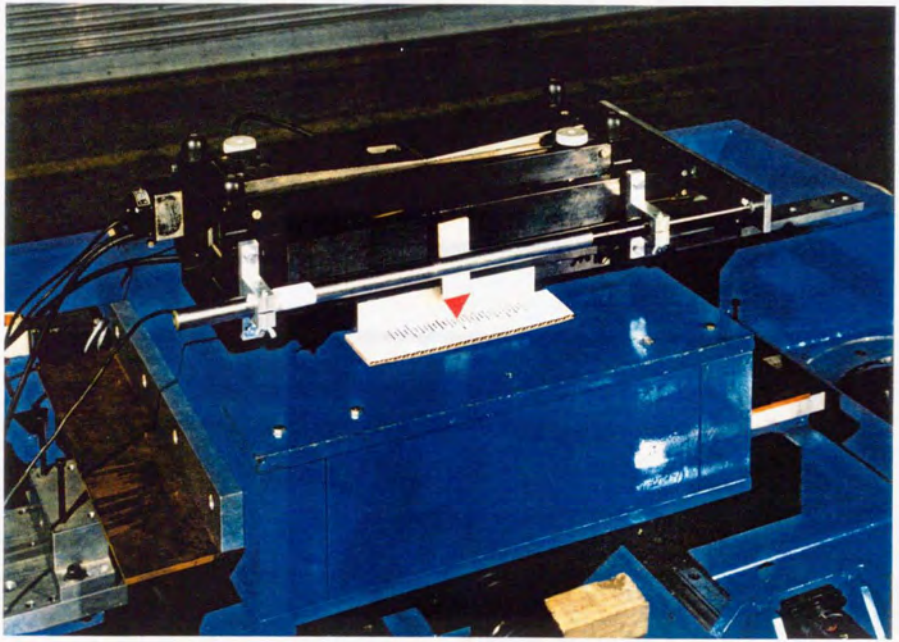

Photo 4.6 Close Up of the Active Mass Drive of the Composite TMD

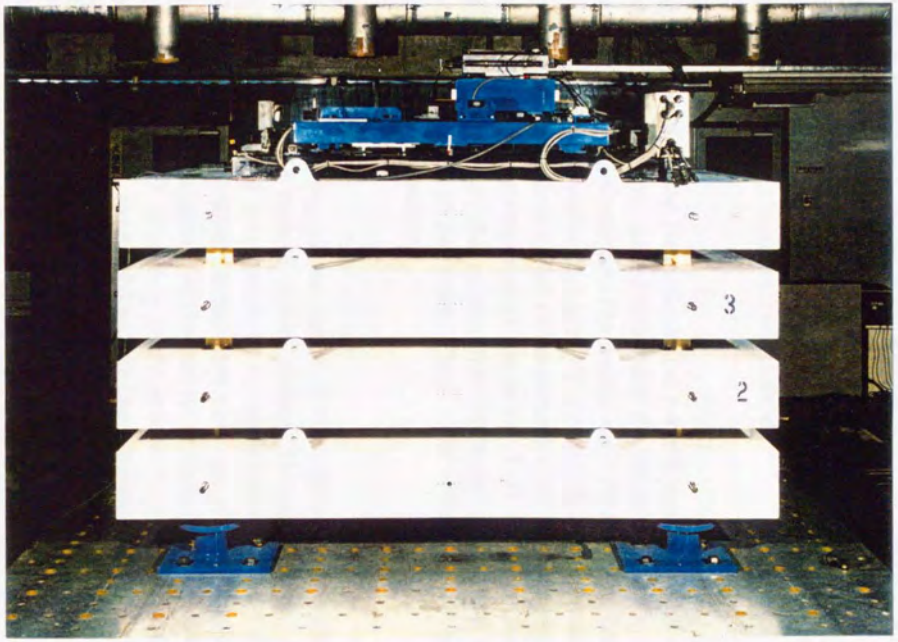

Photo 4.7 Set UP View of the Composite TMD

Conclusion

In this paper, the author proposed a new active control algorithm or the acceleration feedback method which is successfully applied into tuned mass damper. This control algorithm has several unique features which are described in this paper. In accordance with the issues which are pointed out in *Introduction*, the author wishes to summarize the achievements that have been obtained by the acceleration feedback method.

Issue 1:
In the civil engineering field, the active control method is still thought to be dubious and not reliable mainly because of the active tuned mass damper stroke is thought to be extraordinary. The acceleration feedback method proved that the relative displacement response of the active TMD under a harmonic disturbance is equivalent to that of the passive TMD with the same mass ratio. And the steady state response of the active TMD is not influenced by the feedback gain. Hence, the acceleration feedback method has improved the control performance of the active TMD while restricting the auxiliary mass motion as much as possible.

Issues 2:
The physical meaning of the active TMD operation is vague, when we faithfully follow the modern control method. Hence, the tuning adjustment of the auxiliary system was not fully comprehended by the linear quadratic optimum control algorithm. On the other hand, we have successfully obtained a set of closed form solutions for the parameter optimization problem associated with the active TMD, according to the acceleration feedback method. These analytical solutions explicitly tell us the physical meaning of the tuning adjustment and damping selection for the active TMD.

Issue 3:
It is also very important for civil engineering application problems to reduce the required control force and power. The acceleration feedback method clarified the physical meaning of the feedback algorithm. It has two primal feedback quantities: the acceleration of the primal system and the relative

velocity of the auxiliary system. It has become clear that there is a simple relationship between these two feedback quantities that minimize the required control force and power simultaneously without degrading the vibration control efficiency. It is also made clear that there is an optimum ratio between the passive stiffness and the active restoring feedback force. These optimization process is conducted under a white noise disturbance and we obtained a set of closed form solutions.

Issue 4:
The effect of disturbance excitations on the optimization of performance is taken into consideration. First, the parameter optimization of the active TMD is considered. As a result, the formulae of the stiffness and damping adjustment have been obtained under both a harmonic and a white noise wind disturbances. Earthquake disturbances are also considered and it is proposed that the absolute acceleration of the primal system is used as the feedback signal so that the whole derivation and optimization process are identical to those in case of wind blow disturbance. One of the advantages of this method is that the sensing equipment and the control signal processing are not influenced by the types of disturbance excitations.

Issue 5:
The validity of the analytical solutions are numerically evaluated so that the expected vibration control performance is actually checked under several earthquakes. The highly non-stationary random disturbances such as earthquakes are used for this numerical study under various combination of feedback gains and the optimum TMD parameters. The acceleration feedback method is a rather simple methodology so that the response spectra with respect to the natural period of the primal system have been obtained under varied feedback gains. The control performance of the active TMD has been assessed in terms of response spectrum for the first time It is also noted that the passive damping and active braking force combination that has been analytically optimized under a white noise excitation is numerically proved to be the optimum value that eliminates the control power in the average sense in the time domain under several earthquake disturbances.

Issue 6:
The theoretically expected and numerically ascertained vibration control performance has been verified by a shaking table test. The reliability of the test results depend on the precision of the system identification of both the specimen structure and the control device. Careful attention was paid to the dynamic system identification part of the test. Finally, the theoretically expected control effect was realized on the shaking table. The feasibility of the acceleration feedback method is enhanced by the composite TMD which was also tested on the shaking table. The obtained test results are assertive and satisfactory so that the acceleration feedback method is concluded to be the appropriate algorithm especially suitable for the active TMD applied for large building structures.

Acknowledgments

I am indebted to many people in writing this paper. I wish to express thanks to Dr. Kobori, who initiated the project and provided a lot of research opportunities to me. Gratitude is also extended to Mr. Sakamoto, who has been the project manager of the control research, and to Mr. Ishii, who has been the research manager in Kajima Technical Research Institute and always encouraged and helped me a great deal. I must be thankful to Mr. Yamada, who is the inventor of the active and passive composite TMD, for this helpful suggestions. I have been working with him and learned a good deal from this genius engineer. Dr.Koshika is the leader of the research team with the Ando Nishiki-cho project that is the first application of the active-passive composite TMD. I also wish to extend my gratitude for his leadership to accomplish the project. I was encouraged and advised by Prof. Akiyama at Tokyo University who motivated me to write this thesis. His suggestions and advises are greatly appreciated. A research project which was conducted with Prof. Masri at University of Southern California from 1988 to 1990 provided me a good deal of hints and experiences that helped me immensely to conduct the shaking table verification test in chapter 4. My acknowledgment should go to him for that unique opportunity provided to me. I want to appreciate the valuable suggestions and opinions that I obtained from Prof. Takafumi Fujita, Prof. Yozo Fujino, Associate Prof. Kenichi Ohi, and Associate Prof. Hitoshi Kuwamura who are the committee members of this thesis inspection at the University of Tokyo. Finally, my special thanks go to my dear family who have supported me while I was working on this thesis.

Isao Nishimura

Appendix

Integration of Power Spectral Density Function

The following table of the integration is referred to "Theory of Servomechanisms," MIT radiation Laboratory Series, Vol. 25, McGraw-Hill, New York, 1947, pp.333-369.

$$I_n = \frac{1}{2\pi j}\int_{-\infty}^{+\infty} dx \frac{g_n(x)}{h_n(x)\,h_n(-x)}$$

where

$$h_n(x) = a_0 x^n + a_1 x^{n-1} + \cdots + a_n$$

$$g_n(x) = b_0 x^{2n-2} + b_1 x^{2n-4} + \cdots + b_{n-1}$$

under the condition that the roots of $h_n(x)$ all lie in the upper half plane.

$$I_1 = \frac{b_0}{2\,a_0\,a_1}$$

$$I_2 = \frac{-b_0 + \dfrac{a_0 b_1}{a_2}}{2\,a_0\,a_1}$$

$$I_3 = \frac{-a_2 b_0 + a_0 b_1 - \dfrac{a_0 a_1 b_2}{a_3}}{2\,a_0\,(a_0 a_3 - a_1 a_2)}$$

$$I_4 = \frac{b_0(-a_1 a_4 + a_2 a_3) - a_0 a_3 b_1 + a_0 a_1 b_2 + \dfrac{a_0 b_3}{a_4}(a_0 a_3 - a_1 a_2)}{2\,a_0\,(a_0 a_3^2 + a_1^2 a_4 - a_1 a_2 a_3)}$$

References

[1] Den Hartog, J.P., *Mechanical Vibration*, 3rd Edition, McGraw-Hill, New York, pp.112~133, 1947

[2] Ormondroyd,J., Den Hartog,J.P., "The theory of the dynamic vibration absorber," *Trans. ASME* 49/50, A9~A22, 1928

[3] Yao, J.T.P., "Concept of Structural Control," *Journal of the Structural Division, ASCE*, vol. 98, No. ST7, pp.1567~1574, 1972

[4] McNamara, R.J., "Tuned Mass Dampers for Buildings," *Trans. ASCE, Journal of the Structural Division*, vol.103, No.ST9, pp.1785~1798, 1977

[5] Petersen, N.R., "Design of Large-Scale Tuned Mass Dampers," *ASCE National Convention*, Boston, April, 1979

[6] Wiesner, K.B., "Tuned Mass Dampers to Reduce Building Wind Motion," *ASCE National Convention*, Boston, April, 1979

[7] Hust, D.W., "Devices for Damping Lateral Vibrations in Tall Structures," *Proc. Symposium /Workshop on Serviceability of Buildings*, Ottawa, 1988

[8] Lund, R.A., "Active Damping of Large Structures in Winds," *ASCE Convention and Exposition*, Boston, April, 1979

[9] Chang, C.H., Soong, T.T., "Structural Control Using Active Tuned Mass Dampers," *ASCE*, EM6, vol. 106, pp.1091-1098, December, 1980

[10] Morison, J., Karnopp,D., "Comparison of Optimized Active and Passive Vibration Absorber," *14th Annual Joint Automatic Control Conference*, Ohio State University, Columbus, Ohio, pp.932-938, June, 1973

[11] Masri, S.F., "Seismic Response Control of Structural Systems: Closure, " *Proceedings, 9th World Conferences on Earthquake Engineering*, Tokyo-Kyoto, paper No. SE., August, 1988

[12] Soong,T.T., " State-of-the-Art Review: Active Structural Control in Civil Engineering," *Journal of Engineering Structures*, pp.74-84, 1988

[13] Kobori,T., et al. , "Seismic Response Controlled Structure with Active Mass Driver System, Part 1:Design", *Earthquake Engineering and Structural Dynamics*, vol. 20, pp.133~149, 1988

[14] Shiba,K., Tamura,K., Satake,N., Yokota,H., Kitada,Y.," Response Control of Building Utilizing Hybrid Mass Damper System", *Transactions of the Japan National Symposium on Active Structural Response Control* , Tokyo, March, pp.263~270, 1992

[15]Tanida,K.,Koike,Y., "Control of Bending-Torsion Structural Vibration Using a Pair of Hybrid Mass Dampers," *1st International Conf. on Motion and Vibration Control*, Yokohama, vol.1, pp.237~242,September,1992
[16] Watanabe,T., Yoshida,K., "Evaluation and Optimization of Parallel Hybrid Active Dynamic Vibration Absorber," *1st International conf. on Motion and Vibration Control*, Yokohama, pp.285~290, September, 1992
[17] Abiru,H., Fujishiro,M., Matsumoto,T., Yamazaki,S., Nagata,N., "Tuned Active Damper Installed in the Yokohama Land Mark Tower," 1st MOVIC, Yokohama, pp.110~115, 1992
[18] Nishimura,I., Kobori,T., Sakamoto,M., Koshika,N., Sasaki,K., Ohrui,S., , "Acceleration Feedback Method Applied to Active Tuned Mass Damper," *Transactions of the Japan National Symposium on Active Structural Response Control* , Tokyo, pp.187~193, March,1992
[19] Nishimura, I., Kobori,T., Sakamoto,M., Koshika,N., Sasaki,K., Ohrui,S., , "Acceleration feedback method applied to active tuned mass damper,"*1st European Conf. on Smart Structures and Materials*, Glasgow, pp.301~304, May, 1992
[20] Nishimura,I., Kobori,T., Sakamoto,M., Koshika,N., Sasaki,K., Ohrui,S., "Active Tuned Mass Damper," Journal of Smart Materials and Structures, vol.1, pp.306~311,1992
[21] Nishimura,I., Kobori,T., Sakamoto,M., Koshika,N., Sasaki,K., Ohrui,S., , "Acceleration Feedback Method Applied to Active Tuned Mass Damper," 1*st International Conf. on Motion and Vibration Control*, vol.1 , pp.273~278,1993
[22] Yamada,T., Kobori, T., Nishimura, I., "Dynamic Vibration Absorber," application paper submitted to the Japan Patent Bureau, Dec.17, 1986, open to the public in June 29, 1988
[23] Nishimura,I., Kobori,T., Sakamoto,M. ,Yamada,T. ,Koshika,N. ,Sasaki,S. Ohrui,S., "Active Passive Composite Tuned Mass Damper," *Proceedings of the Seminar on Seismic Isolation, Passive Energy Dissipation and Active Control, Applied Technology Council Report* , ATC-17-1, pp.737~748, 1993
[24] Nishimura,I., Kobori,T., Sakamoto,M., Yamada,T., Koshika,N., Sasaki,S., Ohrui,S.,, "An Intelligent Tuned Mass Damper," *A Collection of Technical Papers Part 6, 34th Structures, Structural Dynamics and Materials Conference*, pp.3561~3569, 1993

[25] Nishimura,I., Kobori,T., Sakamoto,M., Koshika,N., Sasaki,S., Ohrui,S., "Satellite Mass Damper," *Proceedings of the 2nd Conference on Recent Advances in Active Control of Sound and Vibration*, pp.875~884, 1993
[26] Timoshenko,S, Yound,D.H., *Vibration Problems in Engineering*, 3rd Edition, D.Van Nostrand Company, Inc., Princeton, New Jersey, pp.210~221, 1955
[27] Crede, C.E., Harris, C.M., *Shock and Vibration*, Vol.1, Chapter 6, McGraw-Hill, New York, 1961
[28] Warburton,G.B., "Optimum absorber parameters for various combinations of response and excitation parameters," *Earthquake Engineering and Structural Dynamics*, vol.10, pp381~401, 1982
[29] Jacquot,R.G., Hoppe,D.L., "Optimal random vibration absorbers," *Journal of Engineering Mechanical Div., ASCE*, 99, pp.612~616, 1973
[30] Ayorinde,E.O.,Warburton,G.B.,"Minimizing Structural Vibrations with Absorbers,"*Earthquake Engineering and Structural Dynamics*, Vol.8, pp.219~236, 1980
[31] Chi-Tsong Chen, *Linear System Theory and Design*, Holt, Rinehart and Winston, Inc., New York, 1984
[32] Bernard Friedland, *Control System Design*, McGraw Hill, New York,1986
[33] *Theory of Servomechanisms*, MIT radiation Laboratory Series, Vol.25, McGraw-Hill, New York, pp.333~369, 1947
[34] Leonard Meirovitch, *Elements of Vibration Analysis*, 2nd Edition,McGraw Hill, New York, 1986
[35] Papoulis, *Probability, Random Variables, and Stochastic Processes*, 2nd Edition, McGraw Hill, New York, 1986
[36] Ray W. Clough, Joseph Penzien, *Dynamics of Structures*, McGraw Hill, New York, 1975
[37] C.Y.Yang, *Random Vibration of Structures*, Hoyn Wiley&Sons, Inc., pp.134~139, 1986
[38] Akiyama,H., *Earthquake-Resistant Limit-State Design for Buildings*, Tokyo University Press, 1980
[39] Akiyama,H., "Ds-values for Multi-Story Frames on the Top Story of which Damage Concentrates", *Trans. of AIJ*, No.362, pp.37~44, 1983

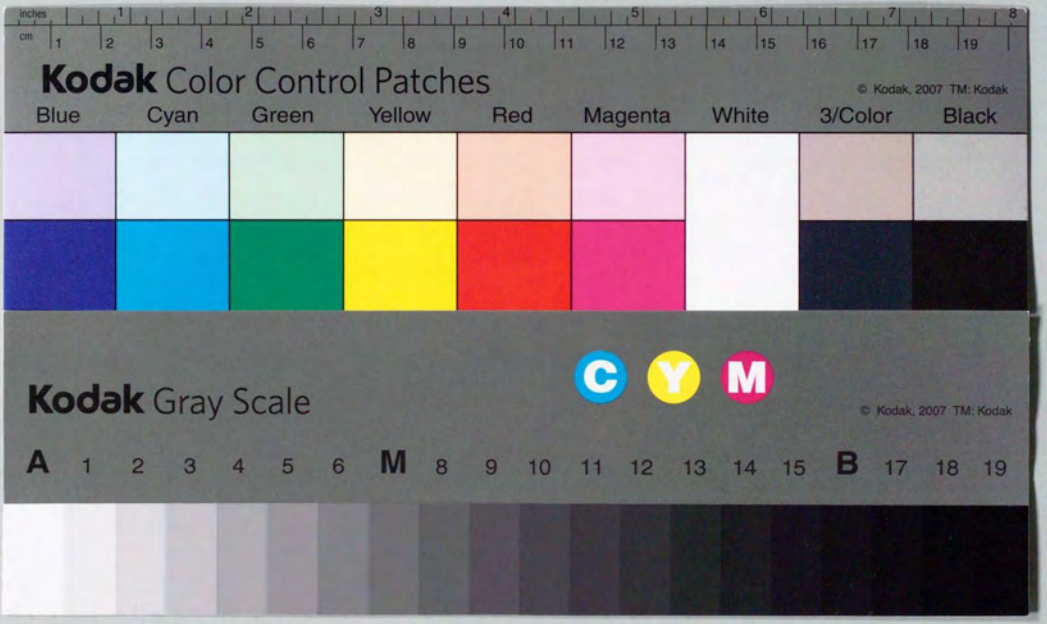
inches
cm
Kodak Color Control Patches
© Kodak, 2007 TM: Kodak
Blue
Cyan
Green
Yellow
Red
Magenta
White
3/Color
Black
Kodak Gray Scale
C
Y
M
© Kodak, 2007 TM: Kodak
A 1 2 3 4 5 6 M 8 9 10 11 12 13 14 15 B 17 18 19